AD 409 456

63-4-2

AFSWC-TDR-63-26

SWC
TDR
63-26

THE DEVELOPMENT OF RECIPROCITY PROCEDURES FOR UTILIZING DATA FROM UNDERGROUND EXPLOSION TESTS

Final Report

May 1963

TECHNICAL DOCUMENTARY REPORT NUMBER AFSWC-TDR-63-26

Research Directorate
AIR FORCE SPECIAL WEAPONS CENTER
Air Force Systems Command
Kirtland Air Force Base
New Mexico

This research has been funded by the
Defense Atomic Support Agency under WEB No. 13.148

Project No. 1080, Task No. 108007

(Prepared under Contract AF 29(601)-5132
by R. E. Hutton, S. Y. Yu, and Y. C.
Fung, Space Technology Laboratories, Inc.
A Subsidiary of Thompson Ramo Wooldridge
Inc. One Space Park, Redondo Beach, Calif.)

HEADQUARTERS
AIR FORCE SPECIAL WEAPONS CENTER
Air Force Systems Command
Kirtland Air Force Base
New Mexico

TDR-63-26

ABSTRACT

A procedure for predicting underground cavity motions resulting from surface air-blast loading is developed on the basis of a dynamic-reciprocity principle for a nonhomogeneous, anisotropic, linear, viscoelastic half space. A computer program for evaluating the integral equations for this medium is presented. Experimental measurements from the RAINIER Event of Operation PLUMBBOB are used to postulate cavity motions arising from a surface burst at the RAINIER site. The effects of variations in the cavity pressure signature, number of measured ground motions, and instrumentation errors are examined. Recommendations are made for experimental programs to obtain needed additional data, and, in general, to ascertain the applicability of the reciprocity to soils.

PUBLICATION REVIEW

This report has been reviewed and is approved.

Harold S. Hamada
Lt USAF
Project Officer

THOMAS J. LOWRY, JR.
Colonel USAF
Chief, Structures Branch

PERRY L. HUIE
Colonel USAF
Chief, Research Division

CONTENTS

CONTENTS (Continued)

PART I -- SUMMARY, CONCLUSIONS, AND RECOMMENDATIONS

I. INTRODUCTION

The central aim of this investigation was to develop a procedure in which ground motion data obtained during an underground explosion could be used to predict the underground motion that would result if there was a surface explosion at that site. Part I summarizes the work performed during the study, while Part II presents the details.

During this study, a digital-computer program was developed which makes it possible to compute cavity deformations caused by a specified pressure loading on the surface of the ground. By using this program the practicality of the proposed procedure is demonstrated and no insurmountable problems are anticipated in its use.

The ground motion and surface pressure pulse data needed to make the cavity motion calculations have been taken during numerous tests and there are no difficulties involved in using these data in the digital computations. Nevertheless, there still remains one important question to be answered; that is, the degree of applicability of this procedure to soil media. This can only be determined when the necessary data become available. Now it is true that soil motions due to a transient loading, say at point C , have been measured, say at point S. However, to test the dynamic-reciprocity theorem in a soil, a reciprocal measurement must be made. That is, the motion at C due to a transient loading at S should

be measured. Such data are not available at present, and suggestions for a test program to gather the necessary data are outlined at the end of this report.

The specific objectives of the present studies were formulated and the study initiated. These four objectives were:

1) Transform the general convolution integrals in the reciprocity theorem to forms that are applicable to the specified problem and that are suitable for digital computation; develop a practical procedure for data reduction.

2) Investigate supplementary techniques for relating average radial displacements to probable displacement variations around the cavity.

3) Evaluate the limitations and possibilities of the basic concept of dynamic reciprocity to the specified problem; delineate possible extensions to nonlinear and dissipative continuous systems, and to other problems in ground shock propagation.

4) Develop criteria for the types and accuracy of instrumentation needed for field measurement; establish reasonable estimates of the number and distribution of measurement stations; investigate interpolation procedures

for estimating ground displacement between stations.

Briefly, the work undertaken to meet the specific objectives was as follows: First, the dynamic-reciprocity relation which is pertinent to the problem was transformed to a form suitable for digital computations. This relation was programmed and checked out by comparing the computed results against some known solutions for beams. Calculations of cavity displacements caused by a postulated nuclear surface detonation were then performed. Ground-motion velocity data taken during the underground PLUMBBOB series of tests were used in these calculations. The underground cavity pressure which caused these ground motions was not available; hence a set of hypothetical cavity-pressure pulse curves were used. Various computer runs were made to investigate the effect on the computed cavity deformations caused by various cavity pressure pulse curves. The influence of errors in the ground-station velocity measurements was also investigated.

Since the cavity displacement calculations provide only the average radial displacement, the relation between the average, distortional, and rigid-body radial displacements was investigated next. Published theoretical results from a related problem were used to estimate the relative magnitude of these radial displacements. The related problem was solved by Baron and Parnes (Reference 6) and dealt with the response of a cylindrical cavity during the passage of a plane compressional wave. They determined the radial and tangential velocities of the cavity boundary as a

function of time for several points around the periphery of the cavity in nondimensional variables. From these published results the average, rigid body, and distortional displacement time-histories for several points around the cavity were determined. This problem differed from the spherical cavity problem considered in this study in two respects. First, the medium was assumed to be homogeneous, isotropic, nondissipative, and linearly elastic; and second, the cavity was cylindrical rather than spherical. In an effort to remove the objection of a different geometry, the analogous problem for a spherical cavity was examined and its solution formulated. However, the calculations of the cavity displacements required the development of another computer program. Since no numerical computations were performed the derivation of this formal solution to the spherical cavity problem was not included in this report but has been documented in STL Report EM 13-7.

II. DIGITAL PROGRAM DEVELOPMENT

A special form of the general dynamic-reciprocity theorem (derived in the Appendix), which has been transformed and programmed on the IBM 7090 so that calculations of cavity motions could be made is

$$\int_o^t \int_{S_c} p_c(t - \tau)u_c(\tau)dS_c d\tau = \int_o^t \int_{S_s} p_s(t - \tau)u_s(\tau)dS_s dt \quad (1)$$

where p and u represent pressure and displacement time-histories and subscripts c and s refer to cavity and surface. This convolution integral relation is integrated over the cavity area S_c and the surface area S_s as well as over time. In the applications of this integral relation it is assumed that the surface responses u_s caused by the cavity pressure p_c have been

measured and the cavity deformation u_c caused by the specified surface pressure p_s is to be determined. Upon examination of the type of ground motion data taken during underground explosions, it appeared that ground velocity data $\dot{u}_s$ or acceleration data $\ddot{u}_s$ were more readily obtainable than ground displacement data. It was decided, therefore, to transform (1) into a form where the digital computations of the unknown cavity deformation $u_c(t)$ depended upon the ground velocities $\dot{u}_s$, and the two pressure pulses p_c and p_s. In the computational scheme adopted, the space integration over the ground surface was replaced by a summation over n stations by assuming that the variations of the integrands over each station were solely time variations. Clearly, this requires that the spacing between stations be small enough so that the variations of p_s and $\dot{u}_s$ from station to station are not too large. From a computational standpoint this does not place any serious restrictions upon the cavity displacement calculations since the computer is capable of handling a large number of stations. Generally, the upper limit to the number of surface stations will be governed by the number of velocity time-histories that can be recorded during the underground detonation. However, from the data to be presented presently, it appears that the number of surface stations required are within the capabilities of the usual instrumentation procedures.

Before the digital program could be used to make cavity deformation calculations it was necessary to obtain surface and cavity pressures and ground velocity time-histories. In the calculations it was assumed that the surface pressures were caused by a surface nuclear explosion. Once a given yield and ground zero were selected, Brode's theoretical pressure pulse was determined for each of the n stations (References 2 and 14). Actually, this was found to be a rather tedious task when a large number of stations used, and therefore, an alternate method for introducing the pressure pulse data was devised. The digital program was modified so that an arbitrary pressure pulse curve at each station can be input. Or alternatively, the weapon yield and the distance from ground zero to each of the n stations are specified, then the computer generates the appropriate Brode pressure pulse curve.

III. CAVITY DISPLACEMENT CALCULATIONS

A search for data on ground motion caused by underground detonation showed that a few measurements had been made on a large number of tests, but there were no tests in which surface motions had been measured at a large number of stations along several lines radiating out from surface ground zero. The most complete ground motion data found were ground-velocity data taken during the Rainier test in the PLUMBBOB series. During this test, ground velocities were measured at seven different stations ranging from ground zero out to a range of 2340 feet. The locations of the underground detonation and respective ground stations for these data are shown in figure 1. The stations were very nearly on a single radial line emanating from surface ground zero.

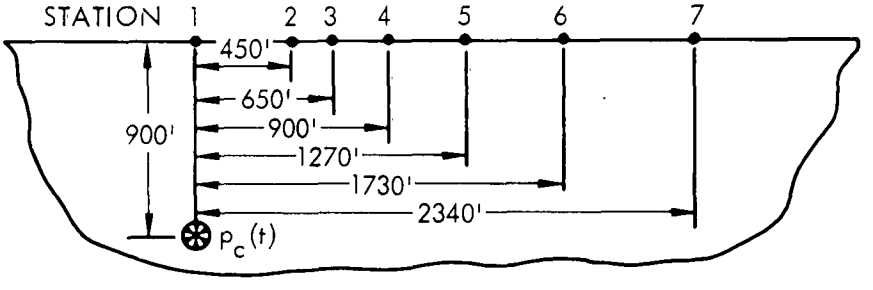

Figure 1. Location of Surface Stations with Respect to Underground Detonation—Rainier Test

Since no ground-motion data were available to indicate the nonisotropic nature of the medium where these data were taken, it was tacitly assumed that the medium was isotropic, and therefore, these measured motions were identical with those along any other radial line.

The ground-motion velocity time-histories at each of these stations are shown in figures 7 and 8 in Part II. Unfortunately, no data were available on the cavity pressure p_c that produced the ground velocities, and therefore, a theoretical pressure pulse was used. For the calculations, it was assumed that the cavity pressure could be expressed in the form

$$p_c(t) = Ae^{-\alpha t} + Be^{-\beta t} \qquad (2)$$

The peak pressure, i.e., A + B, was selected from the theoretical peak pressure curve for various cavity radii presented in figure 8 of Reference 14 for an assumed effective radius of about 10 feet. This corresponds to a pressure of about 100,000 atmospheres. The remaining three constants in equation (2) were arbitrarily selected. These parameters were changed in some of the computations to investigate the influence of variations in the peak cavity pressure and decay rate.

Numerous computations were made using the ground velocity data and cavity pressure pulses for a surface nuclear explosion having its ground zero at one of two locations. The first location was taken as directly above the underground cavity, and therefore, coincident with ground zero for the underground explosion. This case is referred to as the direct-hit example. The second location for ground zero was 1880 feet away from the ground zero for the underground explosion. This case is referred to as the non-direct-hit example. The conclusions drawn from these computations, and to be presented subsequently, are not meant to be interpreted as conclusions that are valid in general, for clearly, they are strongly dependent upon the data used. Nevertheless, the calculations are probably indicative of a typical situation and should provide a guide to the influence of the various parameters. In the calculations it was assumed that the medium was isotropic and, therefore, the measured velocity time-history at any station is the same for any other station at the same distance from surface ground zero.

A. INFLUENCE OF CAVITY PRESSURE PULSE SIGNATURE

The first parameter studied is the influence of various cavity pressure pulse time-histories upon the computed cavity displacements. This is an important parameter to investigate for there is difficulty in measuring this pressure pulse and theoretical computations are strongly dependent upon the properties of the explosive material, cavity size, and the simplifying assumptions. For example, see the theoretical pressure pulse curves computed in Reference 3.

Figure 3 shows the computed cavity displacements for the direct-hit example for the three cavity pressure pulses having peak pressures of 100,000, 81,625, and 61,000 atmospheres shown in figure 2. The pressure pulse curves were selected by initially taking the pressure pulse to be

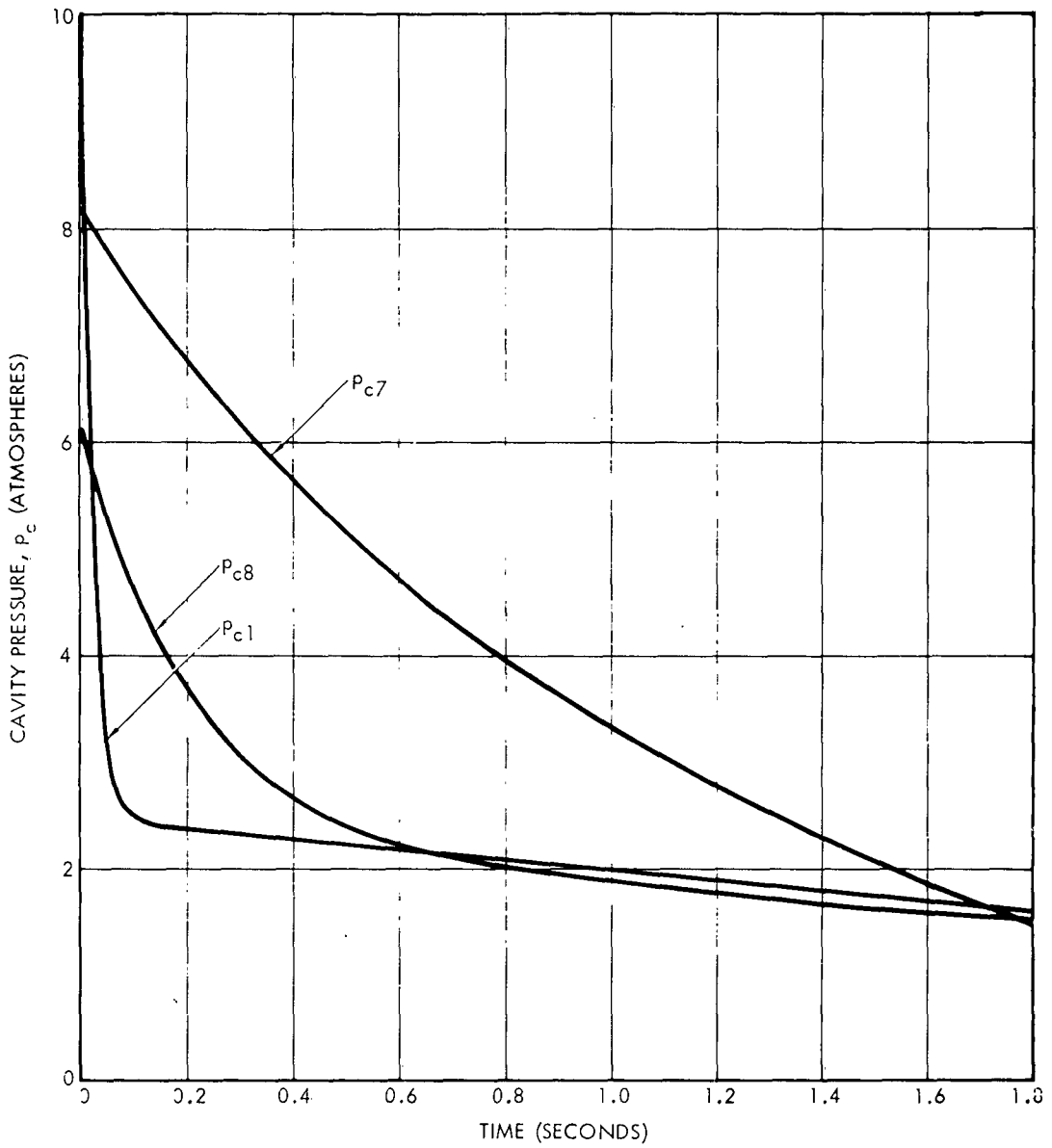

Figure 2. Assumed Cavity Pressures During the Rainier Shot in the PLUMBBOB Series

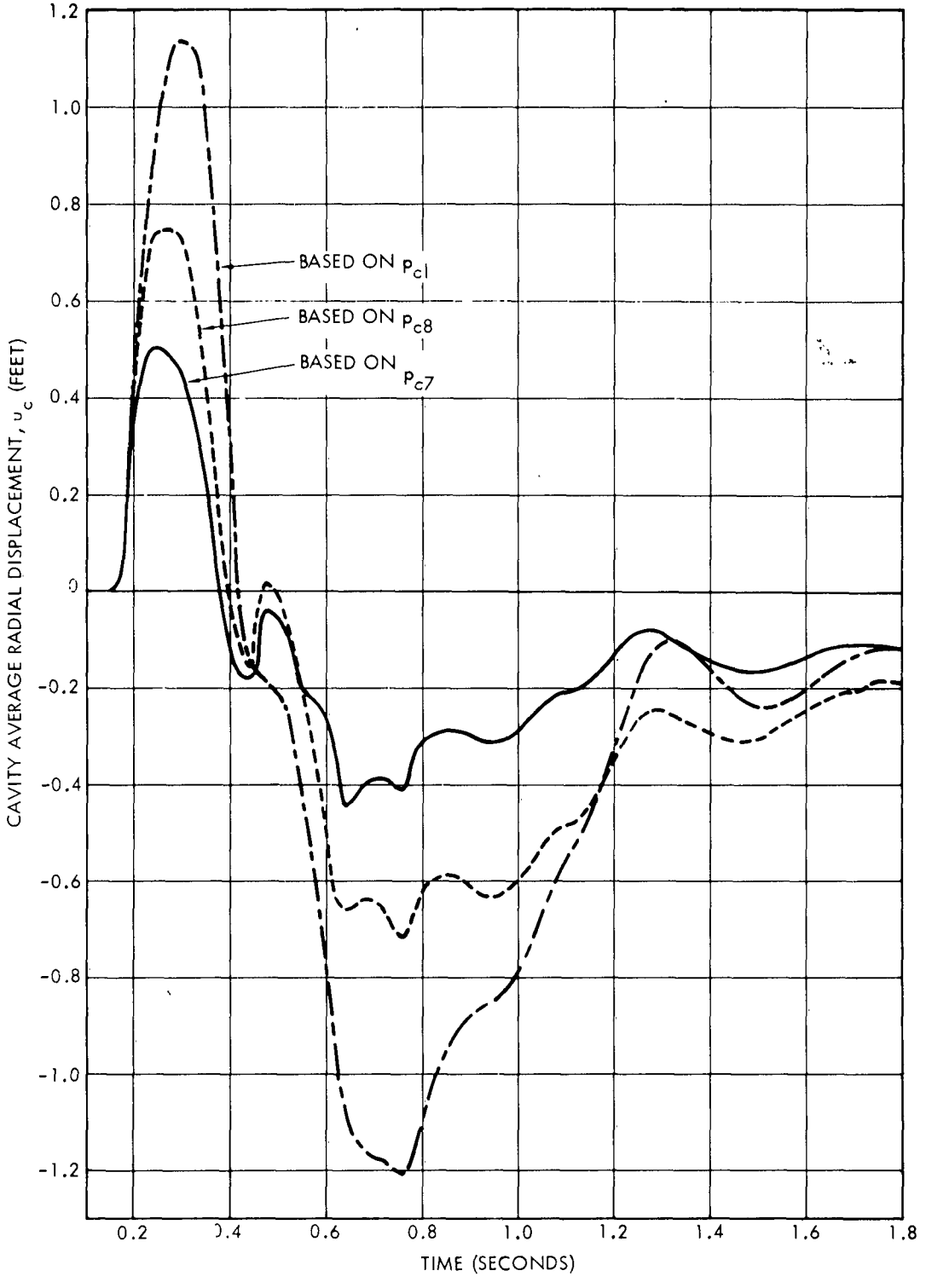

Figure 3. Cavity Displacements for Direct-Hit Example Based on Cavity Pressures of Figure 2.

$$p_c(t) = 75,000\, e^{-50t} + 25,000\, e^{-0.25t} \qquad (3)$$

and then selecting new values of A, B, α, and β subject to the condition that

$$\int_0^\infty p_c(t)\, dt$$

is a constant. Note that in figure 3, the peak cavity displacements are 1.2, 0.75, 0.55 ft for the three pressure pulses, p_{c1}, p_{c7}, p_{c8}, having peak pressures of 100,000, 81,625, and 61,000 atmospheres respectively. These data show that if there were indeed as much uncertainty in the pressure pulse curve as between these extremes, there would be an uncertainty of approximately 2 to 1 in the computed maximum cavity displacement. This suggests that when this procedure is applied to predict the cavity displacement caused by a surface pressure, efforts should be taken to properly define the cavity pressures.

From figure 2 note that p_{c7} is a larger pressure over the first 1.6 seconds except for the initial instant, while figure 3 shows that this cavity pressure pulse curve leads to the smallest predicted cavity displacement. This indicates that if one uses too large a cavity pressure, the computed cavity displacements will be too small. Obviously, it is not necessary to make cavity deformation calculations to note this fact for it is evident from equation (1). If one assumes p_s and u_s are known functions of time, then the right side of equation (1) is some fixed time function. Thus, if on the left side p_c is too large, then u_c will be too small accordingly. Physically, what this means is that if a small cavity pressure produces a large surface motion, then similarly a small surface pressure produces a large cavity motion. These comments suggest that if there is any uncertainty in the cavity pressure pulse, it is conservative to use a cavity pressure curve that is too small.

B. INFLUENCE OF NUMBER OF SURFACE MEASUREMENTS

Several calculations were made to investigate the effect of the number of surface stations used in the computations upon the computed cavity deformations. One such calculation was made by using every other surface station for the same direct-hit example used above. Adopting the

station numbering system shown in figure 1 for the direct-hit example, calculations were made by using the four stations 1, 3, 5, and 7 and the results were compared with those when all seven stations were used. The results of this computation are shown in figure 4. This figure shows that the predicted cavity deformations were larger when four stations were used. This is primarily a consequence of the manner of adjusting the surface areas in the two sets of computations. In the four station computations, the area associated with station 1 was larger than when all seven stations were used. Now, since the surface pressure and velocity were the largest at station 1, the contribution of station 1 to the total cavity deformation is large. Therefore, increasing the area of station 1 increases the predicted cavity response. This example provides an illustration of a case where the spatial variation of the time functions was too large between stations, at least, for those stations closest to ground zero. This does not necessarily infer that four stations are insufficient, but it does show that if fewer stations are used and the maximum pressure and velocity occurring within the area associated with the respective station are assumed to act over the entire area, then a conservative estimate of cavity motion will be obtained.

In an effort to provide additional information regarding the number of surface stations and the effect of instrumentation errors at these stations, some influence functions were computed for both the direct-hit and nondirect-hit examples. These influence functions were defined as the cavity response caused by the surface pressures acting on each station individually. In the results summarized here, the cavity pressure pulse given in equation (3) was used.

The station numbering system shown in figure 1 is again used for the direct-hit example. Figure 5 shows the maximum cavity displacement produced by the pressures acting on each of the seven stations. Probably it should be mentioned that these maximum cavity displacements are proportional to the area lumped at each surface station as well as to the measured ground velocity and prescribed overpressure. For example, the area lumped at station 7 was about three times that lumped at station 6. This larger area associated with station 7 caused the influence of station 7 to be greater than station 6. However, on an influence per unit area basis, the influence of successive stations would clearly decrease as the distance from the cavity to the station increased.

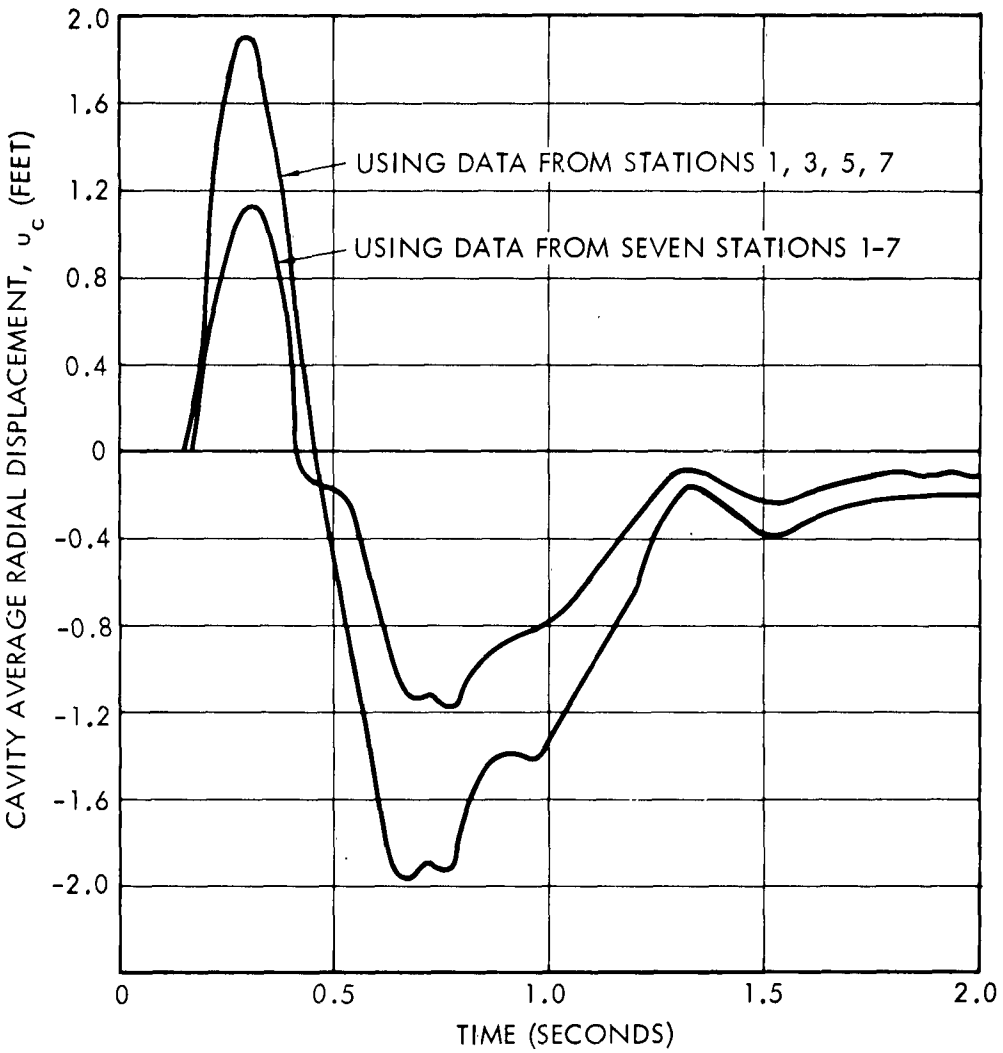

Figure 4. Comparison of Cavity Displacements

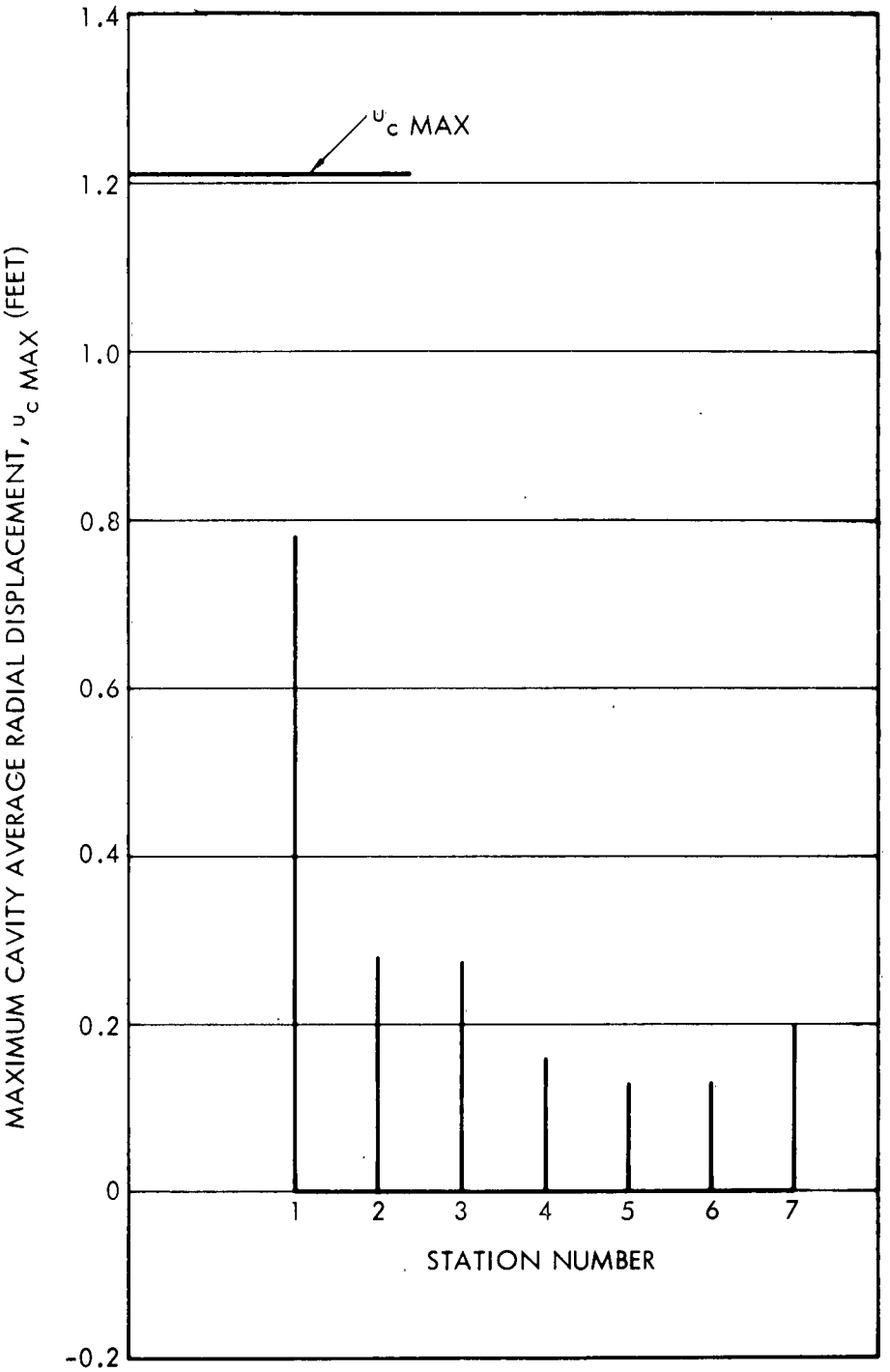

Figure 5. Influence Coefficients — Maximum Cavity Displacements Caused by Pressures Acting on Individual Stations for the Direct-Hit Example

Figure 5 is developed from the cavity motion data presented in figures 14 and 15 of Part II. Note that figure 5 shows that the absolute value of the maximum cavity displacement is 1.21 feet while the maximum value from the first station alone is 0.78 foot. Since the maximum cavity response caused by each surface station does not occur at the same instant of time, the maximum cavity response is not obtained by adding the maximum values shown in figure 5. From figure 3, it is noted that the maximum cavity displacement occurs at 0.76 second for the pressure pulse curve p_{c1}. Figure 6 shows the individual contribution of each station to this maximum cavity displacement at this instant of time. In this figure, it is noted that the contribution from stations 4, 5, 6, and 7 are small compared to the first three stations. In fact, if only the first three stations are used, the computed cavity displacement is -1.14 feet, rather than the value of -1.21 feet when all seven stations are used. In such a case, the computed error using the first three stations would be about 6 percent. Recall that when the four stations 1, 3, 5, and 7 were used, the error was approximately 70 percent. Thus, reasonable predictions of cavity displacements can be made with a limited number of stations; however, the stations must be selected judiciously as indicated later on.

For the nondirect-hit example, the station numbering system is shown in figure 7. More stations are required for the nondirect-hit example than for the direct-hit example because of the loss of some symmetry. Figure 8 shows the maximum cavity displacement caused by each individual station when considered separately. Indicated in this figure is a resultant maximum cavity displacement of 0.26 foot when the properly phased contribution from all stations is summed. Figure 9 shows the actual contribution of each station to this maximum cavity displacement. Since the cavity motion caused by pressures acting on some stations begins after the maximum cavity displacement is reached, their contributions to the maximum are zero. From figure 9, it is noted that if only the six stations, 1, 1a, 1b, 2, 2a, and 2b had been used in the analysis, the predicted maximum cavity displacement would have been -0.268 foot, which is very close to the value of -0.260 foot, when all surface stations are considered.

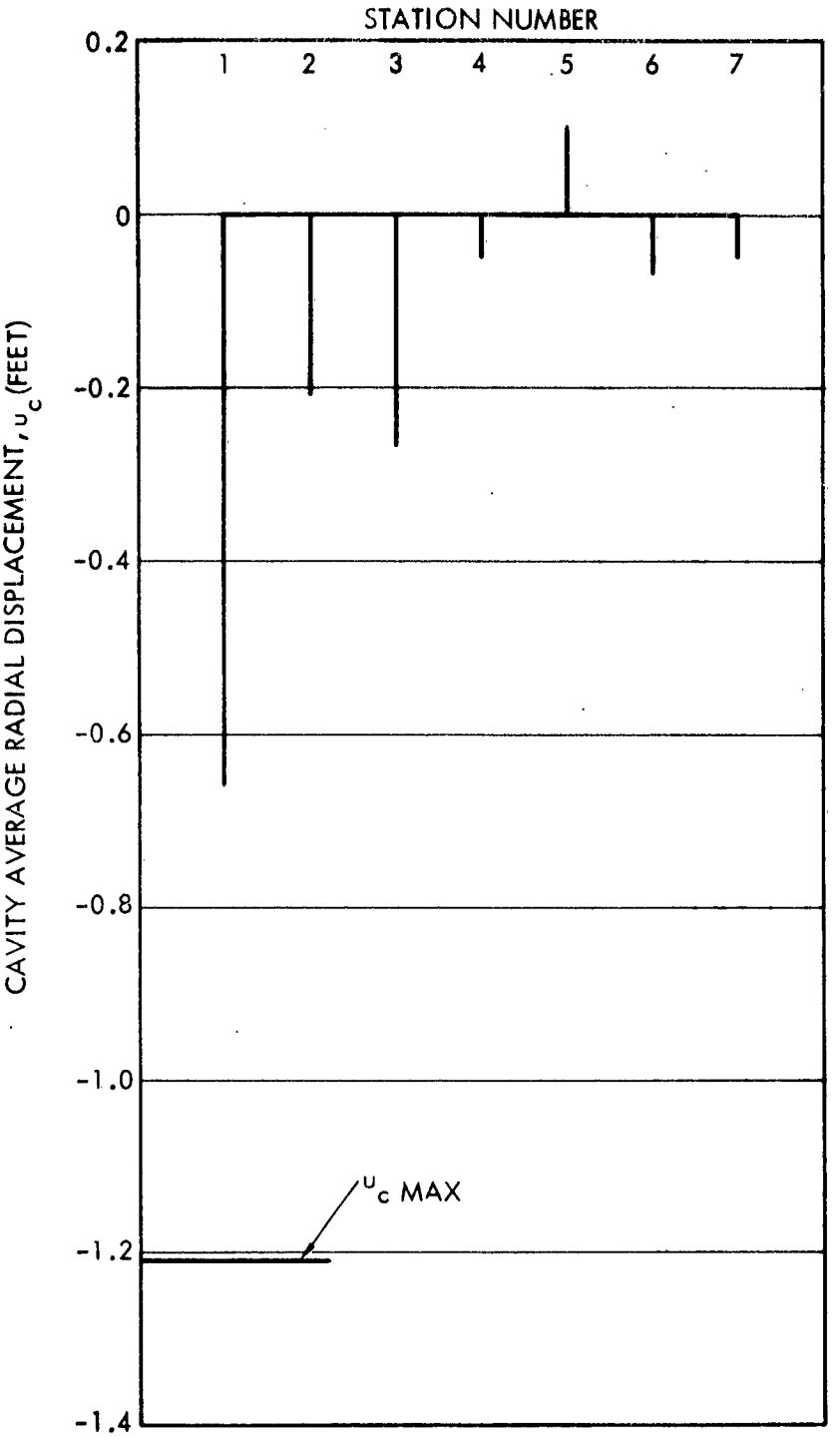

Figure 6. Contribution of Each Individual Station to the Total Maximum Cavity Displacement for the Direct-Hit Example

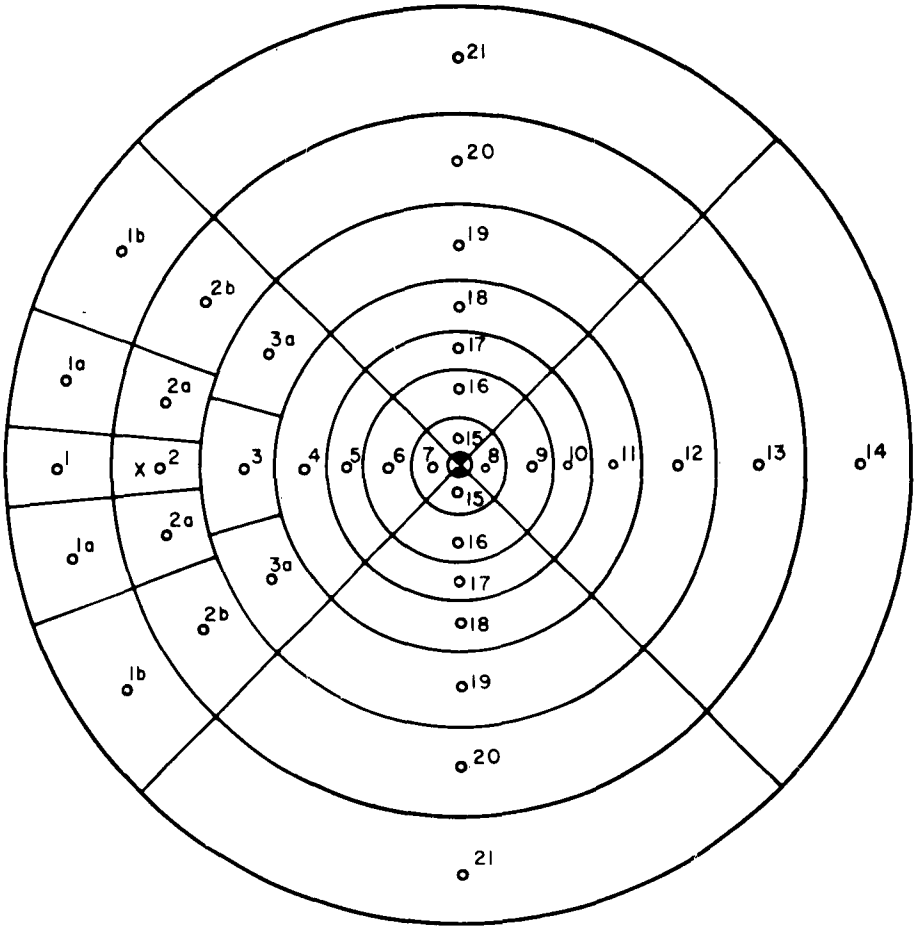

Figure 7. Lumped Stations for the Nondirect-Hit Example

X = surface burst ground zero

◔ = underground explosion ground zero

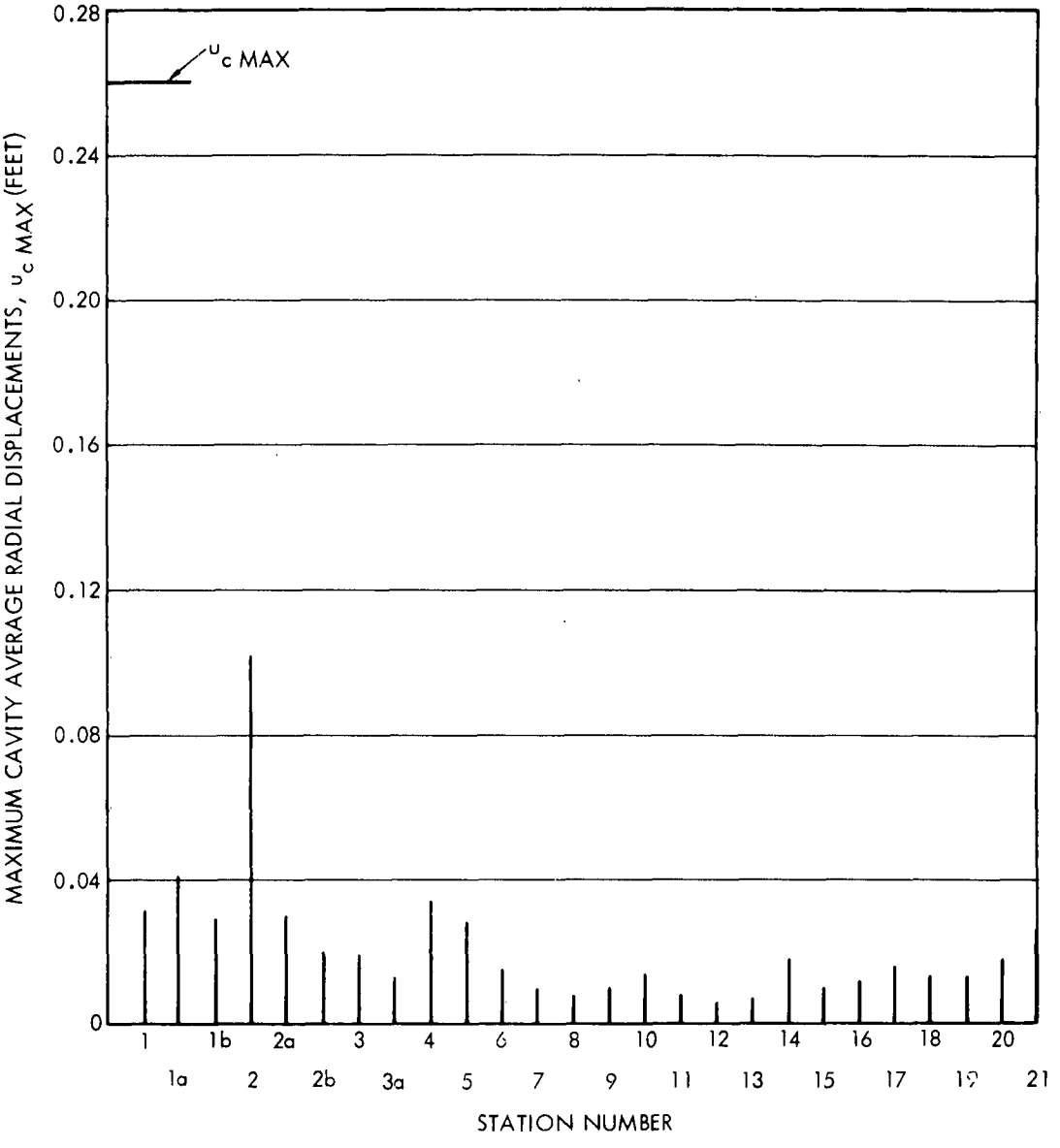

Figure 8. Influence Coefficients — Maximum Cavity Displacements Caused by Pressures Acting on Individual Stations for the Nondirect-Hit Example

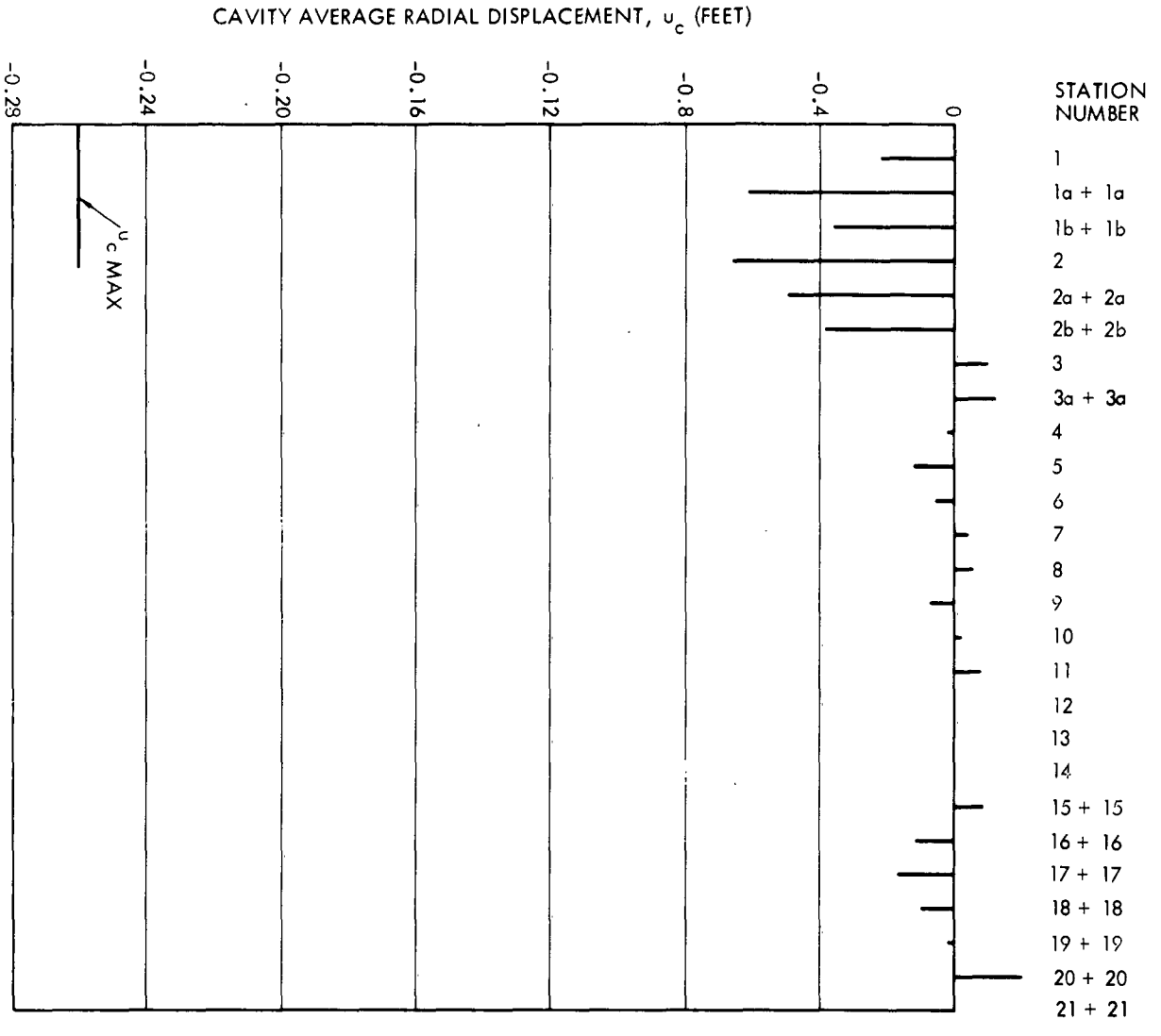

Figure 9. Contribution of Each Individual Station to the Total Maximum Cavity Displacement for the Nondirect-Hit Example

In both the direct-hit and nondirect-hit calculations, a fairly accurate cavity displacement can be predicted using a limited number of surface stations, provided that they are properly selected. The most important stations are those stations where the major portion of the energy from the nuclear surface detonation enters the ground, i.e., in the vicinity of ground zero. In the calculations shown here for an isotropic medium and for the direct-hit example reasonably accurate cavity displacements were predicted using only three stations when full advantage of the problem symmetry is used. For the nondirect-hit example, some symmetry was lost and fairly accurate cavity displacements were predicted using six stations.

C. INFLUENCE OF ERRORS IN SURFACE MEASUREMENTS

Errors in measured surface velocities cause a corresponding error in the computed cavity deformations. For example, since a linear system is assumed, say a 10 percent error in every measured ground velocity produces a 10 percent error in the computed cavity deformation. However, instrumentation errors may be randomly distributed so that the cancelling effects produce a smaller error. Figure 5 can be used to estimate the error in the predicted cavity deformation for a specified error in either the surface pressure or ground velocity at any station. Clearly, the largest error in predicted cavity deformation results from an error in the measurements taken at station 1. Figure 5 shows that the ratio of the contribution from station 1 to the contribution from all the stations is approximately $0.67/1.21 = 0.55$. Therefore, if say the surface velocity data for station 1 had a constant 10 percent error, this would produce an error of 5.5 percent in the predicted cavity deformation. Computations of this type led to the conclusion that errors in the computed cavity deformation caused by instrumental errors in the data taken at the ground surface stations are secondary when compared with the errors caused by the theoretical approximation to the actual pressure pulse curve, and the errors resulting by replacing the space-time integration of the convolution integral over the surface by summation of time integration at each of the n surface stations. These conclusions indicate that the typical accuracy obtainable in ground motion and pressure measurements is entirely satisfactory. The accuracy of cavity motion predictions can be improved more effectively by increasing the number of surface measurements rather than by improving the accuracy of the measurements made at a given set stations.

D. GROUND MOTIONS BETWEEN MEASURED POINTS

The possibility was examined of interpolating between stations to determine the ground motions at some intermediate stations. Here the hope was that fewer ground motion measurements could be made and the accuracy of the cavity computations improved by increasing the number of stations used in the analysis. However, it was soon apparent that no accuracy could be gained by this method and one might just as well use those stations for which data were available.

IV. CAVITY DISPLACEMENTS—AVERAGE, DISTORTION, AND TRANSLATION

Assume ground surface velocity data are obtained from a symmetric pressure pulse having a zero resultant force acting on an underground cavity. If these data are used to compute cavity deformations caused by a pressure loading on the ground surface, only average cavity deformations can be determined by the dynamic reciprocity procedure. The fact that the procedure provides no information regarding the cavity distortion and rigid-body displacement is not a limitation of the dynamic-reciprocity procedure, but rather emphasizes the fact that the cavity pressure pulse, which provided the free-surface velocity data, was symmetric and had a zero resultant force. In fact, if a nonsymmetric pressure pulse having a resultant force can be produced inside the cavity, and if the spatial and time distribution of this pressure pulse is known, then these pressure pulse data and the associated ground velocity data can be used to determine the total cavity displacement that would result from a specified ground-surface pressure loading. It is quite likely, however, that when this dynamic-reciprocity procedure is applied the cavity pressure pulse will be symmetric and have a zero resultant force. For this reason, theoretical computations were conducted to see how the average displacement was related to the distortion and rigid-body displacement. In this study use was made of some results presented by Baron and Parnes in Reference 6.

Baron and Parnes determine the motion of the cylindrical cavity in the infinite elastic medium illustrated in figure 10 during the passage of a plane compressional wave. Presented in their work are plots of the nondimensional radial velocities $\left[w/(\sigma c_p/\mu)\right]$ and tangential velocity $\left[v/(\sigma c_p/\mu)\right]$, as

functions of nondimensional time ($c_p t/2a$) for seven different points around the cavity, where $\dot{w}$ is the radial velocity, $\dot{v}$ the tangential velocity, σ the stress intensity of the wave, μ the shear modulus of the medium, c_p the propagation velocity of the dilatational waves, a the radius of the cylindrical cavity and t the time.

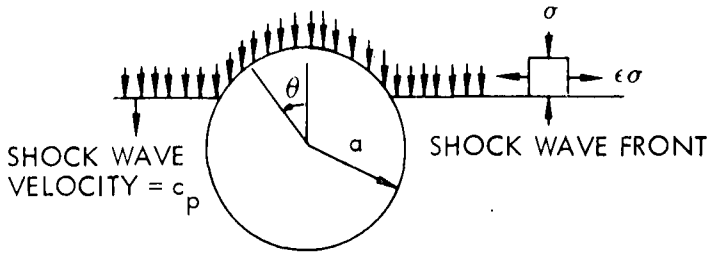

Figure 10. Plane Compressional Wave Engulfing a Cylindrical Cavity in an Infinite Medium

The detailed work presented in Part II consisted of integrating the cavity velocity components to obtain the displacement components $U_c(\theta, t)$ and $V_c(\theta, t)$. Next, the displacements were expanded into a Fourier series to determine individual contributions of the average, distortional, and rigid-body motion to the total radial displacement. This was done by representing the cavity displacements by the equations

$$U_c(\theta, t) = a_o(t) + \sum_{n=1}^{\infty} a_n(t) \cos n\theta$$

$$V_c(0, t) = \sum_{n=1}^{\infty} b_n(t) \sin n\theta$$

so that the component displacements are given by

$$\text{average radial displacement} = a_o(t)$$

$$\text{rigid-body radial displacement} = \frac{a_1(t) - b_1(t)}{2} \cos \theta$$

$$\text{distortional radial displacement} = U_c(\theta, t) - a_o(t) - \frac{a_1(t) - b_1(t)}{2} \cos \theta$$

The results of these computations showed that the maximum displacements occurred at $\theta = 0$. Figure 11 shows a plot of the three displacements at $\theta = 0$, as a function of time. From this figure it is noted that the average displacement and distortional displacement are roughly of the same magnitude. This suggests that, if only the average radial displacement is computed, the total elastic displacement will be obtained approximately by multiplying by a factor of two. Note that after the wave front has propagated one diameter beyond the cavity (nondimensional time equal to two), the cavity translational motion increases nearly at a constant rate. This continuing translational motion is a consequence of the assumption made in this problem that the compressive stress is continually applied. Thus, as the compressive wave front advances with a constant velocity, the entire medium moves with a constant velocity without acceleration. However, such rigid-body translations without distortion of the cavity shape do not cause any stress variations.

V. SUMMARY

During this study, a dynamic-reciprocity procedure was devised and a digital-computer program developed whereby ground-motion data taken during an explosion in an underground cavity could be used to predict cavity motions which would be caused by a specified pressure pulse loading on the ground surface. This digital program was so arranged that the data required to compute cavity motion are the pressure pulse time-history inside the cavity, the corresponding normal velocities of the ground surface, and the prescribed pressure loading on the ground surface. Given these data, the computer evaluates the average radial cavity deformation time-history that the specified surface pressure loading induces. If a nuclear detonation is prescribed on the surface, the yield of the weapon and the distance from ground zero to each of several surface stations can be specified and the computer will generate the approximate Brode pressure pulse curve as is necessary during the cavity calculations. This procedure is rigorously valid in nonisotropic, linear viscoelastic media, and, therefore, can be used for linear dissipative media. Even though the program was written to use ground velocities, acceleration measurements can be used.

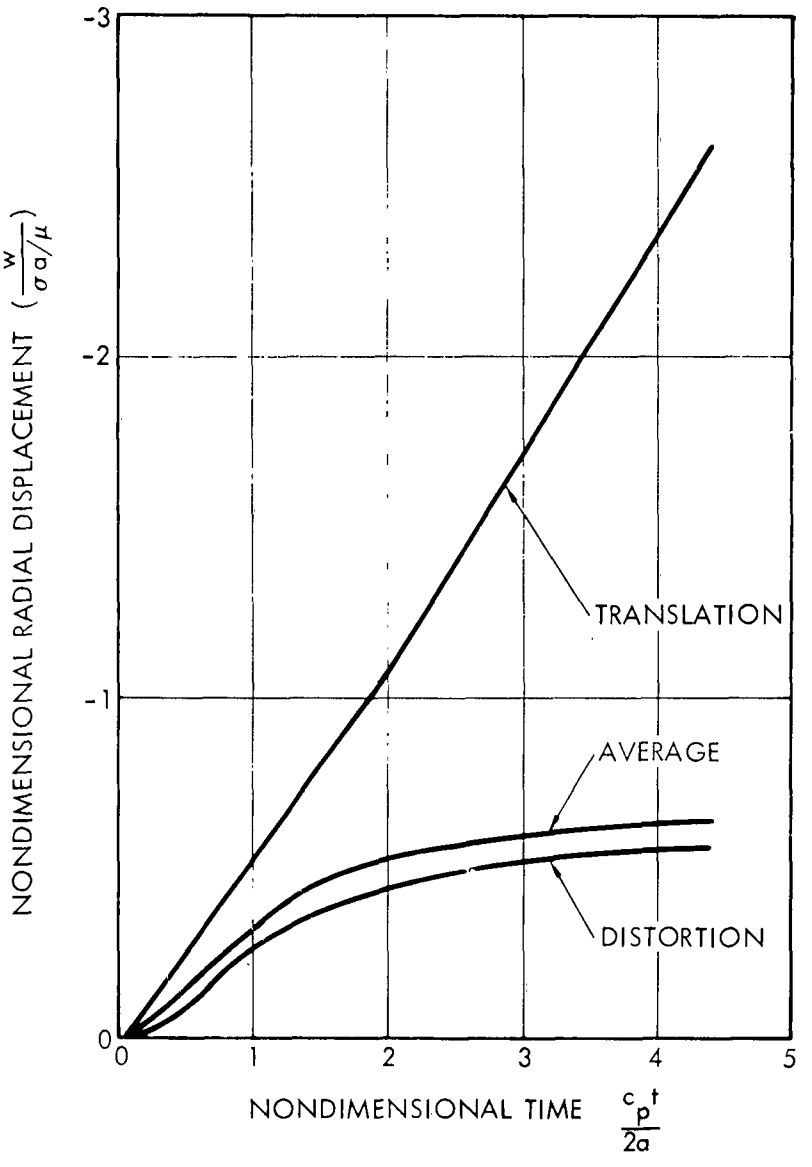

Figure 11. Comparison of Average Displacement, Distortion, and Translation of the Cavity at 0 = 0

The required number of ground motion measurements that must be recorded so as to apply the dynamic-reciprocity procedure is very much dependent upon the nature of the medium. For example, if the medium is isotropic, measurements along one radial line are sufficient. Whereas, if the medium is nonisotropic measurements should be made along three or four radial lines. The number of measurements required along any radial line should be at least 3, but from 4 to 7 or more are recommended. With the data used in this study, it was noted that the error in the calculated average cavity displacement was about 50 percent using only one surface measurement and about 13 percent using three surface measurements, when compared to the calculated average cavity displacement using seven surface measurements.

Cavity distortions can be estimated from the average cavity displacement using the results from the plane wave diffraction problem. Roughly, the maximum distortion is about equal to the average displacement. An alternative and more satisfactory method of estimating the cavity distortion and also translation can be made using experimentally determined transfer functions.

VI. RECOMMENDATIONS

This study demonstrated that a practical procedure utilizing dynamic-reciprocity relations can be used to predict the average cavity displacements caused by a prescribed pressure loading acting on the surface, providing experimental measurements of ground motions caused by a known average pressure acting inside the cavity are available. Although the average radial displacement is vital to the designer of underground structures, the distortional and translational displacements are also important. Theoretically, dynamic reciprocity provides a means for predicting total cavity motion, including translation and distortion as well as the average displacement caused by a hypothetical pressure acting on the surface of the ground. However, such predictions can be made only if one knows the spatial distribution of the pressure time-histories acting around the cavity while the ground motion data are being collected. If only the average pressure time-history acting in the cavity is known, then only the average radial displacement caused by a prescribed surface loading can be predicted. Generally the pressure distribution around the cavity will be nearly uniform unless some clever experimental procedure is adopted.

It is clear that requiring detailed cavity pressure loading imposes a severe constraint upon the test procedure followed when collecting the ground motion data. For this reason, it is desirable to remove this requirement by adopting an alternate procedure. A more practical procedure is to use the combined experimental-theoretical procedure which only requires the average cavity pressure, for predicting the average radial displacement caused by a prescribed ground pressure loading. Then, using the average displacement, along with some additional experimental data, estimate the distortion and translation of the cavity. To use this alternate procedure, data are required which show the relation among the cavity average, distortional, and rigid-body displacements. Such data can be obtained most conveniently on a linear medium using scaled models.

In the appendix, the dynamic reciprocity theorem is derived and shown to be valid for a nonhomogeneous viscoelastic medium provided the stress-strain relationship is linear. At the present time proof does not exist of the validity of the reciprocity relation in a nonlinear medium. Neither is there a proof to the contrary. Lamb, in Reference 16, states on the basis of Lagrange's results that the restriction to linearity may not be necessary, but he did not elaborate on this point, and a proof is lacking.

Clearly, in many applications of dynamic reciprocity one must deal with nonlinear media. For example, while rocks may behave elastically, soils generally do not. It is worthwhile, therefore, to find out experimentally the degree of applicability of the dynamic-reciprocity relationship to such media.

It is recommended that a simple and definitive experimental program be initiated that will fulfill the following two objectives:

1) Gather sufficient test data to determine the relation among cavity translation, distortion, and average displacement in a linear medium.

2) Gather the necessary data to determine the degree of applicability of dynamic reciprocity in a nonlinear medium such as a soil.

The first objective will provide the transfer-function type of data required for estimating cavity distortions and rigid-body translations from the average displacement for a linear medium. The second objective will make it possible to estimate the errors in the predicted cavity displacements caused by nonlinear effects.

PART II -- ANALYTICAL RESULTS

I. TRANSFORMATION OF THE RECIPROCITY RELATION

A special form of the dynamic-reciprocity relation, equation (16) in the Appendix, which is suitable for our purposes is given by

$$\int_{S_c} \int_o^t p_c(x, t-\tau)\, u_c(x, \tau)\, d\tau ds_c = \int_{S_s} \int_o^t p_s(x, t-\tau)\, u_s(x, \tau)\, d\tau ds_s \qquad (1)$$

where p is the pressure, u is the displacement, S is the area, x represents the space coordinates, and t and τ are time coordinates. The subscripts s and c represent surface and cavity respectively. The problem becomes one of solving equation (1) for the unknown cavity displacement u_c caused by a specified surface pressure loading p_s when the normal surface motion u_s has been measured due to a known cavity pressure p_c. To solve this integral equation, several simplifying assumptions are introduced. First, it is realized that the ground surface measurements will only be known at a finite number of surface stations so that space integration over the ground surface must be replaced by a summation over the n measured stations. It is assumed that at each of these n stations, both the pressure and ground motion are the same over the entire station area at any instant of time. It is further assumed that the internal pressure p_c acting on the cavity wall is uniformally distributed and simply varies with time. Under this assumption u_c becomes the average radial cavity displacement produced by the ground surface pressure loading p_s. It is also assumed that the variation of the cavity area with time can be neglected and that this area can be taken as a constant. These assumptions permit equation (1) to be rewritten as

$$S_c \int_o^t p_c(t-\tau) u_c(\tau)\, d\tau = \sum_n S_{sn} \int_o^t p_{sn}(t-\tau) u_{sn}(\tau)\, d\tau \qquad (2)$$

where S_c represents the cavity area, S_{sn} represents the ground surface area of the n^{th} station and the summation is to extend over the n ground surface stations. To cast equation (2) into a form suitable for programming on the IBM 7090, it is necessary that several algebraic manipulations be performed.

Due to the symmetry property of the convolution integral, equation (2) may be rewritten as

$$S_c \int_o^t p_c(t - \tau)\, u_c(\tau)\, d\tau = \sum_n S_{sn} \int_o^t p_{sn}(\tau)\, u_{sn}(t - \tau)\, d\tau \qquad (3)$$

After equation (3) is differentiated with respect to time t, it becomes

$$S_c \int_o^t \dot{p}_c(t - \tau)\, u_c(\tau)\, d\tau + S_c p_c(0)\, u_c(t)$$

$$= \sum_n S_{sn} \int_o^t p_{sn}(\tau)\, \dot{u}_{sn}(t - \tau)\, d\tau + \sum_n S_{sn}\, p_{sn}(t)\, \dot{u}_{sn}(0) \qquad (4)$$

where dots denote differentiation with respect to the independent variable of the functions. It is assumed that the initial displacements at the ground surface $u_{sn}(0)$ are zero so that the last term in equation (4) vanishes. Then, applying the symmetry property of the convolution integral and solving equation (4) for the average radial displacement of the cavity boundary gives

$$u_c(t) = \left(\frac{1}{S_c p_c(0)} \sum_n S_{sn} \int_o^t p_{sn}(\tau)\, \dot{u}_{sn}(t - \tau)\, d\tau \right) - \frac{1}{p_c(0)} \int_o^t \dot{p}_c(\tau)\, u_c(t - \tau)\, d\tau \qquad (5)$$

In equations (4) and (5) $\dot{u}_{sn}$ is the velocity of the ground surface due to an underground explosion and $\dot{p}_c$ is the rate of the pressure change at the cavity boundary during the explosion.

By examining equation (5) it is observed that the first integral contains the known functions p_{sn} and $\dot{u}_{sn}$ whereas the second integral contains the known function $\dot{p}_c$ and the unknown function u_c. It is convenient to separate each of these two integrals into two parts. The first integral will be separated into two parts to save computational time and the second integral into two parts to express u_c entirely in terms of known functions, thereby avoiding the iteration procedure that would be required to solve for u_c from equation (5).

In the first integral in equation (5), it is recognized that the overpressure p_{sn} will be zero until the pressure arrives at station n at the time t_{ln}. Therefore, the lower limit in this integral can be changed from $t = 0$ to $t = t_{ln}$. Now, in general, the pressure p_{sn} decays rapidly after the arrival of the peak overpressure and then is followed by a more slowly decaying pulse, especially when these pressures are caused by a nuclear detonation. Computational time can be reduced by avoiding the small integration step required to evaluate the contribution from the fast decay portion by analytically integrating the fast decay portion and then numerically integrating the remaining portion. By letting ϵ_n represent the duration of the fast decay part of p_{sn}, the integral is replaced by an integral covering the period from $\tau = t_{ln}$ to $\tau = t_{ln} + \epsilon_n$ and another integral for the period from $\tau = t_{ln} + \epsilon_n$ to $\tau = t$.

The second integral is separated into two parts, covering the period from $\tau = 0$ to $\tau = \Delta t$, and from $\tau = \Delta t$ to $\tau = t$ where Δt represents the time interval selected for evaluating the cavity displacements. In this manner, the integral from Δt to t contains only known functions, since when u_c is being determined at time t it will be known for all times up to $(t - \Delta t)$. However, the integral from 0 to Δt contains the time portion of u_c that is being determined, so that this integral will require further examination. After these manipulations, equation (5) is rewritten as

$$u_c(t) = \frac{1}{S_c p_c(0)} \left[\sum_n S_{sn} \left(\int_{t_{ln}}^{t_{ln}+\epsilon_n} p_{sn}(\tau)\dot{u}_{sn}(t - \tau)\, d\tau \right.\right.$$

$$\left.\left. + S_{sn} \int_{t_{ln}+\epsilon_n}^{t} p_{sn}(\tau)\dot{u}_{sn}(t - \tau)\, d\tau \right) \right]$$

$$- \frac{1}{p_c(0)} \left[\int_0^{\Delta t} \dot{p}_c(\tau)u_c(t - \tau)\, d\tau + \int_{\Delta t}^{t} \dot{p}_c(\tau)u_c(t - \tau)\, d\tau \right] \qquad (6)$$

For sufficiently small ϵ_n, the value of $\dot{u}_{sn}$ can be considered constant during the period t_{ln} to $(t_{ln} + \epsilon_n)$ and the approximation

$$\dot{u}_{sn}(t - \tau) \cong \dot{u}_{sn}(t - t_{ln}) \qquad (7)$$

is made during this period. For this period, the pressure p_{sn} is approximated by a double exponential decay equation

$$p_{sn}(\tau) = A_{sn} e^{-\alpha_{sn}(\tau - t_{ln})} + B_{sn} e^{-\beta_{sn}(\tau - t_{ln})}, \quad t_{ln} \leq \tau \leq t_{ln} + \epsilon_n \tag{8}$$

where A_{sn}, B_{sn}, α_{sn}, β_{sn} are constants. If equations (7) and (8) are substituted into equation (6), the first integral in equation (6) becomes

$$S_{sn} \int_{t_{ln}}^{t_{ln}+\epsilon_n} p_{sn}(\tau)\dot{u}_{sn}(t - \tau)\, d\tau$$

$$= S_{sn}\dot{u}_{sn}(t - t_{ln}) \int_{t_{ln}}^{t_{ln}+\epsilon_n} \left[A_{sn} e^{-\alpha_{sn}(\tau - t_{ln})} + B_{sn} e^{-\beta_{sn}(\tau - t_{ln})} \right] d\tau \tag{9}$$

which upon integration gives

$$S_{sn} \int_{t_{ln}}^{t_{ln}+\epsilon_n} p_{sn}(\tau)\dot{u}_{sn}(t - \tau)\, d\tau$$

$$= S_{sn}\dot{u}_{sn}(t - t_{ln}) \left[\frac{A_{sn}}{\alpha_{sn}} \left(1 - e^{-\alpha_{sn}\epsilon_n} \right) + \frac{B_{sn}}{\beta_{sn}} \left(1 - e^{-\beta_{sn}\epsilon_n} \right) \right] \tag{10}$$

In a similar manner, it is assumed that the cavity pressure p_c can be represented by a double exponential decay equation during the time interval from 0 to Δt. Thus, p_c is taken as

$$p_c(\tau) = A_c e^{-\alpha_c \tau} + B_c e^{-\beta_c \tau}, \quad 0 \leq \tau \leq \Delta t \tag{11}$$

where again A_c, B_c, α_c, and β_c are constants. Previously, it was pointed out that when u_c is being determined at time t, u_c will be known for the entire period from 0 to $(t - \Delta t)$ so that the last integral in equation (6) involves an integration of known functions. However, the third integral in equation (6) concerns that period of time for which u_c is not yet known. To circumvent this difficulty and express this integral in terms of the

values of u_c at the beginning and end of time interval $0 \leq \tau \leq \Delta t$, another approximation is introduced. The approximation is made that the variation in $u_c(\bar{\tau})$ which represents the function $u_c(t - \tau)$ in the interval $0 \leq \tau \leq \Delta t$ can be expressed by the parabola

$$u_c(\bar{\tau}) = a\bar{\tau}^2 + b\bar{\tau} + c \quad , \qquad 0 \leq \bar{\tau} \leq \Delta t \quad , \qquad \bar{\tau} = \Delta t - \tau \tag{12}$$

subjected to the conditions:

at $$\bar{\tau} = 0 \quad , \qquad u_c(\bar{\tau}) = u_{ci} \tag{13}$$

$$\bar{\tau} = 0 \quad , \qquad \dot{u}_c(\bar{\tau}) = \dot{u}_{ci} \tag{14}$$

$$\bar{\tau} = \Delta t \quad , \qquad u_c(\bar{\tau}) = u_c(t) \tag{15}$$

where u_{ci} = the radial displacement of the cavity at the end of the previous time interval $(t - \Delta t)$ and $\dot{u}_{ci}$ = the radial velocity of the cavity at the end of the previous time interval $(t - \Delta t)$. By imposing these conditions, equation (12) becomes

$$u_c(\bar{\tau}) = \left[\frac{u_c(t) - u_{ci}}{(\Delta t)^2} - \frac{\dot{u}_{ci}}{\Delta t}\right]\bar{\tau}^2 + \dot{u}_{ci}\bar{\tau} + u_{ci} \tag{16}$$

and the function $u_c(t - \tau)$ is

$$u_c(t - \tau) = \left[\frac{u_c(t) - u_{ci}}{(\Delta t)^2} - \frac{\dot{u}_{ci}}{\Delta t}\right](\Delta t - \tau)^2 + \dot{u}_{ci}(\Delta t - \tau) + u_{ci} \tag{17}$$

Then the third integral of equation (6) may be written as

$$\frac{1}{p_c(0)} \int_o^{\Delta t} \dot{p}_c(\tau) u_c(t - \tau)\, d\tau$$

$$= -u_c(t) + \frac{2u_c(t)}{p_c(0)(\Delta t)^2} \int_o^{\Delta t} (\Delta t - \tau) p_c(\tau)\, d\tau$$

$$- \frac{2}{p_c(0)} \left(\frac{\dot{u}_{ci}}{\Delta t} + \frac{u_{ci}}{(\Delta t)^2} \right) \int_o^{\Delta t} (\Delta t - \tau) p_c(\tau)\, d\tau$$

$$+ \frac{\dot{u}_{ci}}{p_c(0)} \int_o^{\Delta t} p_c(\tau)\, d\tau + \frac{u_{ci}}{p_c(0)} p_c(\Delta t) \qquad (18)$$

where the procedure of integration by parts has been used.

Finally, by introducing equations (10), (11), and (18) into equation (6), the cavity displacement u_c becomes

$$u_c(t) = u_{ci} + \dot{u}_{ci}\Delta t + \frac{\Delta t^2}{2\left[\frac{A_c}{\alpha_c^2}\left(e^{-\alpha_c \Delta t} + \alpha_c \Delta t - 1\right) + \frac{B_c}{\beta_c^2}\left(e^{-\beta_c \Delta t} + \beta_c \Delta t - 1\right)\right]}$$

$$\sum_n \left\{ \frac{S_{sn}}{S_c} \left\langle \left[\frac{A_{sn}}{\alpha_{sn}} \left(1 - e^{-\alpha_{sn}\epsilon_n}\right) + \frac{B_{sn}}{\beta_{sn}} \left(1 - e^{-\beta_{sn}\epsilon_n}\right) \right] \dot{u}_{sn}(t - t_{ln}) \right.\right.$$

$$\left.\left. + \int_{t_{ln}+\epsilon_n}^{t} p_{sn}(\tau) \dot{u}_{sn}(t - \tau)\, d\tau \right\rangle \right] - \int_{\Delta t}^{t} \dot{p}_c(\tau) u_c(t - \tau)\, d\tau$$

$$\left. - u_{ci} p_c(\Delta t) - \dot{u}_{ci} \left[\frac{A_c}{\alpha_c} \left(1 - e^{-\alpha_c \Delta t}\right) + \frac{B_c}{\beta_c} \left(1 - e^{-\beta_c \Delta t}\right) \right] \right\} \qquad (19)$$

II. DIGITAL PROGRAM

An IBM 7090 digital program was developed to solve equation (19) for the cavity radial motion u_c. To use this program, the velocity and pressure data must first be introduced into the computer. Some of the methods of introducing these data and several other salient points will be discussed next before presenting computed results.

A. GROUND VELOCITIES $\dot{u}_{sn}$

The digital program is so arranged that ground velocity data measured normal to the ground surface and caused by an underground explosion are used. These data are input into the computer in tabular form, that is, the measured velocities at a discrete set of times. If ground acceleration or displacement data are recorded during the underground explosion, it will be necessary to integrate or differentiate such data to derive the corresponding velocity data before they are introduced into the computer. Clearly, acceleration data are preferable to displacement data to avoid any loss of accuracy through the differentiation process.

B. SURFACE PRESSURES p_{sn}

The surface pressures acting on each of the n stations can be introduced into the computer in one of two ways. The first method provides a means of handling those cases where the pressure pulse signature is completely arbitrary. The second method is restricted to a nuclear surface detonation. This second method of introducing the pressure pulse data for a nuclear detonation was developed to simplify the input procedure. This seemed to be a worthwhile simplification because it was anticipated that most problems to be considered will be those in which the cavity motion must be determined for a nuclear explosion on the surface.

1. Arbitrary Pressure Pulse

The procedure for introducing the pressure pulse acting at each of the n stations is identical to that used for the ground velocities. That is, a tabular listing of the discrete set of times and pressures is stored in the computer. A slight variation of this procedure can be followed when the pressure pulse decays rapidly following the peak pressure. In this variation, the fast-decay portion is approximated by the double

decaying-exponential pulse as expressed by equation (8), and a tabular listing for the remaining time interval. The analytical pressure pulse is generated internally in the computer as required during the computations, once the constants A_{sn}, B_{sn}, α_{sn}, β_{sn}, and t_{ln} are prescribed for each station.

2. Nuclear Pressure Pulse

The overpressure acting at each of the n stations caused by a nuclear surface detonation is also generated within the computer once the weapon yield and the distance from ground zero to each of the n stations are specified. This generated overpressure pulse is an approximation to the theoretical overpressures derived by Brode (Reference 2). These overpressure pulses were approximated by the double decaying-exponential equation

$$p_{sn}(\tau) = A_{sn} e^{-\alpha_{sn}(\tau - t_{ln})} + B_{sn} e^{-\beta_{sn}(\tau - t_{ln})}, \quad t_{ln} \leq \tau \leq t_{ln} + \epsilon_n \quad (20)$$

during the fast decay time interval and by

$$p_{sn}(\tau) = A'_{sn} e^{-\alpha'_{sn}\left[\tau - (t_{ln} + \epsilon_n)\right]} + B'_{sn} e^{-\beta'_{sn}\left[\tau - (t_{ln} + \epsilon_n)\right]}, \quad t_{ln} + \epsilon_n \leq \tau \quad (21)$$

for the subsequent time period, where ϵ_n is set to 0.01 second. The values of A_{sn}, B_{sn}, α_{sn}, β_{sn}, t_{ln}, and the corresponding primed parameters are internally evaluated in the computer by fitting the above two equations to Brode's data for the specified range from ground zero and for a nominal yield.

Once the weapon yield W and the distances R_n of each station n from ground zero are specified, the computer evaluates the pressures p_{sn} and arrival times t_{ln} by the following steps. First the computer evaluates the equivalent distance R_E for the nominal yield weapon W_N at which the same overpressures would be observed using the equation (Reference 11).

$$R_E = \left(\frac{W_N}{W}\right)^{1/3} R_n \quad (22)$$

The value of R_E is then used to evaluate the constants A_{sn}, B_{sn}, α_{sn}, β_{sn}, the corresponding primed constants and the arrival times $(t_{1N})_n$ for the nominal yield weapon. Finally, the overpressures p_{sn}, acting on each station, are computed according to equations (20) and (21) and the arrival times at these stations from the equation

$$t_{1n} = (t_{1N})_n \left(\frac{W}{W_N}\right)^{1/3} \tag{23}$$

C. CAVITY PRESSURE p_c

The cavity pressure time-history can be introduced into the computer in one of two ways. Either:

1) Prescribe the constants A_c', B_c', α_c', β_c', and the computer evaluates the pressure at any time t from the equation

$$p_c(t) = A_c' e^{-\alpha_c' t} + B_c' e^{-\beta_c' t} \tag{24}$$

or

2) Prescribe the constants A_c, B_c, α_c, β_c, and the computer evaluates the pressure for the first time interval 0 to Δt using equation (11). The cavity pressures following this period are prescribed by a tabular listing of discrete pressure and time values.

D. INTEGRATION STEP SIZE

The integration step size can be specified in one of two ways in the Adams-Moulton, Runge-Kutta method used for numerically integrating the integrals in equation (19). Either a constant step size can be prescribed, or limits placed on the truncation error allowed in any integration step. In the latter method, a variable step size is used with the computer selecting its own step size by comparing the error introduced at each step with the prescribed allowable error, and then, adjusting the step size to keep the error within the specified limits.

III. PROGRAM CHECKOUT

A. BEAM EXAMPLE

The programming of equation (1), and also the steps leading to equation (19) from the reciprocity relation (1) were verified by computations for problems in which exact solutions were known or obtainable. One such problem used for this purpose was the response at some point of a simply supported beam due to transient loadings applied at three other points.

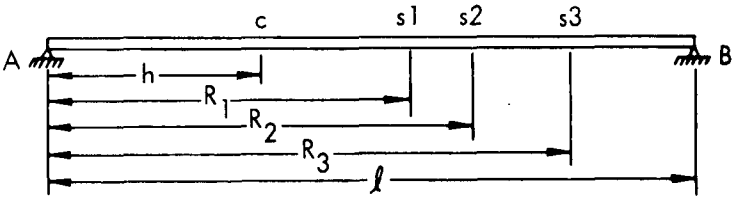

Figure 1. Beam Geometry

Figure 1 shows the beam used for this check where the three loading points are s1, s2, s3 and the response is determined at point c. In order that this problem can bear some resemblance to the half space problem to be considered later, the loadings at the three points approximate a pressure pulse traveling across the beam with different arrival times and reduced peak pressures at successive points along the beam. The loadings selected are shown in figure 2 and are expressed mathematically as

$$\left.\begin{aligned} p_{s1}(t) &= P_{11}H(t - t_{11}) - P_{12}H(t - t_{12}) - P_{13}H(t - t_{13}) - P_{14}H(t - t_{14}) \\ p_{s2}(t) &= P_{21}H(t - t_{21}) - P_{22}H(t - t_{22}) - P_{23}H(t - t_{23}) - P_{24}H(t - t_{24}) \\ p_{s3}(t) &= P_{31}H(t - t_{31}) - P_{32}H(t - t_{32}) - P_{33}H(t - t_{33}) - P_{34}H(t - t_{34}) \end{aligned}\right\} \quad (25)$$

where H(t) is the Heaviside unit step function.

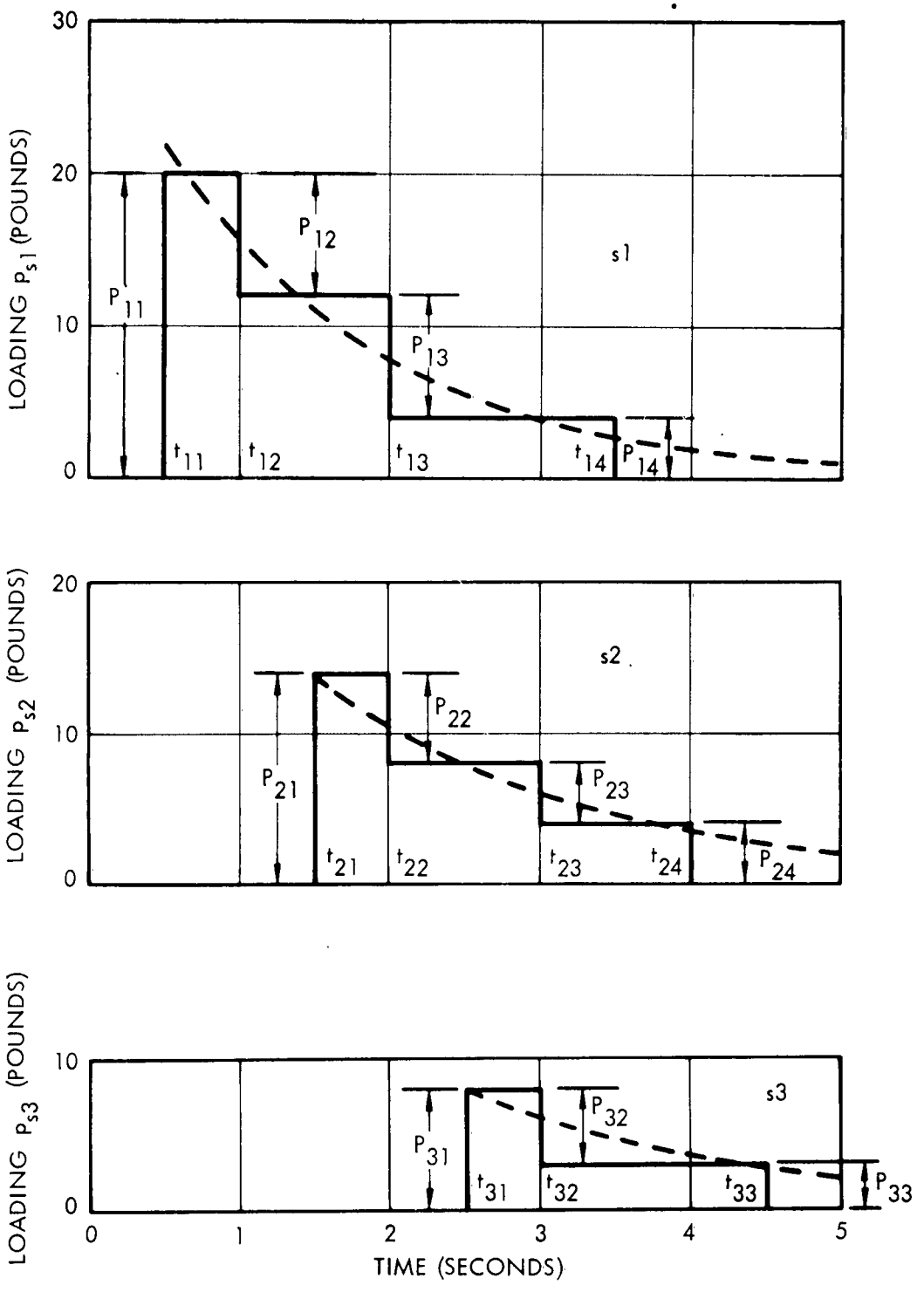

Figure 2. Beam Loadings at Points s1, s2, and s3

It is found by analysis that these loadings produce a displacement at point c given by

$$u_c(t) = \sum_{n=1}^{3} \sum_{m=1}^{\infty} \frac{1}{M\omega_m^2} \sin\frac{m\pi h}{\ell} \sin\frac{m\pi R_n}{\ell} \left\{ P_{n1}\left[1 - \cos\omega_m(t - t_{n1})\right]H(t - t_{n1}) \right.$$

$$- P_{n2}\left[1 - \cos\omega_m(t - t_{n2})\right]H(t - t_{n2}) - P_{n3}\left[1 - \cos\omega_m(t - t_{n3})\right]H(t - t_{n3})$$

$$\left. - P_{n4}\left[1 - \cos\omega_m(t - t_{n4})\right]H(t - t_{n4}) \right\} \qquad (26)$$

Now, to apply equation (19) to find u_c, the velocity at the three stations must be determined for a known loading at point c. The loading chosen to be applied at point c is shown in figure 3

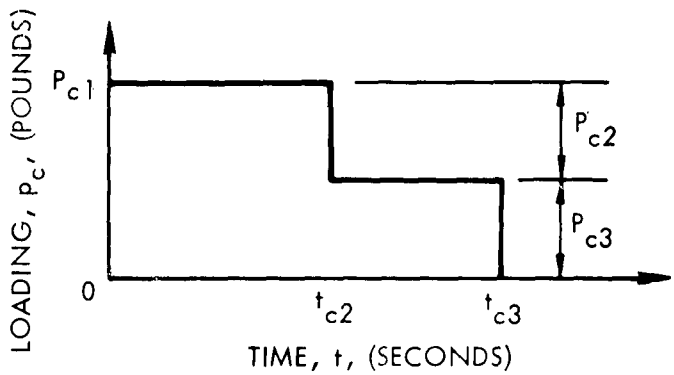

Figure 3. Loading at Point c

and is expressed mathematically as

$$p_c(t) = P_{c1}H(t - t_{c1}) - P_{c2}H(t - t_{c2}) - P_{c3}H(t - t_{c3}) \qquad (27)$$

The velocities at points s_n caused by the loading [equation (27)] are found analytically to be

$$\dot{u}_{sn}(t) = \sum_{m=1}^{\infty} \frac{1}{M\omega_m} \sin\frac{m\pi h}{\ell} \sin\frac{m\pi R_n}{\ell} \left\{ P_{c1} \sin\omega_m(t - t_{c1})H(t - t_{c1}) \right.$$

$$\left. - P_{c2} \sin\omega_m(t - t_{c2})H(t - t_{c2}) - P_{c3} \sin\omega_m(t - t_{c3})H(t - t_{c3}) \right\} \qquad (28)$$

for n = 1, 2, 3. These velocities were evaluated for the modes m = 1 to 7 and are shown in figure 4. The velocity time-history data and the pressure loadings p_{sn} and p_c were introduced into the computer and u_c determined with a constant integration step size of 0.05 second.

For these computations, the following values were used:

$$\frac{EI}{M\ell^3} = \frac{1}{25\pi^4} \qquad \frac{R_2}{\ell} = 0.7$$

$$\omega_n = \frac{m^2}{5} \qquad \frac{R_3}{\ell} = 0.8$$

$$M = 30 \text{ lb/in} \qquad t_{c1} = 0 \text{ sec} \qquad P_{c1} = 14 \text{ lb}$$

$$\frac{h}{\ell} = 0.25 \qquad t_{c2} = 2.0 \text{ sec} \qquad P_{c2} = 8 \text{ lb}$$

$$\frac{R_1}{\ell} = 0.55 \qquad t_{c3} = 4.5 \text{ sec} \qquad P_{c3} = 6 \text{ lb}$$

The results of these calculations are shown in figure 5 where the value of the analytical solution of u_c was determined from equation (26) by summing the terms from m = 1 to m = 7. The higher mode contributions for $m > 7$ for both u_c and $\dot{u}_{sn}$ were negligible compared to the first seven mode contributions. Figure 5 shows that the computer solution and the analytical solution are quite close with the maximum difference about 5 percent. These results suggested that the coding and the manipulation of equation (1) into the form given by equation (19) were correct, and therefore, the digital program was then used to investigate the cavity displacements caused by surface pressure loadings.

B. INTEGRATION STEP SIZE

Several beam deflection calculations were made to investigate the effect of the integration step size used in the digital computations. The step size selected in any given computation depends on the data to be integrated and the accuracy demanded. The data used in these calculations are the loading curves shown in figure 2 and the velocity curves shown in figure 4. It is clear that when the loading and velocity data vary rapidly, the integration step size must be reduced accordingly provided these rapid

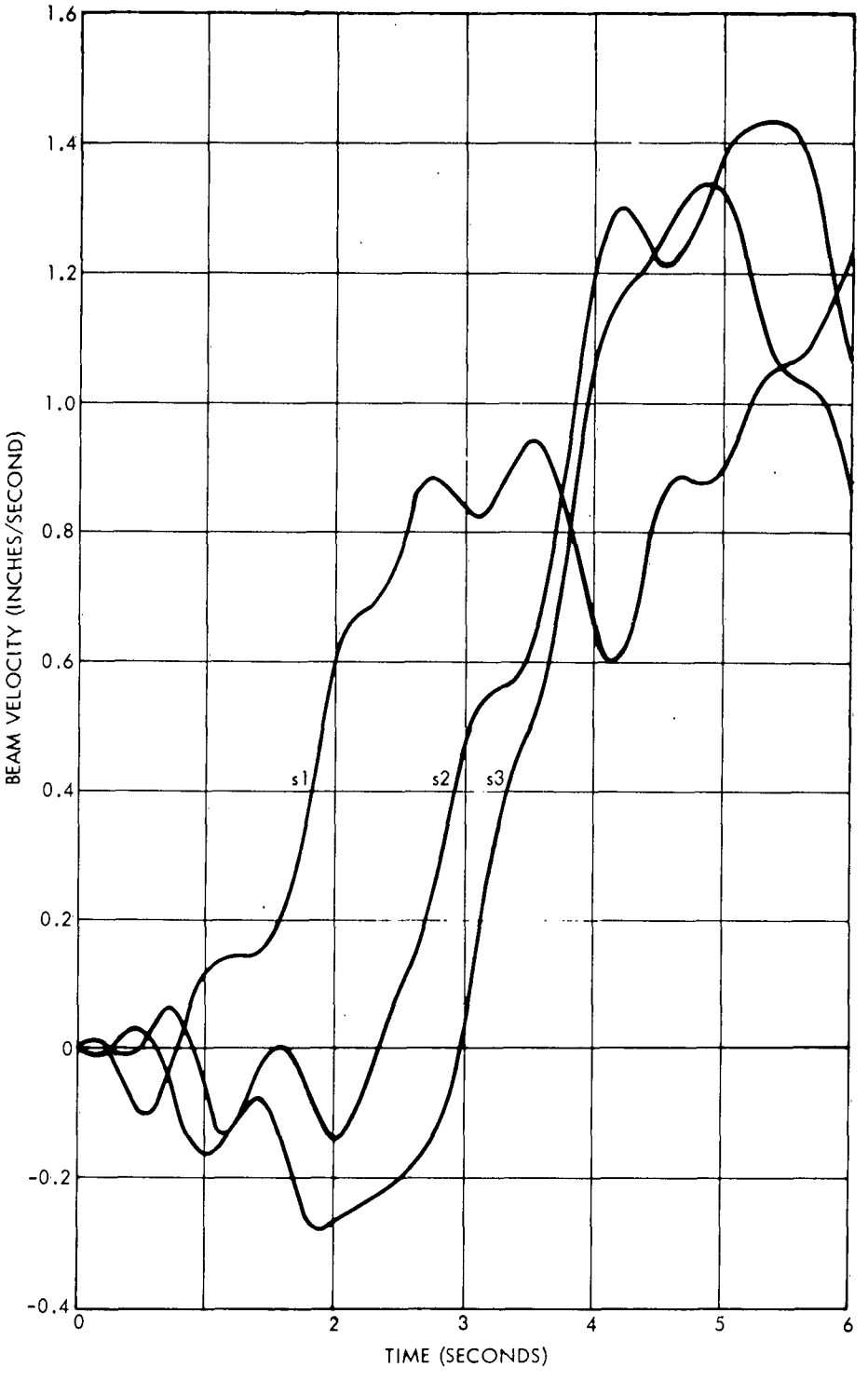

Figure 4. Beam Velocities at Points s1, s2, and s3 Due to Loading at Point c

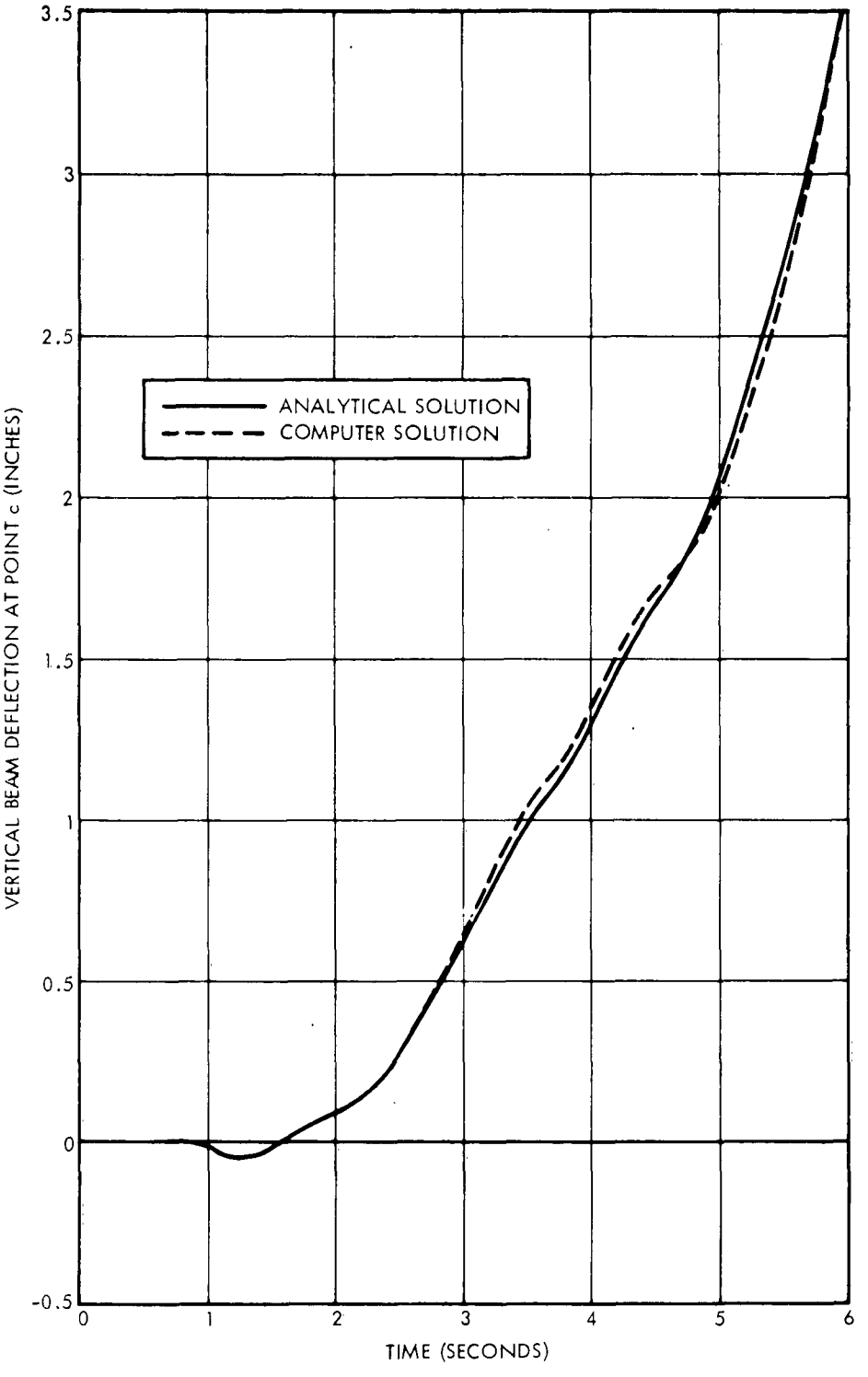

Figure 5. Comparison of Analytical Solution and Computer Solution for the Beam Problem

fluctuations are large enough to significantly affect the final results. By examining figure 4, it is observed that the primary velocity curve has a rise time of about five seconds while the individual fluctuations have a minimum rise time of about 0.1 second. The discontinuities in the loading curve shown in figure 2 also give rise to higher frequency fluctuations (this would be evident if the loading curve is replaced by its Fourier series expansion). Several calculations were made using various integration step sizes. Figure 6, which shows the results for integration step sizes of 0.05 and 0.5 second, indicates that the difference between the two predicted deflections at t = 5.5 seconds is about 10 percent. Figure 5 shows that the deflection computed by using 0.05 second step size agrees fairly well with the exact deflection, so that the integration step size of 0.05 second is entirely satisfactory, and even the 0.5 second step size is probably adequate in this problem.

IV. CAVITY DISPLACEMENT CALCULATIONS

To compute the average cavity radial displacement caused by a prescribed pressure acting on the ground surface, it is necessary to know the ground motions caused by a known underground cavity pressure loading. The most nearly complete ground motion data that could be found were ground velocity measurements obtained during the Rainier shot in the PLUMBBOB series (Reference 22). These data consist of seven surface measurements that are nearly on one radial line extending from surface ground zero out to a distance of 2340 feet. Figures 7 and 8 show these data for the stations at distances of 0, 450, 650, 900, 1270, 1730, and 2340 feet from surface ground zero. The cavity pressures that gave rise to these ground motions were not recorded during the test and therefore, a pressure pulse must be assumed. Reference 14 indicates that the cavity radius before the shot was 3 feet and after the explosion, the crushed radios before collapse was 55 feet. For the calculations which follow an effective radius of 10 feet will be assumed. For this radius, the cavity area S_c is 1200 square feet. Figure 8 in Reference 14 shows the theoretical peak pressure inside the cavity as a function of cavity radius. For the cavity radius of 10 feet, the peak pressure is about 100,000 atmospheres. In the following calculations,

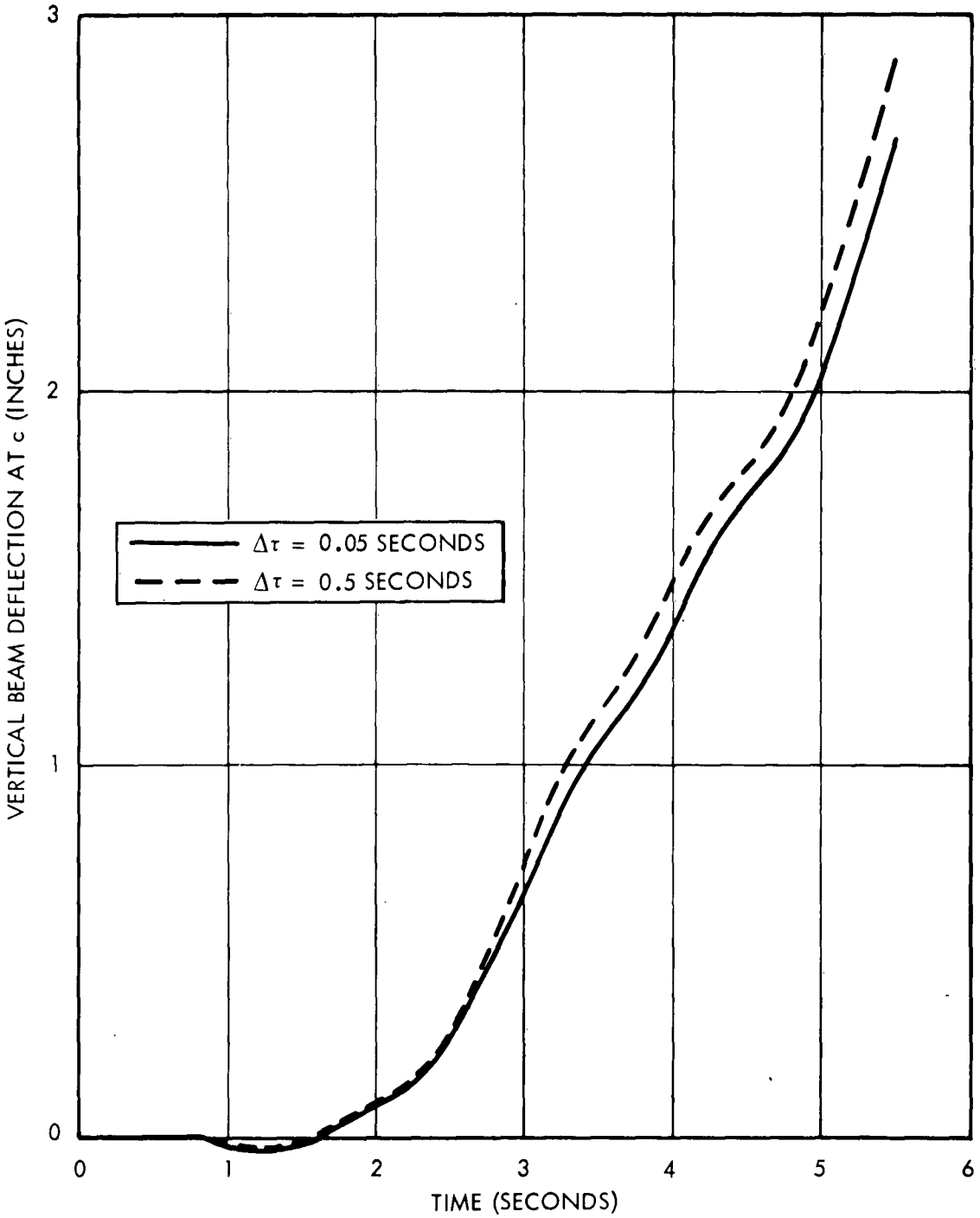

Figure 6. Comparison of Calculated Beam Deflection Using Two Integration Step Sizes

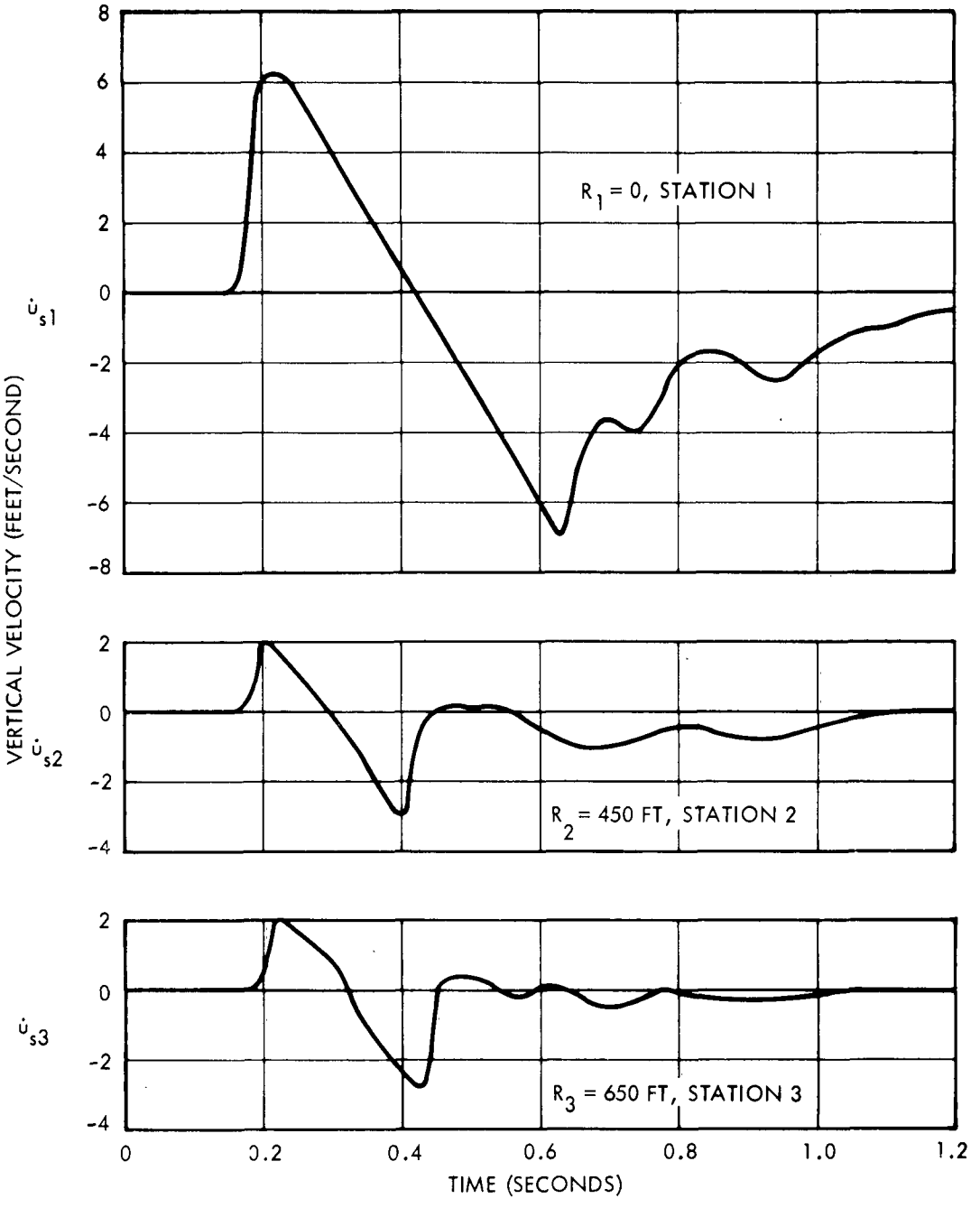

Figure 7. Ground Velocity Data for the Rainier Shot in the PLUMBBOB Series for Ranges 0, 450, and 650 ft

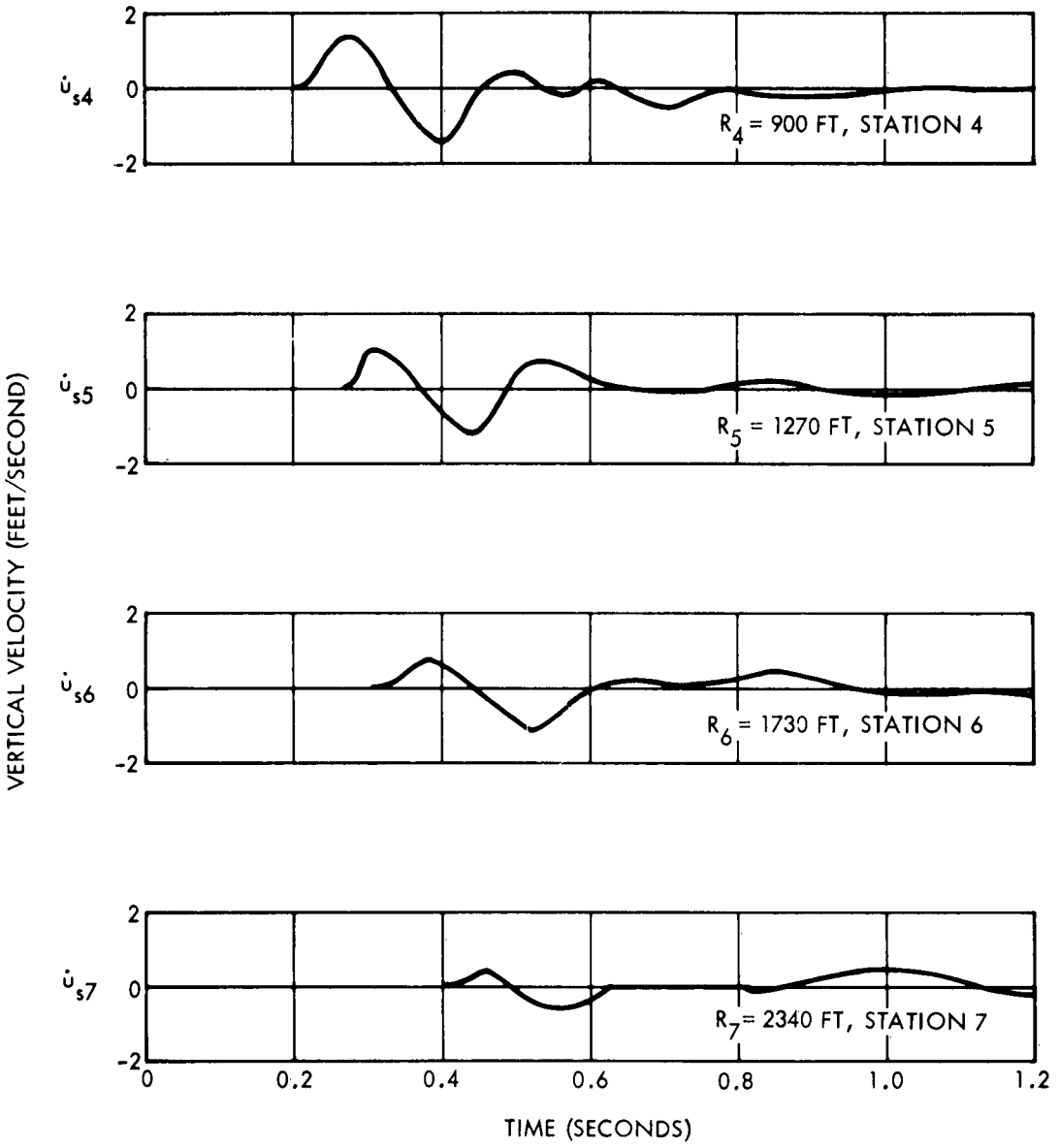

Figure 8. Ground Velocity Data for the Rainier Shot in the PLUMBBOB Series for Ranges 900, 1270, 1730 and 2340 ft

it is assumed that the pressure pulse has a zero rise time to the maximum pressure and then decays exponentially as described by equation (24). One pressure pulse used for many of the calculations to follow was taken as

$$p_c = 75,000\, e^{-50t} + 25,000\, e^{-0.25t} \qquad (29)$$

With these ground velocity data and cavity pressure pulse, the average cavity response was computed for a nuclear surface detonation at one of two locations. These two cases are called the direct-hit and nondirect-hit examples.

A. DIRECT-HIT EXAMPLE

For the direct-hit example, it is assumed that a nuclear detonation occurs on the surface with its ground zero coinciding with the surface ground zero for the underground detonation. Brode's theoretical overpressures (Reference 2) are used for the overpressures acting on each of the ground stations, and are axisymmetrical about the ground zero location.

1. Ground Surface Stations

It is assumed that the medium is isotropic and homogeneous so that the recorded velocities during the underground explosion would have been the same if they had been measured along any other radial line from surface ground zero. Since both the ground pressures p_s and ground velocities $\dot{u}_s$ are symmetric about ground zero, the surface areas used in the solution of equation (19) are the ring shaped areas around ground zero indicated in figure 9. These surface areas are listed in table 1.

Table 1. Station Areas in the Direct-Hit Example Using 7 Stations

Station n	Area ft^2
1	159.4
2	791,300
3	936,600
4	1,811,000
5	3,370,000
6	5,941,000
7	14,330,000

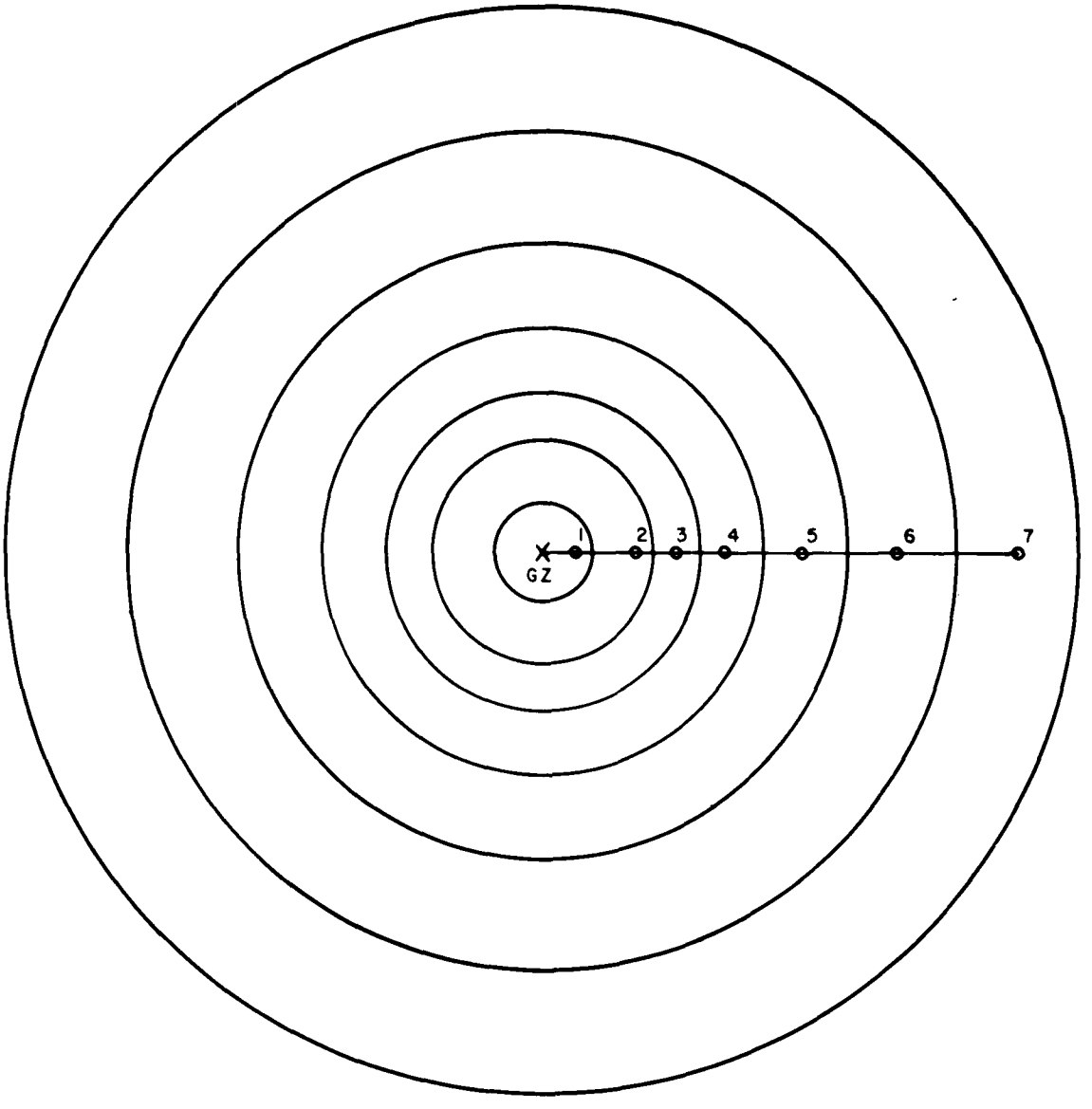

Figure 9. Lumped Stations for the Direct-Hit Example

2. Ground Overpressures

Since Brode's theoretical overpressure is infinite at ground zero, the first ground station was arbitrarily moved out to a point 150 feet from ground zero. The overpressure used at this first station is that corresponding to Brode's overpressure at a range of 150 feet, whereas the ground velocity used there is the actual velocity recorded at surface ground zero. The overpressure data for the fast decay portion were computed from equation (20) using the values listed in table 2. For the remaining period, the overpressures were input into computer in tabular form by reading overpressure and time values from the overpressures shown in figure 10.

Table 2. Overpressure Constants Used in equation (20)

Station n	A_{sn} atmos	B_{sn} atmos	α_{sn} sec^{-1}	β_{sn} sec^{-1}	t_{1n} sec
1	97,500	2500	.6000	250	0.01
2	2,600	800	1500	195	0.007
3	900	200	520	200	0.0035
4	320	80	420	25	0.0045
5	120	10	120	20	0.01
6	40	19	70	10	0.02
7	17	7.4	31	5	0.076

3. Influence of Cavity Pressure Signature

Since there is considerable uncertainty in the cavity pressure pulse, calculations were made using various pressure pulses so that the influence of the cavity pressure signature could be observed. The basic pressure pulse is taken as that expressed in equation (29). Other pulses are selected arbitrarily subject to the constraint condition.

$$\int_0^\infty p_c(\tau)\, d\tau = \text{constant}$$

Figure 12 shows the computed average cavity displacements caused by the nuclear explosion on Station 1 for the five cavity pressures shown in figure 11.

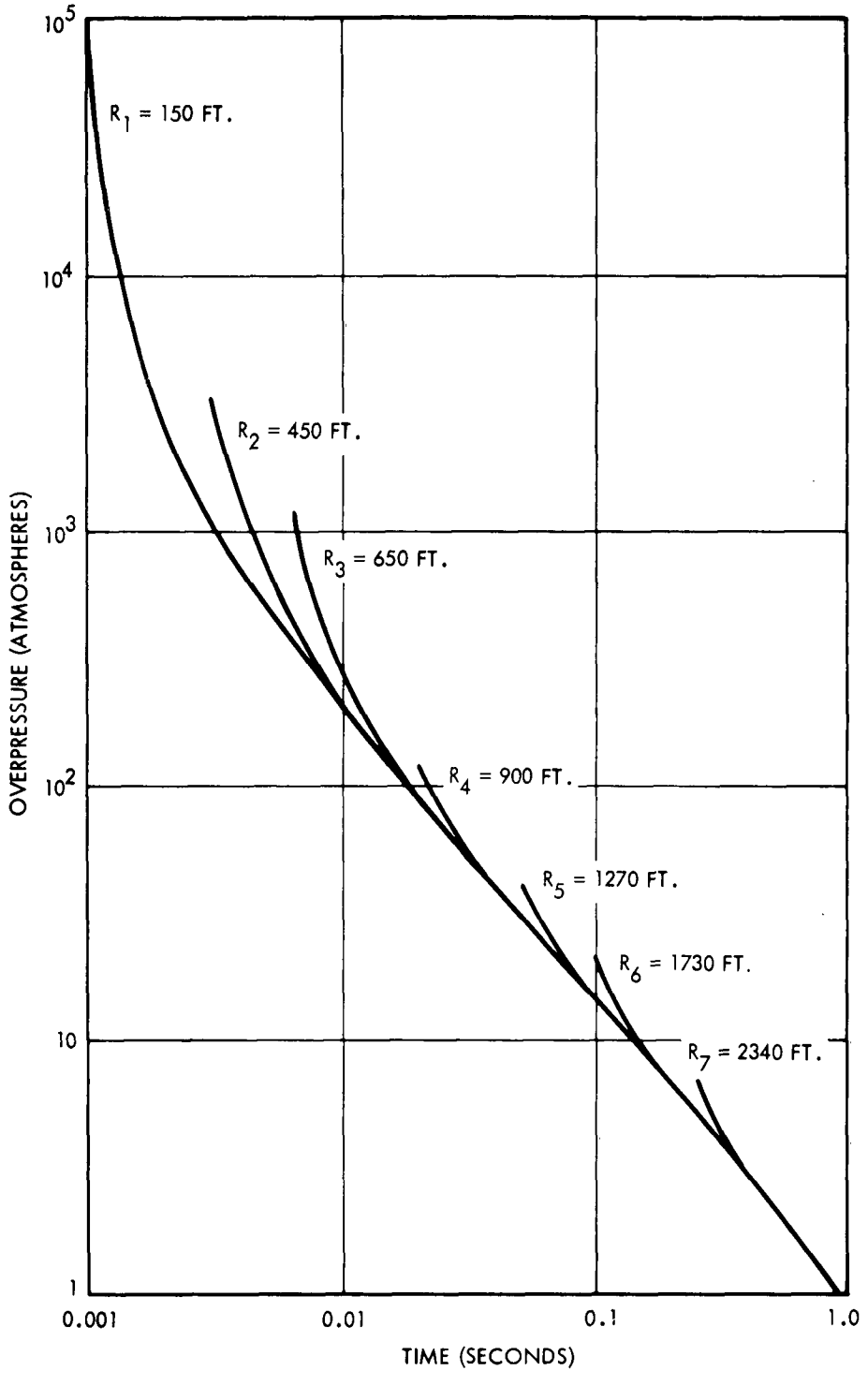

Figure 10. Overpressures Acting on the Seven Ground Stations for the Direct-Hit Example

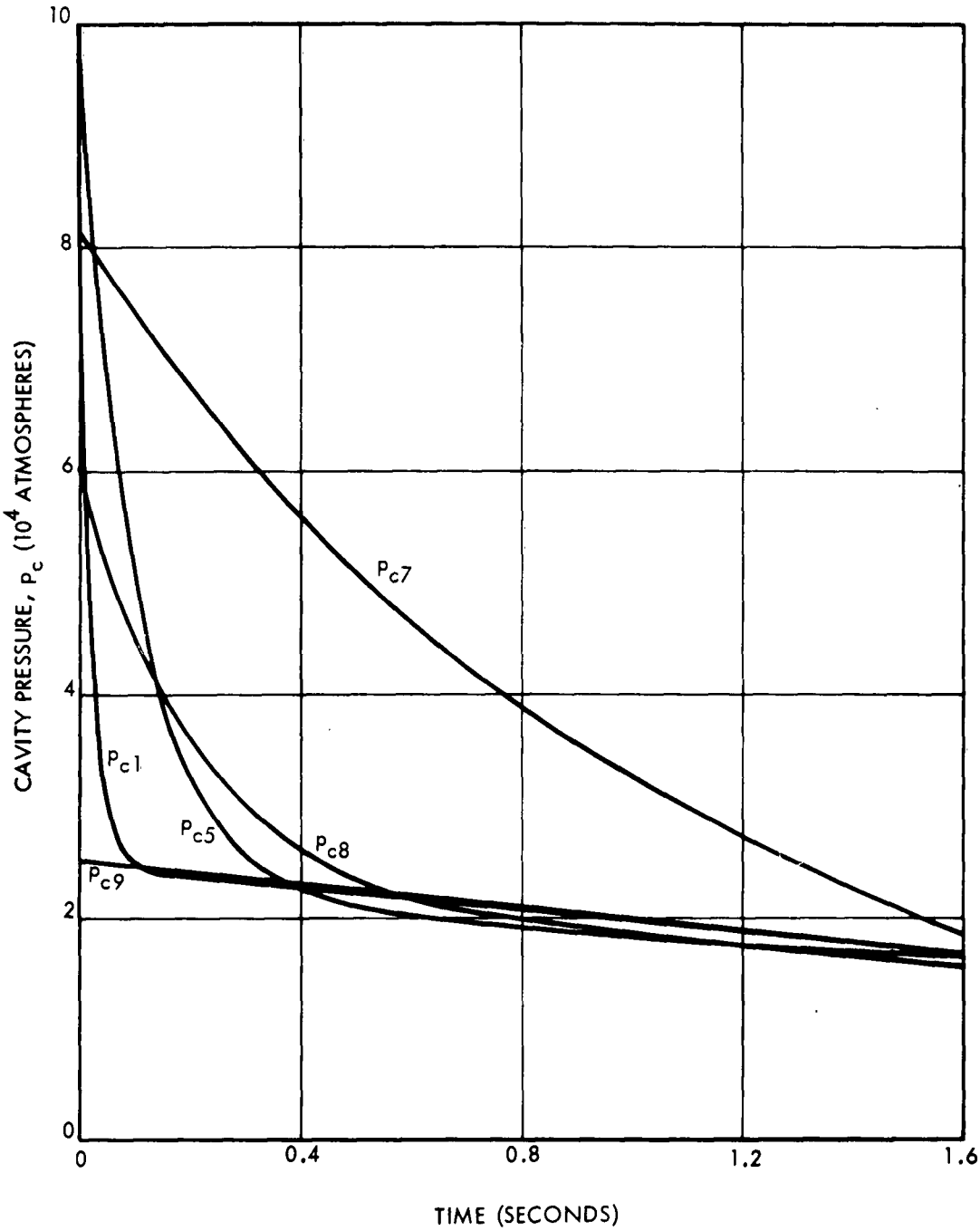

Figure 11. Typical Cavity Pressures Used in the Calculations

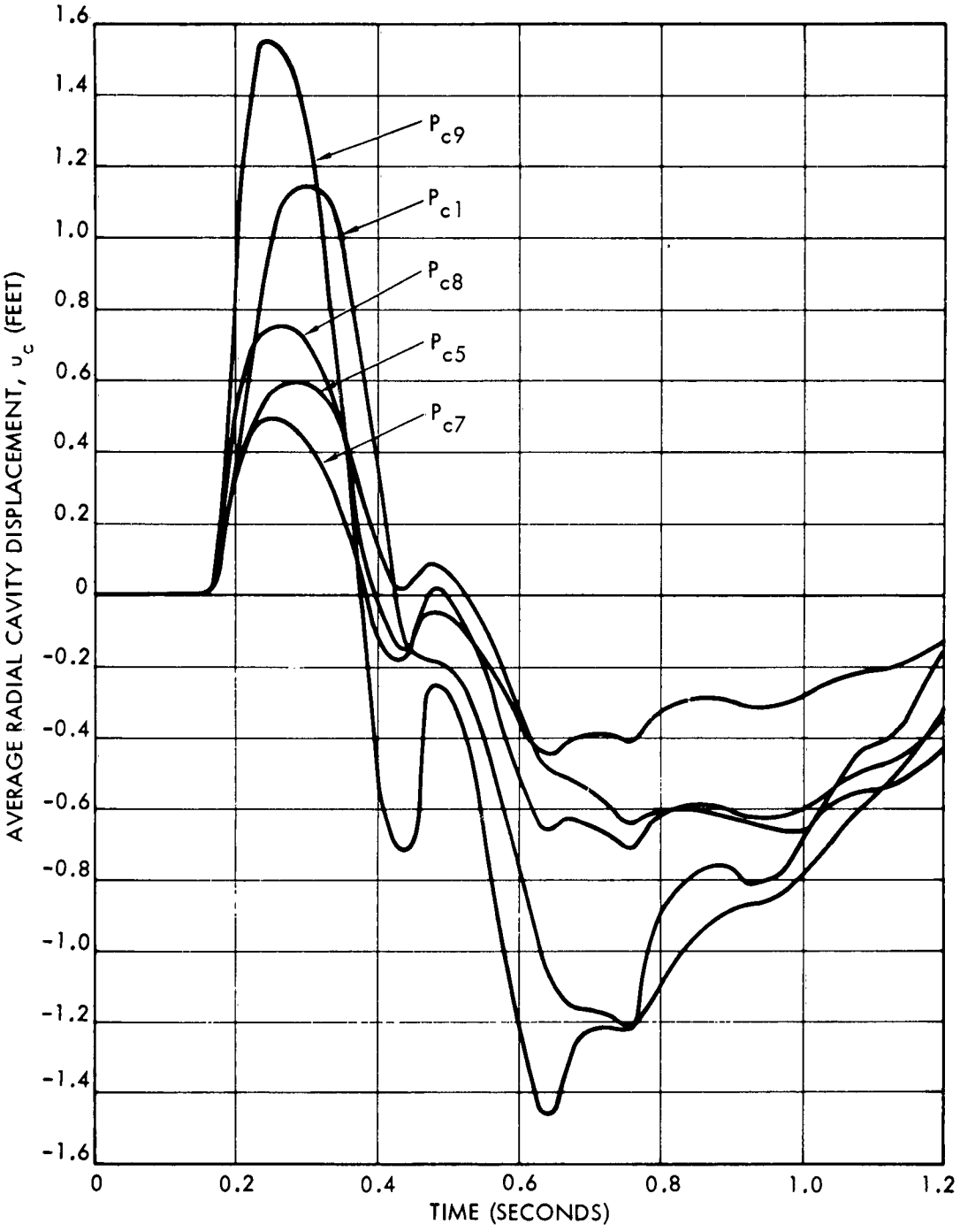

Figure 12. Cavity Displacements Produced by the Direct-Hit Burst for the Five Cavity Pressures Shown in Figure 11

4. Influence of Ground Surface Stations

In order to estimate the effect of using a fewer number of stations while computing cavity displacements, calculations were made using every other station shown in figure 9, i.e., stations 1, 3, 5, and 7. The adjusted surface areas for this case are shown in table 3.

Table 3. Station Areas for the Direct-Hit Example Using Four Stations

Station n	Area 10^3 ft^2
1	332
3	2,560
5	7,340
7	15,700

The results of these calculations are shown in figure 13 where the p_{c1} curve given by equation (29) was again used. In figure 13 it is noted that this four-station lumping predicts a larger cavity motion. This is primarily a consequence of the increased area used for station 1 in the four-station computations.

Figures 14 and 15 show the results of another set of calculations made to investigate the influence of each surface station. These curves were computed by using all seven stations shown in figure 9. Each curve on figures 14 and 15 shows the cavity motion caused by the overpressures acting on each of the seven stations individually. For example, figure 14 shows that the maximum cavity displacement caused by the overpressure acting on station 1 alone is -0.75 foot, whereas figure 12 shows the maximum to be -1.21 feet when the properly phased contributions from all seven stations are considered.

B. NONDIRECT-HIT EXAMPLE

The nondirect-hit example is defined as one in which the location of the surface nuclear detonation does not coincide with the surface ground zero for the underground explosion. In this example, it is assumed that a surface burst having the same yield as in the direct-hit example takes place at a point 1880 feet from surface ground zero. Once again, Brode's

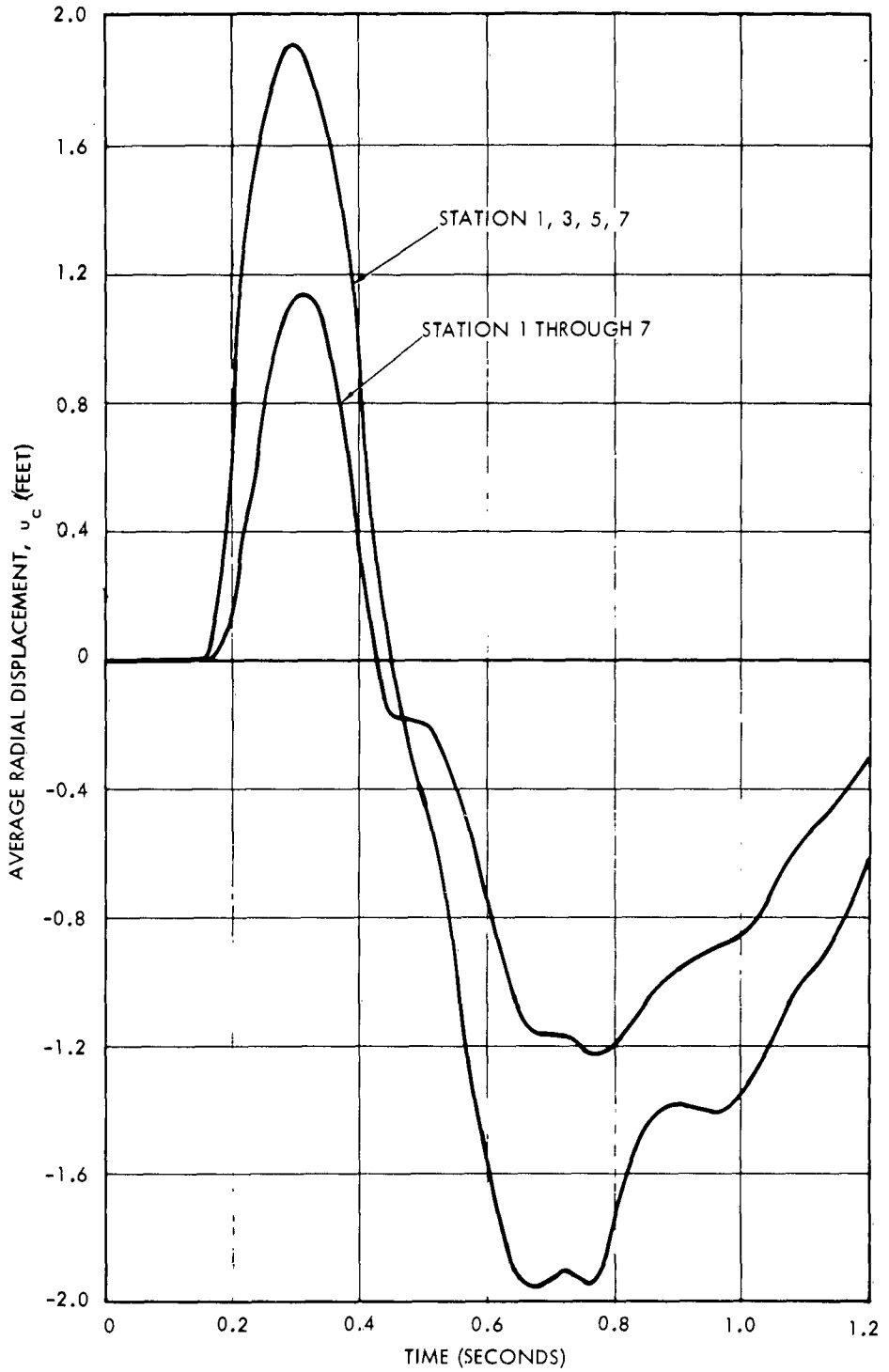

Figure 13. Comparison of Cavity Displacements Using Four and Seven Stations

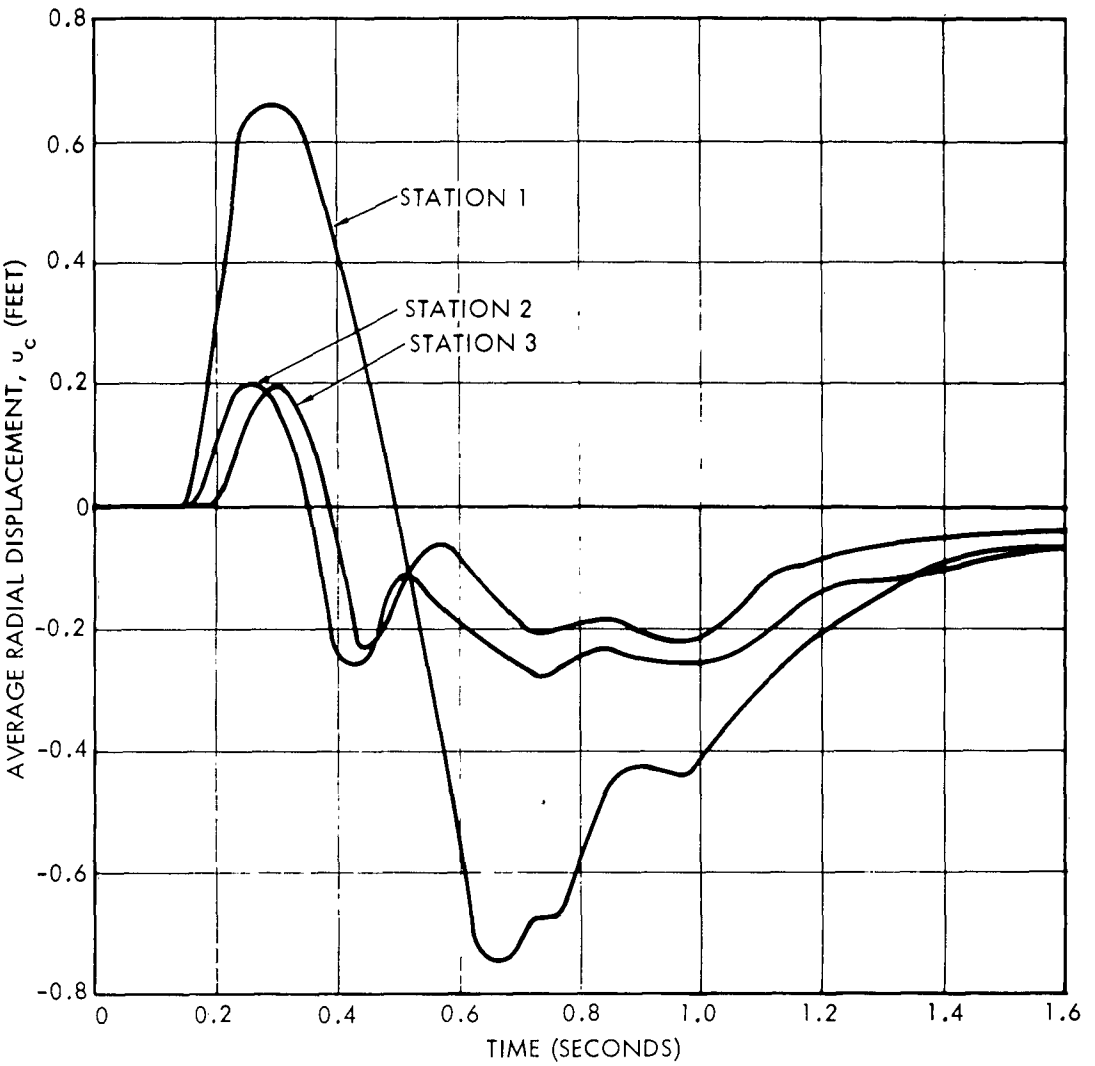

Figure 14. Influence Coefficients — Cavity Displacements Caused by Surface Pressure Loadings Acting on Stations 1, 2, and 3 for the Direct-Hit Example

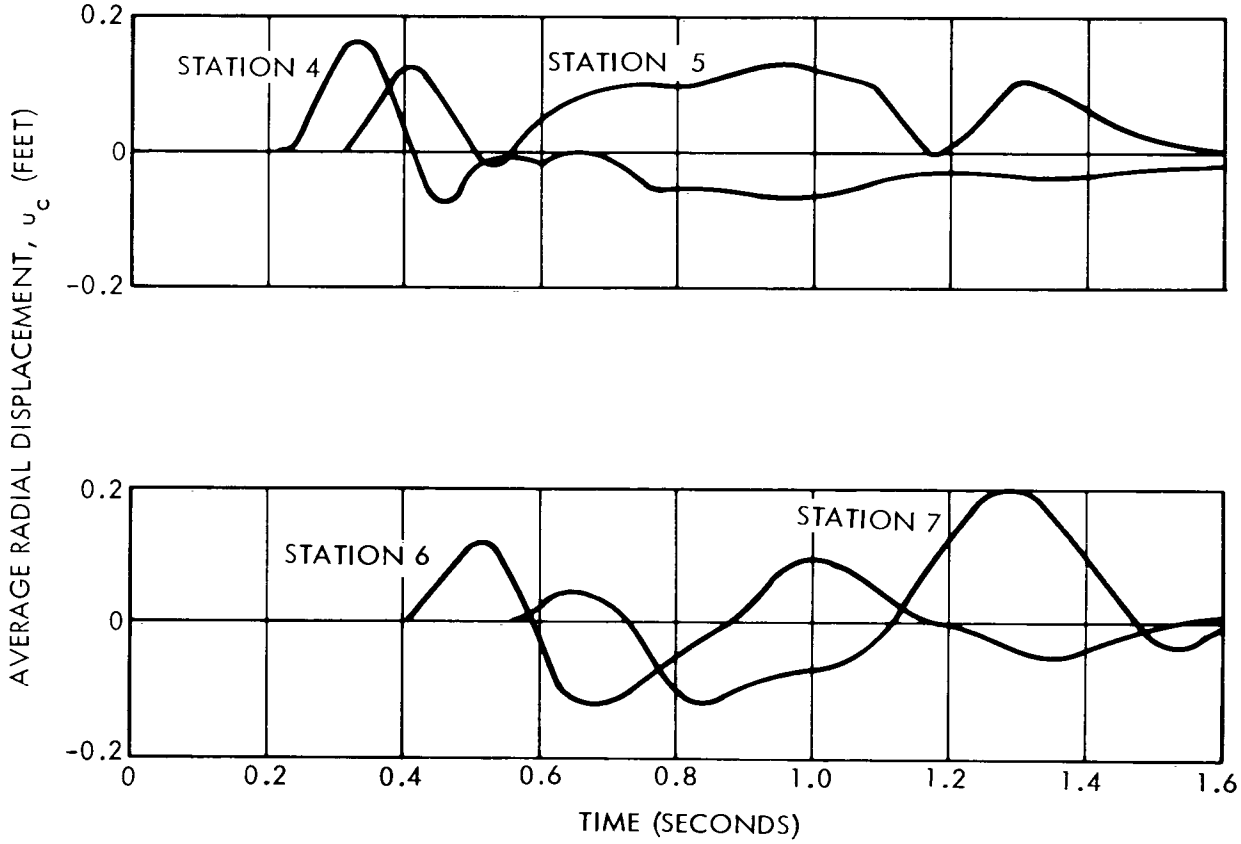

Figure 15. Influence Coefficients—Cavity Displacements Caused by Surface Pressure Loadings Acting on Stations 4, 5, 6, and 7 for the Direct-Hit Example

theoretical overpressures are used for the p_{sn} data and the Rainier ground velocities for the $\dot{u}_{sn}$ data. The cavity pressure signature used is given by equation (29) and denoted by p_{c1}.

For these calculations, the 38 stations shown in figure 16 are used. Note that even though the surface overpressure has symmetry about ground zero for the surface detonation and the ground velocities have symmetry about the surface ground zero for the underground explosion, the products of the overpressures and velocities only have symmetry about the line passing through the two ground zero locations. Thus, when full advantage is taken of this symmetry, the cavity motion caused by the surface pressures acting on all 38 stations can be determined by using the 26 stations 1, 1a, 1b, . . . , 20, and 21. However, this is considerably more than was required for the direct-hit example. Table 4 lists the geometrical data required in these calculations. Shown in the table are the areas of each of the different 26 stations, the distance from surface ground zero for the underground explosion to the respective station, and the distance from the surface burst to each station.

The cavity-displacement calculations made using the above data are summarized in figures 17 to 21 in the form of influence curves. That is, each curve shows the cavity motion caused by the overpressure acting on each of the stations individually. The total cavity motion caused by the pressures acting on all the stations is obtained from the sum of these individual curves.

These figures can be used to compare the relative importance of those stations where the surface pressures are the largest with those where the ground velocities are the largest. For example, compare the effect of station 2 where the surface explosion acts with that of the four stations around surface ground zero for the underground explosion. Even though table 4 shows that the area of station 2 is approximately equal to the total area of the four stations, figures 17, 18, and 19 show that the effect of station 2 is about twice as large as the combined effect of the four stations surrounding surface ground zero. Thus in this example the largest contribution to the cavity displacements comes from the stations around ground zero where the ground overpressures are the largest.

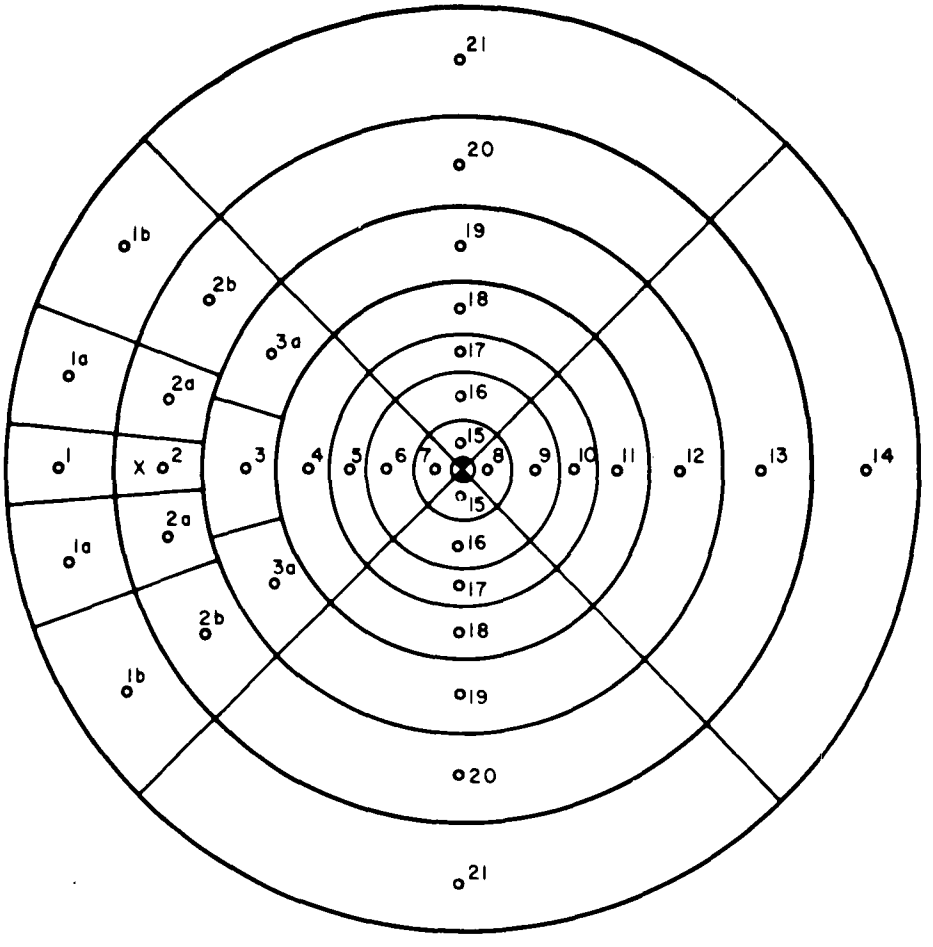

Figure 16. Lumped Stations for the Nondirect-Hit Example

X = surface burst ground zero

⊗ = underground explosion ground zero

Table 4. Geometrical Parameters for the Nondirect-Hit Example

Station No.	Station Area $ft^2 \times 10^3$	Distance From Underground Explosion Ground Zero (ft)	Distance From Surface Burst Ground Zero (ft)
1	398	2340	460
1a	597	2340	660
1b	995	2340	1270
2	165	1730	150
2a	248	1730	415
2b	413	1730	1030
3	281	1270	610
3a	281	1270	1010
4	453	900	980
5	234	650	1230
6	198	450	1430
7	39.8	150	1730
8	39.8	150	2030
9	198	450	2330
10	234	650	2530
11	453	900	2780
12	843	1270	3150
13	1485	1730	3610
14	3582	2340	4220
15	39.8	150	1880
16	198	450	1930
17	234	650	1990
18	453	900	2080
19	843	1270	2270
20	1485	1730	2560
21	3582	2340	3010

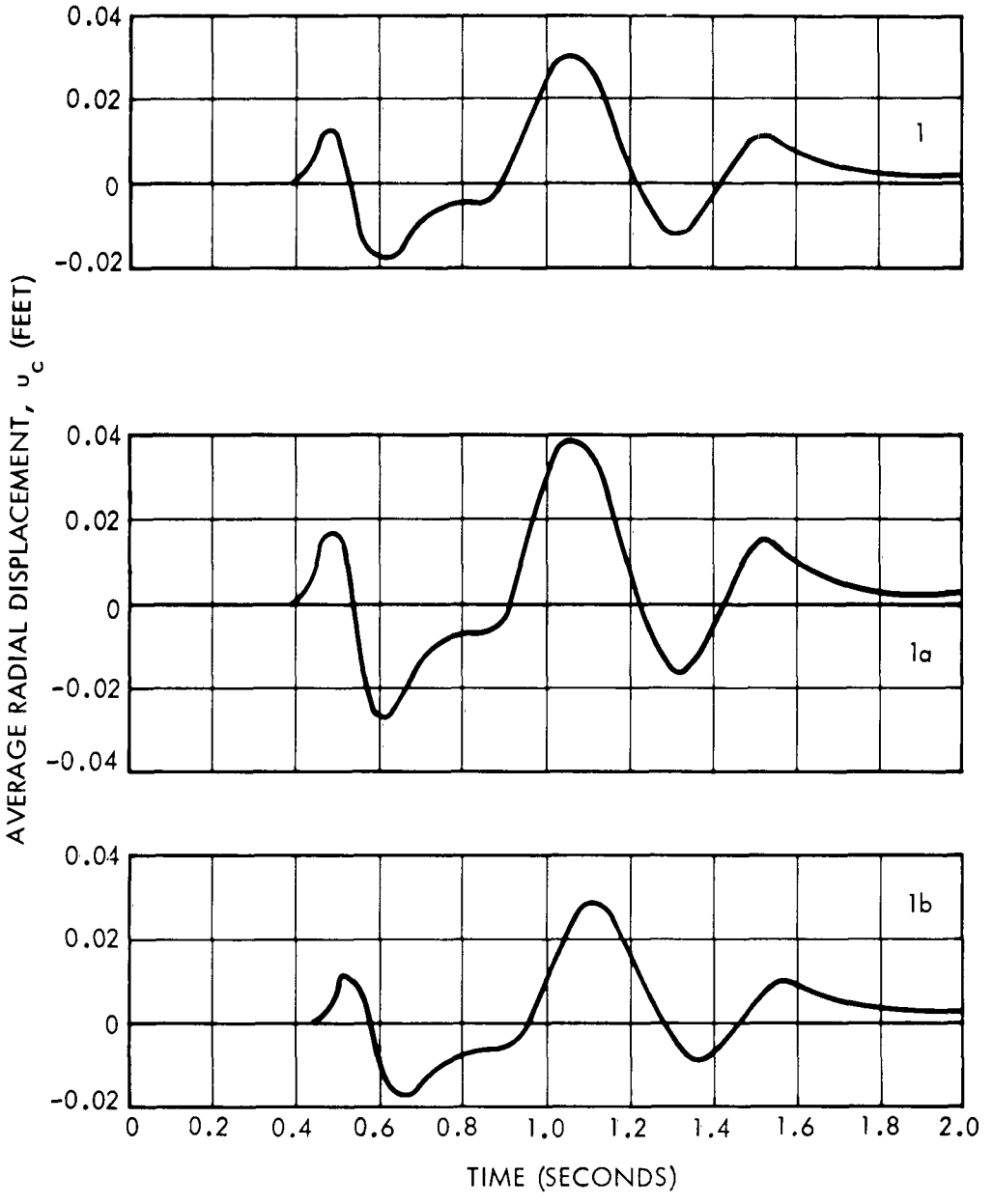

Figure 17. Influence Coefficients — Cavity Displacements Caused by Surface Pressure Loadings Acting on Stations 1, 1a, and 1b for the Nondirect-Hit Example

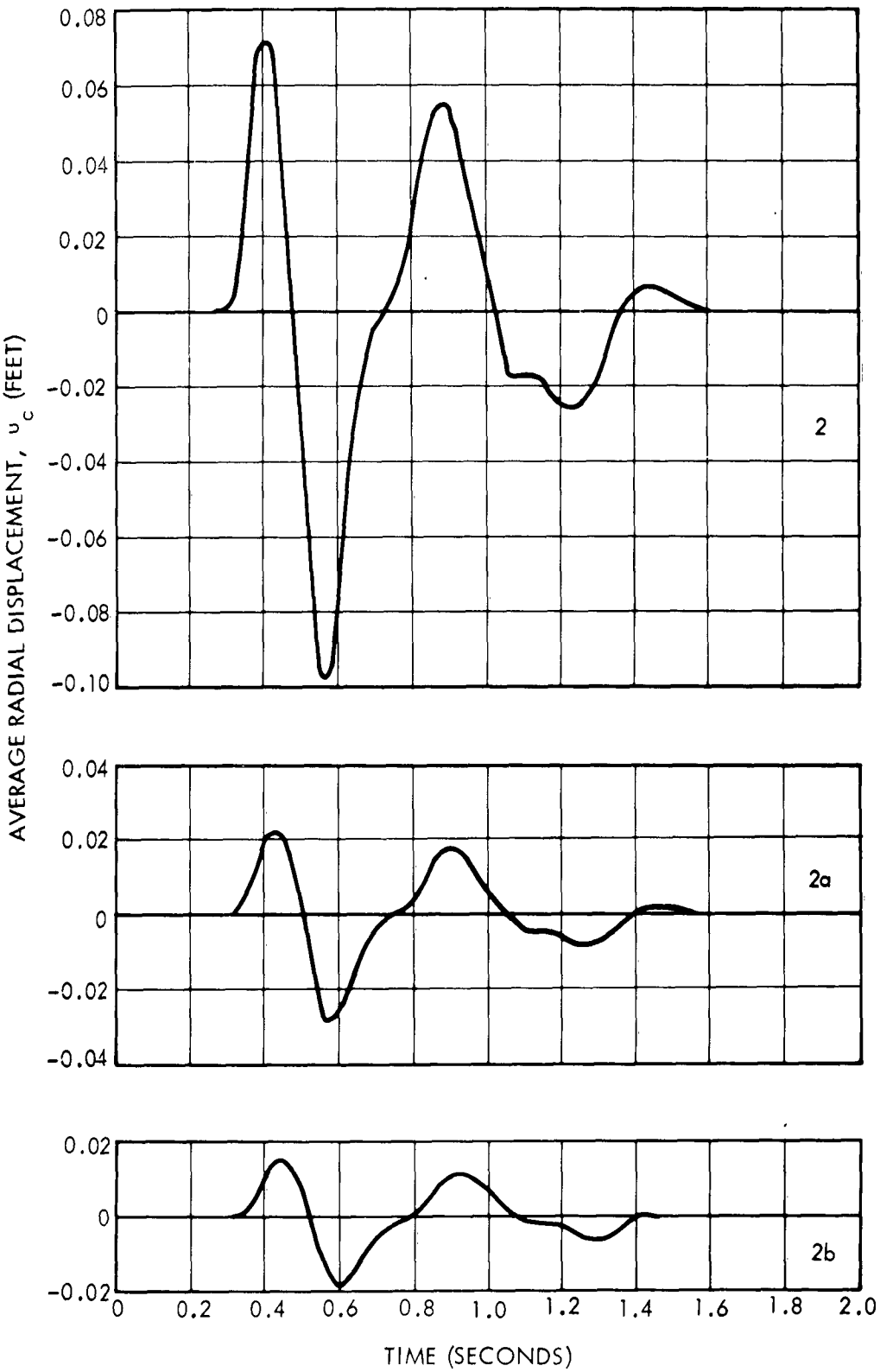

Figure 18. Influence Coefficients — Cavity Displacements Caused by Surface Pressure Loadings Acting on Stations 2, 2a, and 2b for the Nondirect-Hit Example

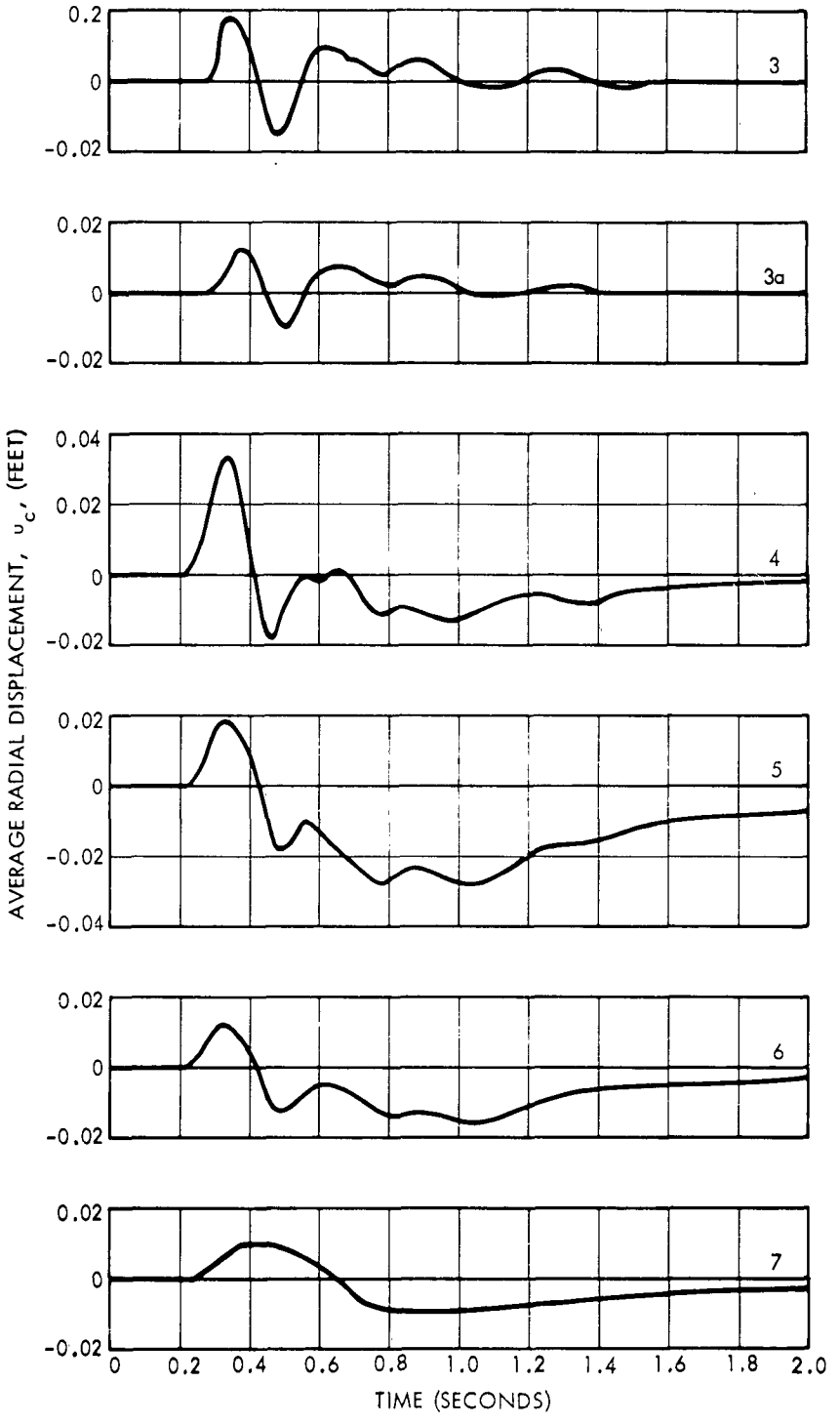

Figure 19. Influence Coefficients — Cavity Displacements Caused by Surface Pressure Loadings Acting on Stations 3, 3a, 4, 5, 6, and 7 for the Nondirect-Hit Example

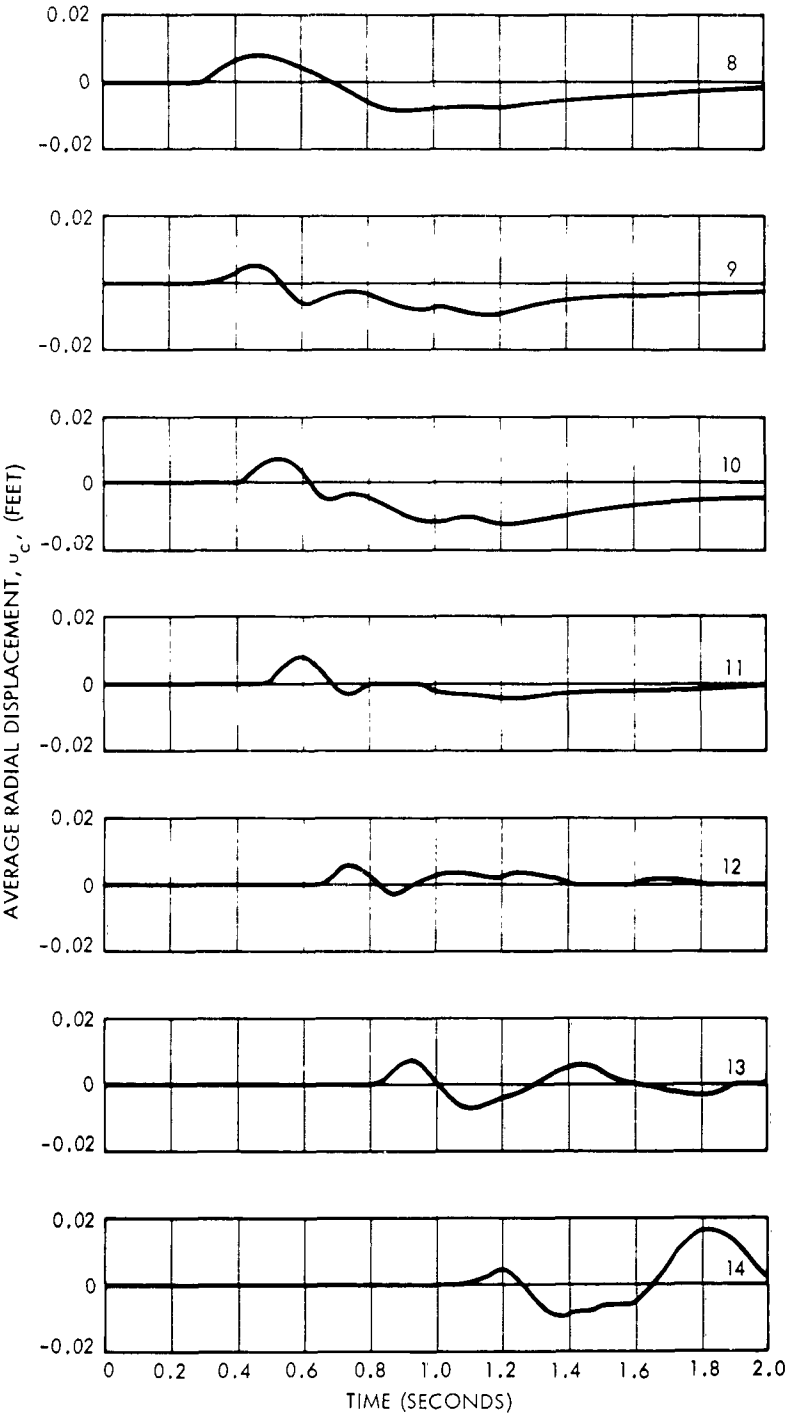

Figure 20. Influence Coefficients — Cavity Displacements Caused by Surface Pressure Loadings Acting on Stations 8 to 14 for the Nondirect-Hit Example

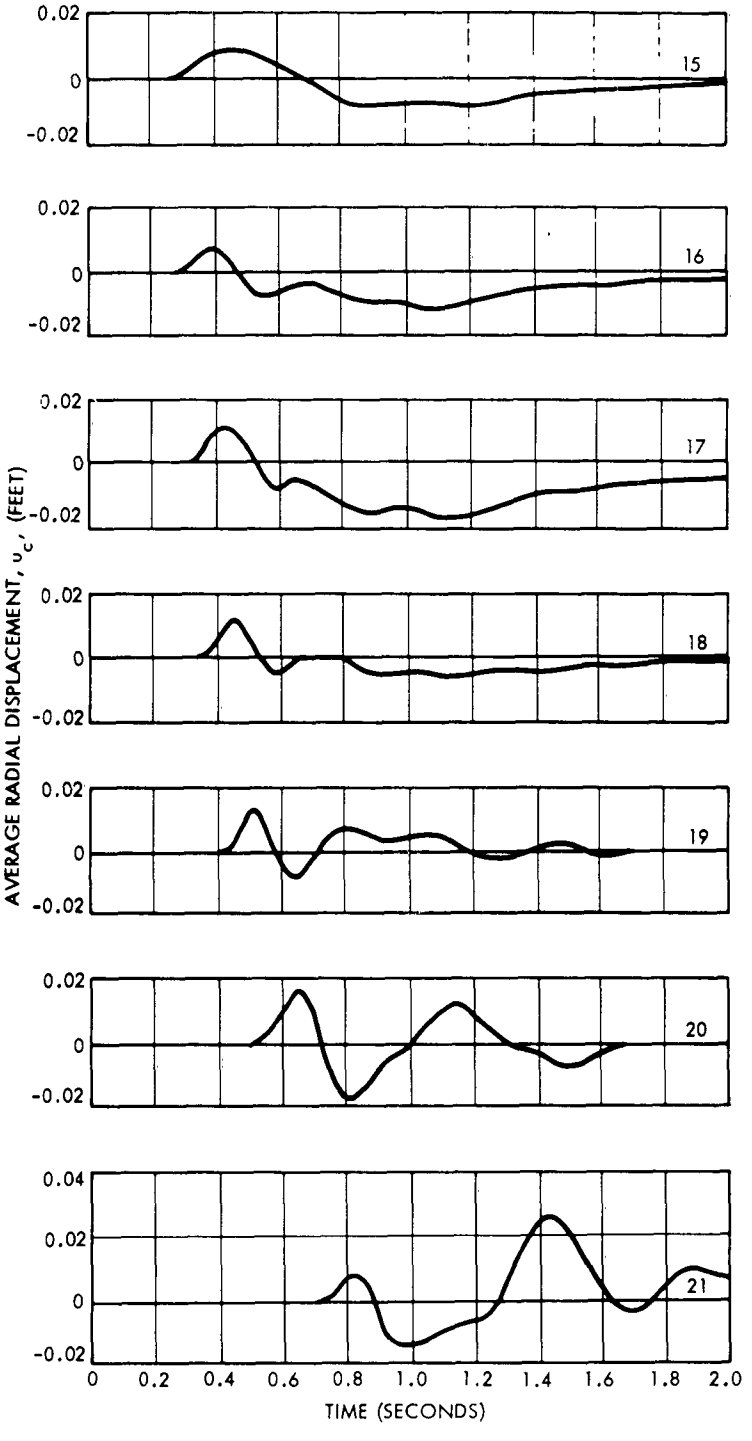

Figure 21. Influence Coefficients — Cavity Displacements Caused by Surface Pressure Loadings Acting on Stations 15 to 21 for the Nondirect-Hit Example

V. COMPARISON OF CAVITY AVERAGE DISPLACEMENT AND DISTORTION

Even though the average cavity displacement caused by a specified nuclear burst on the surface is of vital interest, cavity distortions are also important. The numerical procedure used in the examples only predicts the average cavity displacement. This section examines a theoretical problem in which the average displacement and distortion are computed to investigate the relative magnitudes of each of these types of displacements. The calculations of average displacement and distortion and also rigid-body translation, are determined from some published results of Baron and Parnes (Reference 6). Baron and Parnes find the motion of a cylindrical cavity during the passage of a plane compressional wave. They assume that the medium is homogeneous, isotropic, and elastic with a Poisson's ratio of 1/4 which corresponds to a granite-rock medium. The plane compressional wave front has a step distribution in time and propagates at the constant velocity of the dilatational waves c_p in a direction normal to the generators of the cylindrical cavity. Figure 22 shows the geometrical relations and the points on the cylinder surface where the radial displacements are computed.

The average and distortional radial displacements of points on the cylindrical surface are derived from the data shown in Reference 6. Figures 7 and 8 of Reference 6 show the radial and tangential velocities as functions of time in terms of nondimensional coordinates ($\dot{w}\mu/\sigma c_p$ and $\dot{v}\mu/\sigma c_p$ versus $c_p t/2a$) for the twelve points around the cavity $\theta_1 = 0$, $\theta_2 = \pm 22.5^\circ$, $\theta_3 = \pm 45^\circ$, $\theta_4 = \pm 67.5^\circ$, $\theta_5 = \pm 90^\circ$, $\theta_6 = \pm 135^\circ$, and $\theta_7 = 180^\circ$. In these plots $\dot{w}$ and $\dot{v}$ represent the radial and tangential velocities respectively, σ the stress intensity of the incoming wave, c_p the propagation velocity of the incoming waves, μ the shear modulus of the medium, t the time, and a the cavity radius. The radial velocity data have been reproduced and are shown in figure 23 of this report.

Let U_c and V_c represent the nondimensional radial and tangential displacements and let these displacements be represented by the Fourier expansions

$$U_c(\theta, t) = a_o(t) + \sum_{n=1}^{\infty} a_n(t) \cos n\theta \qquad (30)$$

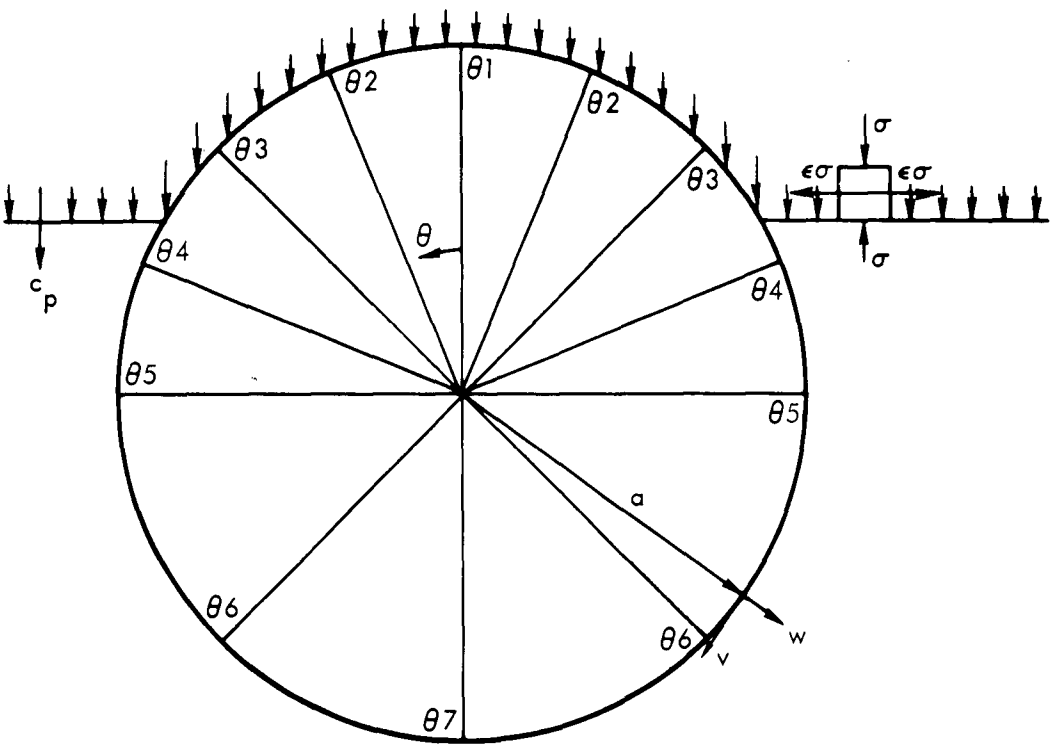

Figure 22. Geometry of Baron and Parnes Cylindrical Cavity Problem

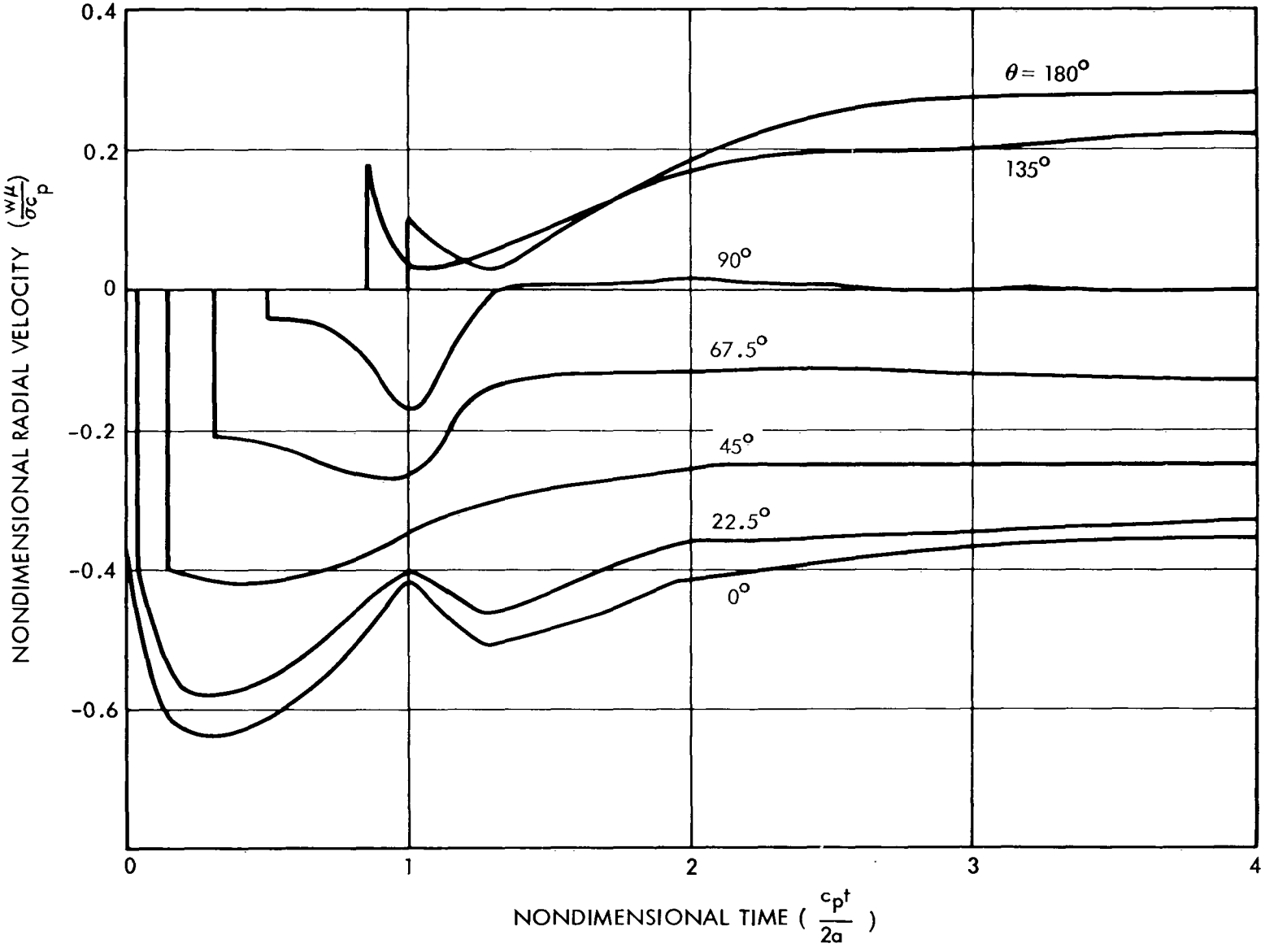

Figure 23. Radial Velocities of the Cavity for Various Angular Locations (Reproduced from Figure 7 of Reference 6)

$$V_c(\theta, t) = \sum_{n=1}^{\infty} b_n(t) \sin n\theta \tag{31}$$

In this notation, the nondimensional average and distortional radial displacements and rigid-body translations in the radial direction can be written as

$$\text{average radial displacement} = a_o(t) \tag{32}$$

$$\text{rigid-body radial translation} = \frac{a_1(t) - b_1(t)}{2} \cos\theta \tag{33}$$

$$\text{distortional radial displacement} = U_c(\theta, t) - a_o(t) - \frac{a_1(t) - b_1(t)}{2} \cos\theta \tag{34}$$

The average radial displacement is evaluated by numerically integrating the data in figure 23, to obtain the $U_c(\theta, t)$ shown in figure 24. Then, $a_o(t)$ is evaluated by numerically integrating the following equation

$$a_o(t) = \frac{1}{\pi} \int_o^{\pi} U_c(\theta, t)\, d\theta \tag{35}$$

and is shown in figure 25.

The rigid-body radial translation is computed from equation (33) by using the values of $(a_1 - b_1)/2$ presented in figure 10 of Reference 6. Finally, the radial distortional displacements are calculated from equation (34) and these results are presented in figures 26 and 27. Comparing figures 25 and 26, it is noted that the average and the maximum distortional radial displacements, which occur on $\theta = 0$, have about the same magnitude.

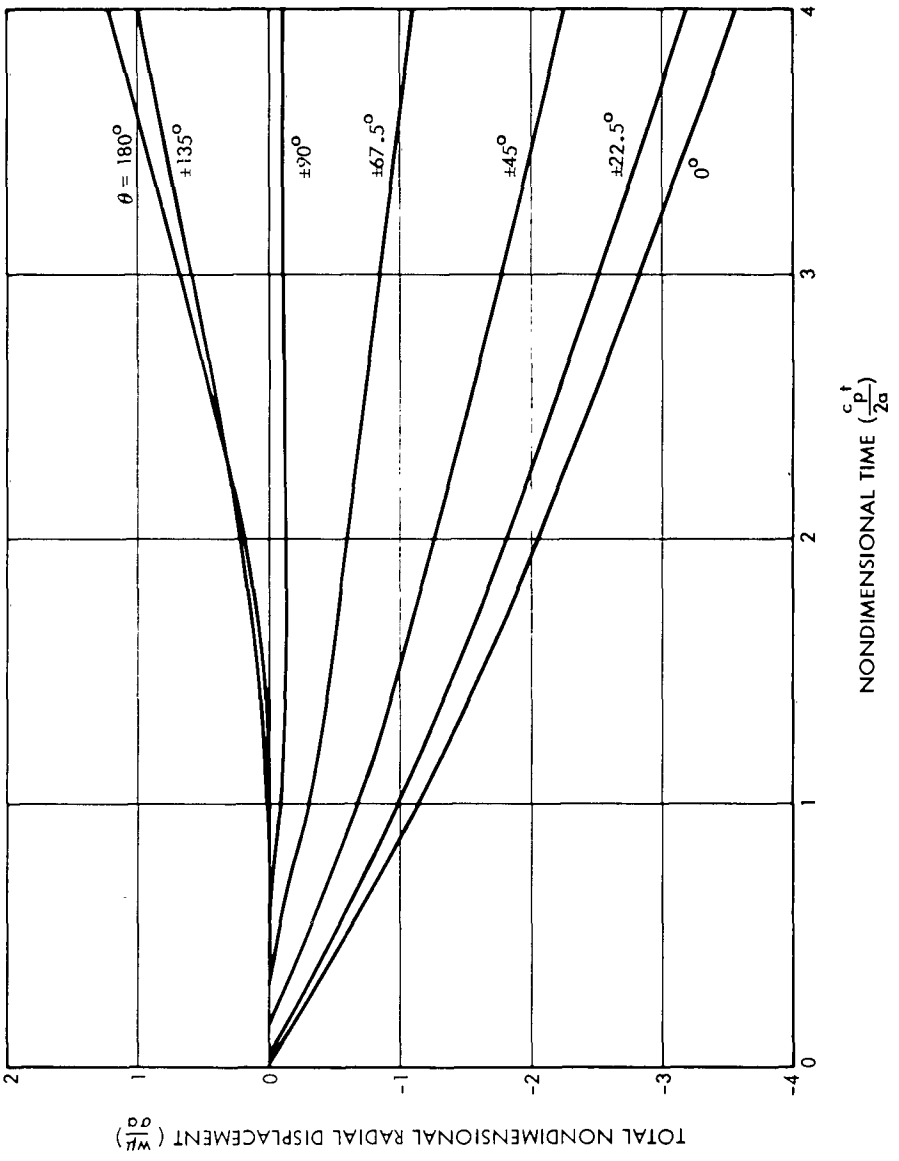

Figure 24. Total Cavity Displacements at θ = 0, ±22.5°, ±45°, ±67.5°, ±90°, ±135°, 180°
(Derived from Reference 6 Figure 7 data)

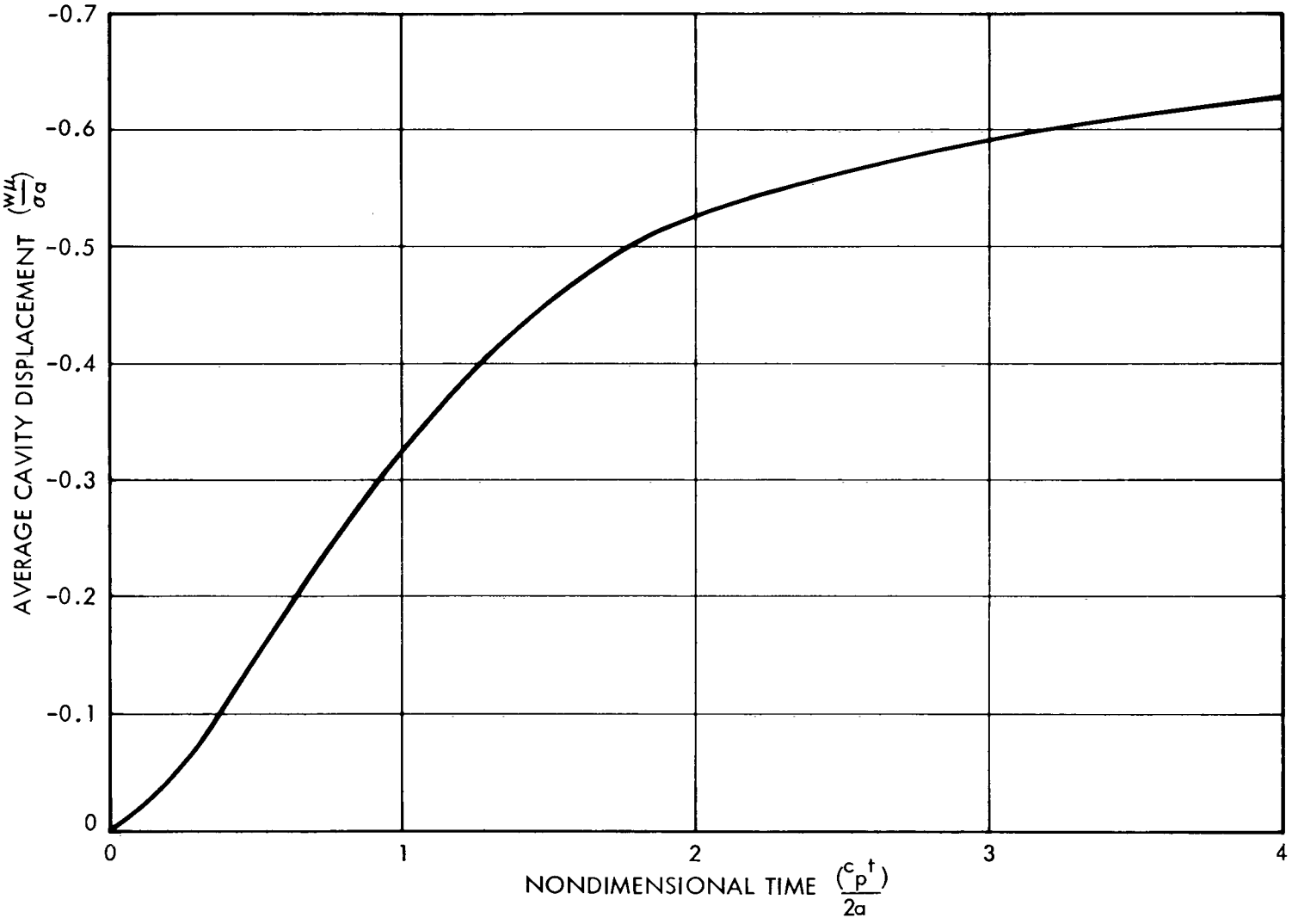

Figure 25. Average Cavity Displacement
(Derived from Reference 6 Figure 7 data)

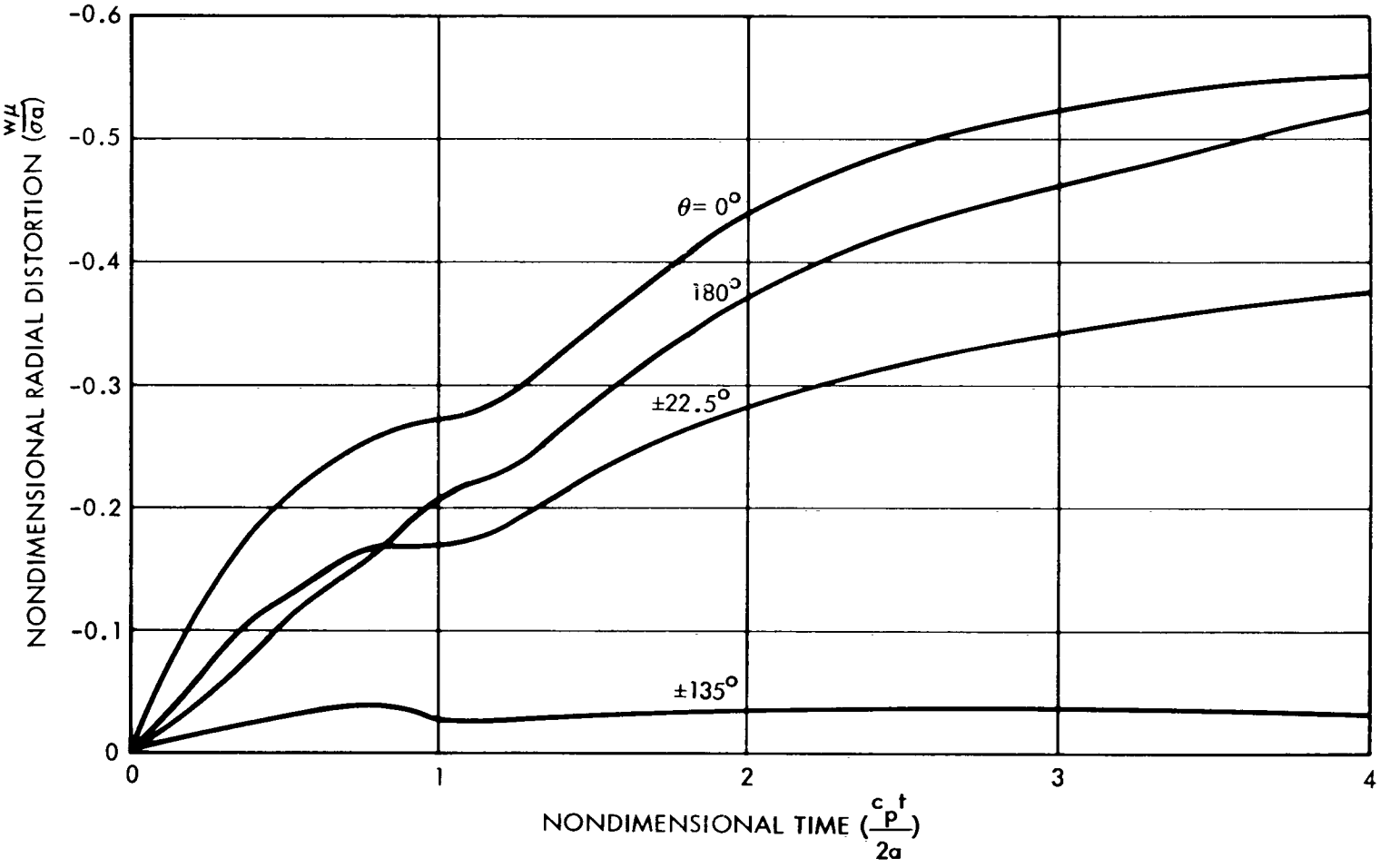

Figure 26. Cavity Distortions at $\theta = 0^o$, 180^o, $\pm 22.5^o$, $\pm 135^o$
(Derived from Reference 6 Figure 7 data)

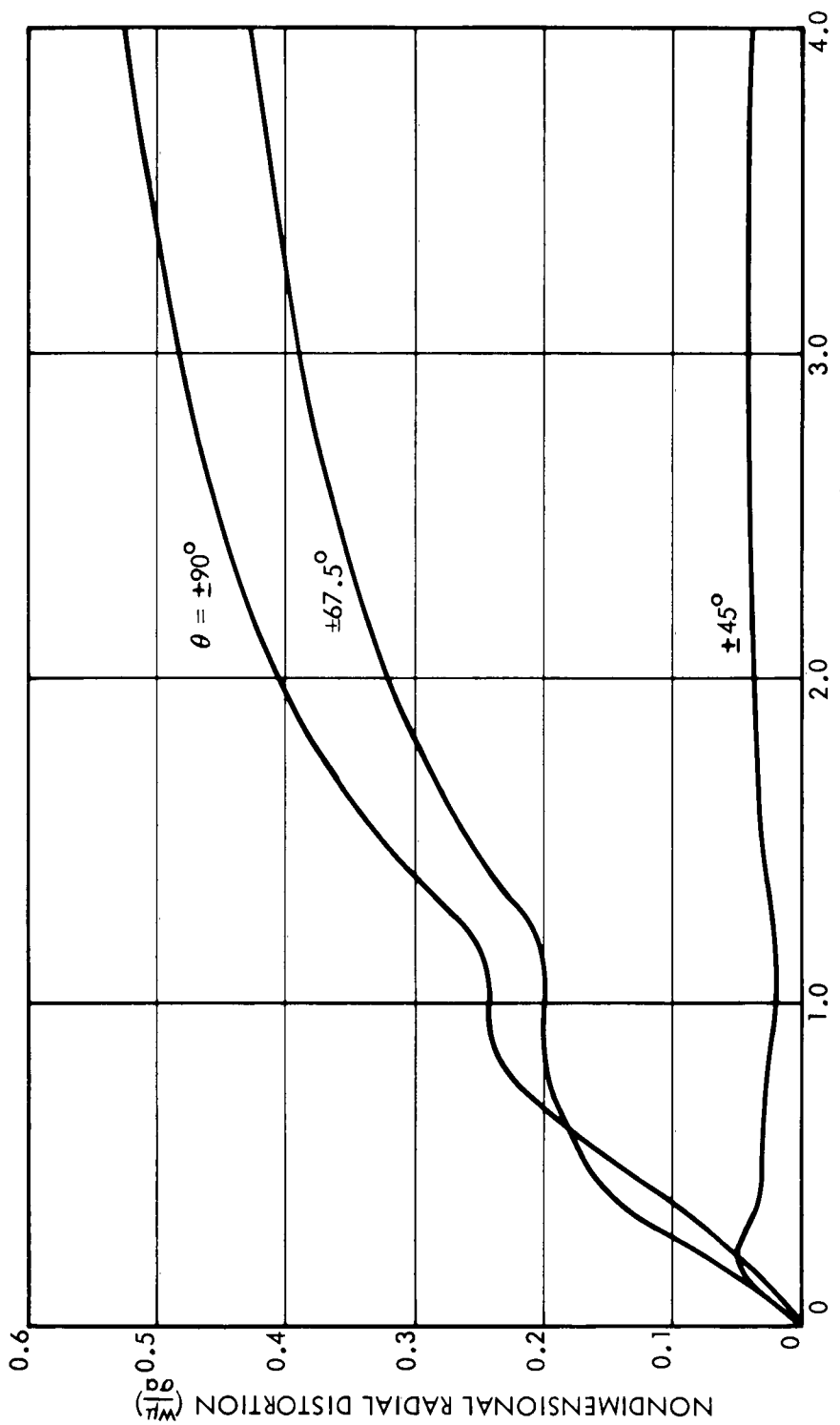

Figure 27. Cavity Distortions at $\theta = \pm 45^{\circ}$, $\pm 67.5^{\circ}$, $\pm 90^{\circ}$
(Derived from Reference 6 Figure 7 data)

APPENDIX

RECIPROCITY RELATIONS IN ELASTIC AND VISCOELASTIC WAVE PROPAGATION

I. SUMMARY

By a slight extension of Graffi's proof of the reciprocity relations in dynamics, it is pointed out that dynamic reciprocity applies as well to viscoelastic media and also to traveling loads.

II. INTRODUCTION

The most general reciprocal theorem in dynamics was asserted by Horace Lamb (Reference 16) to be derivable from a remarkable formula established by Lagrange in the "Mécanique Analytique" (1809) by way of a prelude to his theory of the variation of arbitrary constants. Lamb showed how the reciprocal theorems of von Helmholtz in the theory of least action in acoustics and optics and of Lord Rayleigh in acoustics, can be derived from Lagrange's formula. Rayleigh (Reference 21) extends the reciprocal theorem to include the action of dissipative forces and Lamb shows the complete reciprocity relationship in a moving fluid with reversed flow conditions. These theorems are best stated and proved in terms of generalized coordinates.

In the theory of static elasticity, a well known reciprocal theorem is associated with the names of Maxwell, Betti, and Rayleigh. A generalization of this theorem to dynamic problems in elasticity is given by Graffi (References 12 and 13), and certain applications of Graffi's results to the problem of elastic wave propagation, in particular, of the reciprocity between certain results of Pekeris' problem (Reference 19) of a suddenly applied vertical load and Chao's problem (Reference 7) of a suddenly applied horizontal load, was pointed out by Di Maggio and Bleich (Reference 9). However, there seems to have been no mention in the literature about reciprocity relations that hold for traveling loads. It is the purpose of this Appendix to state such a relationship, to extend it to viscoelastic media, and to demonstrate some interesting applications.

III. DERIVATION OF EQUATIONS

Consider a linear isotropic viscoelastic medium, which is described by the stress-strain relationship (in the usual tensor notations)

$$\left(\sum_{n=o}^{N} a_n \frac{d^n}{dt^n}\right)\sigma_{ij} = \left(\sum_{n=o}^{N} b_n \frac{d^n}{dt^n}\right)u_{k,k}\,\delta_{ij} + \left(\sum_{n=o}^{N} c_n \frac{d^n}{dt^n}\right)\left(u_{i,j} + u_{j,i}\right) \quad (1)$$

where σ_{ij} is the stress tensor, u_i is the displacement vector, a_n, b_n, c_n are constants if the medium is homogeneous, and are functions of space coordinates if the medium is nonhomogeneous. If N = 0, the material obeys Hooke's law and the above relationship is written

$$\sigma_{ij} = \lambda u_{k,k}\delta_{ij} + \mu(u_{i,j} + u_{j,i}) \quad (2)$$

where λ, μ are the Lamè constants which may depend on space coordinates. If X_i is the body force per unit mass, the equation of motion is

$$\rho \frac{d^2 u_i}{dt^2} = \rho X_i + \sigma_{ij,j} \quad (3)$$

If the material occupies a finite volume V with a boundary surface $S = S_\sigma + S_u$, surface traction being specified over S_σ and displacement being specified over S_u, the boundary conditions that must be satisfied are

$$\begin{aligned} \sigma_{ij}n_j &= \overset{\nu}{T}_i \qquad \text{on } S_\sigma \\ u_i &= w_i \qquad \text{on } S_u \end{aligned} \quad (4)$$

where n_j is the direction cosine of the normal ν of S. Let us consider problems in which $X_i(x_1, x_2, x_3; t)$, $\overset{\nu}{T}_i(x_1, x_2, x_3; t)$, and $w_i(x_1, x_2, x_3; t)$ are given functions of space and time, which starts its action at $t > 0$, under the initial conditions

$$u_i = \frac{du_i}{dt} = \ldots = \frac{d^N u_i}{dt^N} = 0 \quad \text{when } t \leq 0 \quad (5)$$

The response $u_i\,(x_1, x_2, x_3; t)$ is sought. To this end, we apply Laplace transformation with respect to the time t to every dependent variable under the assumption of suitable continuity conditions so that the transforms exist. Let the Laplace transform of u be written as $\underline{u}$

$$\underline{u} = \mathcal{L}\{u(t) \mid s\} = \int_0^\infty e^{-st} u(t)\, dt \tag{6}$$

We have, on account of the initial conditions named above

$$\left.\begin{aligned} \underline{\sigma}_{ij} &= \lambda(s)\underline{u}_{k,k}\delta_{ij} + \mu(s)(\underline{u}_{i,j} + \underline{u}_{j,i}) \\ s^2\rho\underline{u}_i &= \rho\underline{X}_i + \underline{\sigma}_{ij,j} \qquad \text{in } V \\ \underline{\sigma}_{ij}n_j &= \overset{\nu}{\underline{T}}_i \qquad \text{on } S_\sigma \\ \underline{u}_i &= \underline{w}_i \qquad \text{on } S_u \end{aligned}\right\} \tag{7}$$

where

$$\lambda(s) = \sum b_n s^n \Big/ \sum a_n s^n \quad , \quad \mu(s) = \sum c_n s^n \Big/ \sum a_n s^n \tag{8}$$

When the mathematical problem is solved for $\underline{u}_i\,(x_1, x_2, x_3; s)$, the inverse transform must be performed in order to obtain the desired solution $u_i\,(x_1, x_2, x_3; t)$.

Now consider two problems in which the applied body force and the surface tractions and displacements are differently specified. Let the variables involved in these two problems be distinguished by superscripts. Then

In V : $s^2\rho\underline{u}_i^{(1)} = \rho\underline{X}_i^{(1)} + \underline{\sigma}_{ij,j}^{(1)}$ (9a) $\qquad s^2\rho\underline{u}_i^{(2)} = \rho\underline{X}_i^{(2)} + \underline{\sigma}_{ij,j}^{(2)}$ (10a)

On S_σ : $\underline{\sigma}_{ij}^{(1)}n_j = \overset{\nu}{\underline{T}}_i^{(1)}$ (9b) $\qquad \underline{\sigma}_{ij}^{(2)}n_j = \overset{\nu}{\underline{T}}_i^{(2)}$ (10b)

On S_u : $\underline{u}_i^{(1)} = \underline{w}_i^{(1)}$ (9c) $\qquad \underline{u}_i^{(2)} = \underline{w}_i^{(2)}$ (10c)

Multiplying equation (9a) by $\underline{u}_i^{(2)}$ and (10a) by $\underline{u}_i^{(1)}$, subtracting, and integrating over the volume V, we obtain

$$\int_V \rho \underline{X}_i^{(1)} \underline{u}_i^{(2)} dv + \int_V \underline{\sigma}_{ij,j}^{(1)} \underline{u}_i^{(2)} dv = \int_V \rho \underline{X}_i^{(2)} \underline{u}_i^{(1)} dv + \int_V \underline{\sigma}_{ij,j}^{(2)} \underline{u}_i^{(1)} dv \qquad (11)$$

Now

$$\begin{aligned}
\int_V \underline{\sigma}_{ij,j}^{(1)} \underline{u}_i^{(2)} dv &= \int_V \left[\left(\lambda \underline{u}_{k,k}^{(1)} \delta_{ij} \right)_{,j} \underline{u}_i^{(2)} + \left(\mu \underline{u}_{i,j}^{(1)} + \mu \underline{u}_{j,i}^{(1)} \right)_{,j} \underline{u}_i^{(2)} \right] dv \\
&= \int_S \lambda \underline{u}_{k,k}^{(1)} \delta_{ij} \underline{u}_i^{(2)} n_j ds - \int_V \lambda \underline{u}_{k,k}^{(1)} \delta_{ij} \underline{u}_{i,j}^{(2)} dv \\
&\quad + \int_S \mu \underline{u}_{i,j}^{(1)} \underline{u}_i^{(2)} n_j ds + \int_S \mu \underline{u}_{j,i}^{(1)} \underline{u}_i^{(2)} n_j ds \\
&\quad - \int_V \mu \underline{u}_{i,j}^{(1)} \underline{u}_{i,j}^{(2)} dv - \int_V \mu \underline{u}_{j,i}^{(1)} \underline{u}_{i,j}^{(2)} dv \\
&= \int_S \lambda \underline{u}_{k,k}^{(1)} \underline{u}_i^{(2)} n_i ds - \int_V \lambda \underline{u}_{k,k}^{(1)} \underline{u}_{j,j}^{(2)} dv \\
&\quad + \int_S \mu \underline{u}_{i,j}^{(1)} \underline{u}_i^{(2)} n_j ds + \int_S \mu \underline{u}_{j,i}^{(1)} \underline{u}_i^{(2)} n_j ds \\
&\quad - \int_V \mu \underline{u}_{i,j}^{(1)} \underline{u}_{i,j}^{(2)} dv - \int_V \mu \underline{u}_{j,i}^{(1)} \underline{u}_{i,j}^{(2)} dv \qquad (12)
\end{aligned}$$

A similar expression is obtained for the integral

$$\int_V \underline{\sigma}_{ij,j}^{(2)} \underline{u}_i^{(1)} dv \qquad (13)$$

When these expressions are substituted into equation (11), we see that a number of volume integrals cancel each other. The surface integrals contributed by the integrals (12) and (13) to (11) are

$$\begin{aligned}
&\int_S \lambda \underline{u}_{k,k}^{(1)} \underline{u}_i^{(2)} n_i ds + \int_S \mu \underline{u}_{i,j}^{(1)} \underline{u}_i^{(2)} n_j ds + \int_S \mu \underline{u}_{j,i}^{(1)} \underline{u}_i^{(2)} n_j ds \\
&= \int_S \lambda \underline{u}_{k,k}^{(2)} \underline{u}_i^{(1)} n_i ds + \int_S \mu \underline{u}_{i,j}^{(2)} \underline{u}_i^{(1)} n_j ds + \int_S \mu \underline{u}_{j,i}^{(2)} \underline{u}_i^{(1)} n_j ds \qquad (14)
\end{aligned}$$

or

$$\int_S \sigma_{ij}^{(1)} u_i^{(2)} n_j ds = \int_S \sigma_{ij}^{(2)} u_i^{(1)} n_j ds \tag{14a}$$

If we now recall the definitions of S_σ and S_u, and the boundary conditions (9b), (9c), (10b), (10c), and substituting all these into equation (11), we obtain finally

$$\int_V \rho \underline{X}_i^{(1)} \underline{u}_i^{(2)} dv + \int_{S_\sigma} \underline{T}_i^{\nu(1)} \underline{u}_i^{(2)} ds + \int_{S_u} \underline{\sigma}_{ij}^{(1)} \underline{w}_i^{(2)} n_j ds$$

$$= \int_V \rho \underline{X}_i^{(2)} \underline{u}_i^{(1)} dv + \int_{S_\sigma} \underline{T}_i^{\nu(2)} \underline{u}_i^{(1)} ds + \int_{S_u} \underline{\sigma}_{ij}^{(2)} \underline{w}_i^{(1)} n_j ds \tag{15}$$

This is a general reciprocal relation in the Laplace transformation form. It is of the same form as Betti's reciprocal relation in elastostatics.

Since the inverse transform of the product of two functions is the convolution of the inverses, we obtain

$$\int_V \int_o^t \rho(\mathbf{x}) X_i^{(1)}(\mathbf{x}, t-\tau) u_i^{(2)}(\mathbf{x}, \tau) d\tau dv + \int_{S_\sigma} \int_o^t T_i^{\nu(1)}(\mathbf{x}, t-\tau) u_i^{(2)}(\mathbf{x}, \tau) d\tau ds$$

$$+ \int_{S_u} \int_o^t \sigma_{ij}^{(1)}(\mathbf{x}, t-\tau) w_i^{(2)}(\mathbf{x}, \tau) n_j d\tau ds$$

$$= \int_V \int_o^t \rho(\mathbf{x}) X_i^{(2)}(\mathbf{x}, t-\tau) u_i^{(1)}(\mathbf{x}, \tau) d\tau dv + \int_{S_\sigma} \int_o^t T_i^{\nu(2)}(\mathbf{x}, t-\tau) u_i^{(1)}(\mathbf{x}, \tau) d\tau ds$$

$$+ \int_{S_u} \int_o^t \sigma_{ij}^{(2)}(\mathbf{x}, t-\tau) w_i^{(1)}(\mathbf{x}, \tau) n_j d\tau ds \tag{16}$$

This is the general reciprocal theorem for elasto-kinetics. Whether the material is viscoelastic or purely elastic makes no difference in the final result. Note that this result holds for variable density $\rho(x_1, x_2, x_3)$ and nonhomogeneous material properties.

IV. GENERALIZATION TO INFINITE REGION

A generalization of the above result to an infinite or semi-infinite region is possible. Since a finite wave speed exists there always exists a boundary surface at any finite $t > 0$ which is yet uninfluenced by the loading initiated at $t = 0$. Let S_u be such a surface. Then $w_i = 0$ on S_u and the remainder of the equation holds without question.

V. SPECIFICATION AND APPLICATIONS

Space-time Separable Body Forces, Surface Tractions, and Displacements

If

$$X_i^{(1)} = \Xi_i^{(1)}(x)g(t) \qquad X_i^{(2)} = \Xi_i^{(2)}(x)g(t)$$

$$\overset{\nu}{T}{}_i^{(1)} = P_i^{(1)}(x)g(t) \qquad \overset{\nu}{T}{}_i^{(2)} = P_i^{(2)}(x)g(t)$$

$$w_i^{(1)} = W_i^{(1)}(x)g(t) \qquad w_i^{(2)} = W_i^{(2)}(x)g(t)$$

then equation (15) can be written, on cancelling $\mathcal{L}\{g(t)\}$ from every term, as

$$\int_V \rho \Xi_i^{(1)} \underline{u}_i^{(2)} dv + \int_{S_\sigma} P_i^{(1)} \underline{u}_i^{(2)} ds + \int_{S_u} W_i^{(2)} \underline{\sigma}_{ij}^{(1)} n_j ds$$

$$= \int_V \rho \Xi_i^{(2)} \underline{u}_i^{(1)} dv + \int_{S_\sigma} P_i^{(2)} \underline{u}_i^{(1)} ds + \int_{S_u} W_i^{(1)} \underline{\sigma}_{ij}^{(2)} n_j ds$$

The inverse transformation gives

$$\int_V \rho \Xi_i^{(1)} u_i^{(2)}(x,t) dv + \int_{S_\sigma} P_i^{(1)} u_i^{(2)}(x,t) ds + \int_{S_u} W_i^{(2)} \sigma_{ij}^{(1)}(x,t) n_j ds = 1\backslash 2$$

or

$$\int_V \rho X_i^{(1)}(x,t) u_i^{(2)}(x,t) dv + \int_{S_\sigma} \overset{\nu}{T}{}_i^{(1)}(x,t) u_i^{(2)}(x,t) ds + \int_{S_u} w_i^{(2)}(x,t) \sigma_{ij}^{(1)}(x,t) n_j ds = 1\backslash 2$$

where $\overline{1}\overline{2}$ indicates the same expression as on the left-hand side except that the superscripts (1) and (2) are interchanged. Graffi's well-known formula results if $w_i^{(1)}$, $w_i^{(2)} = 0$ on S_u.

Forces Applied at Different Times

Graffi also gives the following case. If

$$X_i^{(1)} = \Xi_i^{(1)}(x)g(t - T_1) \qquad X_i^{(2)} = \Xi_i^{(2)}(x)g(t - T_2)$$

$$T_i^{\nu(1)} = P_i^{(1)}(x)g(t - T_1) \qquad T_i^{\nu(2)} = P_i^{(2)}(x)g(t - T_2)$$

$$w_i^{(1)} = 0 \qquad w_i^{(2)} = 0$$

then equation (15) becomes, on cancelling $\mathcal{L}\{g(t)|s\}$,

$$\int_V \rho \Xi_i^{(1)} e^{-sT_1} \underline{u}_i^{(2)} dv + \int_{S_\sigma} P_i^{(1)} e^{-sT_1} u_i^{(2)} ds = \overline{1}\overline{2}$$

The inverse transform gives

$$\int_V \rho \Xi_i^{(1)}(x) u_i^{(2)}(x, t - T_1) dv + \int_{S_\sigma} P_i^{(1)}(x) u_i^{(2)}(x, t - T_1) ds$$

$$= \int_V \rho \Xi_i^{(2)}(x) u_i^{(1)}(x, t - T_2) dv + \int_{S_\sigma} P_i^{(2)}(x) u_i^{(1)}(x, t - T_2) ds$$

Concentrated Forces

If the loading consists of concentrated loads $f_i^{(1)}$ and $f_i^{(2)}$ acting at points p_1, p_2 respectively, we may consider $\rho\Xi_i$ or P_i as suitable delta function and obtain at once

$$f_i^{(1)}(p_1) u_i^{(2)}(p_1, t - T_1) = f_i^{(2)}(p_2) u_i^{(1)}(p_2, t - T_2)$$

or, if $T_1 = T_2$

$$f_i^{(1)}(p_1)u_i^{(2)}(p_1, t) = f_i^{(2)}(p_2)u_i^{(1)}(p_2, t)$$

This is the extension of the conventional elastostatic Betti-Rayleigh reciprocal relation to kinetics.

Impulsive and Traveling Concentrated Forces

Let an impulsive concentrated force act at a point p_1

$$\rho X_i^{(1)} = f_i^{(1)}\delta(p_1)\delta(t)$$

and a concentrated force $f_i^{(2)}$ be applied at the origin at $t = 0$ and thereafter moved along the x_1 axis at uniform speed U

$$\rho X_i^{(2)} = f_i^{(2)}\delta\left(t - \frac{x_1}{U}\right)\delta(x_2)\delta(x_3)$$

No other surface loading or displacement is imposed. Then equation (16) gives

$$f_i^{(1)}u_i^{(2)}(p_1, t)$$

$$= f_i^{(2)}\int\int\int \delta(x_2)\delta(x_3)dx_1dx_2dx_3 \int_0^t \delta\left(\tau - \frac{x_1}{U}\right)u_i^{(1)}(x_1, x_2, x_3, t - \tau)d\tau$$

and therefore

$$f_i^{(1)}u_i^{(2)}(p_1, t) = f_i^{(2)}\int_{-\infty}^{\frac{x_1}{U}} u_i\left(x_1, 0, 0, t - \frac{x_1}{U}\right)dx_1$$

If $u_i^{(1)}\left[x_1, 0, 0, t - (x_1/U)\right]$ is known, then $u_i^{(2)}(p_1, t)$ can be found from the above equation.

Suddenly Started Line Load Over an Elastic Half-Space

The steady-state solution of the problem of a line load traveling at constant speed over an elastic half-space (a two-dimensional problem) was first solved by Sneddon (Reference 20) and later by Cole and Huth

(Reference 8) by means of Fourier transformation and by analytic functions of a complex variable. A singularity was found if the load travels at the Rayleigh wave speed of the medium. To examine this singularity Ang (Reference 1) considered the problem of suddenly started line load. Now according to the reciprocal theorem Ang's problem can be solved by one integration of the solution of Lamb's problem: the impulsive loading at one point (not traveling) inside a two-dimensional half-space. Only the surface displacement due to the point loading needs to be known.

Figure 1. Illustration of the Loading in Lamb's and Ang's Problems

Suddenly Started Point Load Over an Elastic Half-Space

The corresponding three-dimensional problem of a concentrated load suddenly applied at a point on the surface of an elastic half-space and thereafter moved at a constant velocity U in the x-direction has not yet been solved. However, from the reciprocal theorem named about, it becomes apparent that the solution to this problem can be obtained by an integration of Pekeris' solution to a suddenly applied vertical load and Chao's solution to a suddenly applied horizontal load at a given point in an elastic half-space.

REFERENCES

1. Ang, D. D., "Transient Motion of a Line Load on the Surface of an Elastic Half-Space," Quarterly of Applied Mathematics, vol. XVIII, No. 3 (October 1960), pp. 251-256.

2. Brode, H. L., "Point Source Explosion in Air," Research Memorandum RM-1824, December 1956, The Rand Corporation.

3. Brode, H. L., "Cavity Explosion Calculations for the Cowboy Program," Research Memorandum RM-2624, 5 August 1960, The Rand Corporation.

4. Baron, Bleich, and Weidlinger, "Theoretical Studies of Ground Shock Phenomena," Report SR-19, October 1960, Mitre Corporation.

5. Baron, M. L. and Matthews, A. T., "Diffraction of a Pressure Wave by a Cylindrical Cavity in an Elastic Medium," Journal of Applied Mechanics, vol. 28 (September 1961), pp. 347-354.

6. Baron, M. L. and Parnes, R., "Displacements and Velocities Produced by the Diffraction of a Pressure Wave by a Cylindrical Cavity in an Elastic Medium," Journal of Applied Mechanics, vol. 29 (1962), pp. 385-395.

7. Chao, C. C., " Dynamical Response of an Elastic Half-Space to Tangential Surface Loadings," Columbia University Contract Nonr-266(20), Technical Report No. 11 (March 1958), and Journal of Applied Mechanics, vol. 27 (September 1960), pp. 559-567.

8. Cole, J. and Huth, J., "Stresses Produced in a Half-Plane by Moving Loads," Journal of Applied Mechanics, vol. 25 (December 1958), pp. 433-436.

9. DiMaggio, F. L. and Bleich, H. H., "An Application of a Dynamic Reciprocal Theorem," Journal of Applied Mechanics, vol. 26 (December 1959), pp. 678-679.

10. Eringen, A. C., "Elasto-Dynamic Problem Concerning the Spherical Cavity," Quarterly Journal of Mechanics and Applied Mathematics, vol. X, part 3 (1957), pp. 257-270.

11. Glasstone, S. (Ed.), The Effects of Nuclear Weapons, United States Atomic Energy Commission (April 1962).

12. Graffi, D., "Sui Teoremi di Reciprocità nei Fenomeni Dipendenti dal Tempo," Annali di Mathematica, series 4, vol. 18 (1939), pp. 173-200.

REFERENCES (Continued)

13. Graffi, D., "Sul Teorema di Reciprocità nelle Dinamica Dei Corpi Elastici," Memoria della Accademia della Scienze, Bologna, series 10. vol. 4 (1946-1947), pp. 103-111.

14. Johnson, G. W. and Violet, C. E., "Phenomenology of Contained Nuclear Explosions," UCRL-5124. rev. I, December 1958, University of California, Lawrence Radiation Laboratory, Livermore, California.

15. Knopoff, L. and Gangi, A. F., "Seismic Reciprocity," Geophysics, vol. 24, No. 4 (October 1959), pp. 681-691.

16. Lamb, H., "On Reciprocal Theorems in Dynamics," Proceedings of London Mathematical Society, vol. 19 (1888), pp. 144-151.

17. Morse, R. M. and Feshback, H., Methods of Theoretical Physics, McGraw-Hill and Company, Inc., New York (1953).

18. Naghdi, P. M., "Reciprocity Theorem for Dynamic Elasticity," Internal STL Memorandum (11 September 1961).

19. Pekeris, C. L. and Lifson, H. "Motion of the Surface of a Uniform Elastic Half-Space Produced by a Buried Pulse," The Journal of the Acoustical Society of America, vol. 29, No. 11 (November 1957), pp. 1233-1238.

20. Sneddon, I. N., Fourier Transforms, McGraw-Hill and Company, Inc., New York (1951), pp. 445-449.

21. Strutt, J. W. (Lord Rayleigh), "Some General Theorems Relating to Vibrations," Proceedings of London Mathematical Society, vol. 4 (1873), pp. 357-368.

22. Swift, L. M. and Sachs, D. C., "Surface Motion from an Underground Detonation," WT-1528, Operation PLUMBBOB, Project 26.4a, (1 April 1959).

23. Timoshenko, S. and Goodier, J. N., Theory of Elasticity, Second Edition, McGraw-Hill and Company, Inc., New York (1951).

DISTRIBUTION

No. cys	
	HEADQUARTERS USAF
1	Hq USAF (AFOCE), Wash 25, DC
1	Hq USAF (AFRST), Wash 25, DC
1	Hq USAF (AFNIN), Wash 25, DC
1	USAF Dep, The Inspector General (AFIDI), Norton AFB, Calif
1	USAF Directorate of Nuclear Safety (AFINS), Kirtland AFB, NM
1	AFCRL, ATTN: Norm Haskell (CRRA),Hanscom Fld, Bedford, Mass
1	AFOSR, Bldg T-D, Wash 25, DC
	MAJOR AIR COMMANDS
	AFSC (SCT), Andrews AFB, Wash 25, DC
1	SAC (OAWS), Offutt AFB, Nebr
1	AFLC, Wright-Patterson AFB, Ohio
1	AUL, Maxwell AFB, Ala
2	USAFIT (USAF Institute of Technology), Wright-Patterson AFB, Ohio
	AFSC ORGANIZATIONS
	ASD, Wright-Patterson AFB, Ohio
1	(ASAPRL)
1	(Director of Systems Management, Col Sam Lowry)
1	BSD (BSR), Norton AFB, Calif
	ESD, Hanscom Fld, Bedford, Mass
1	(ESAT)
1	(CRRA)
1	(CRZG)
	KIRTLAND AFB ORGANIZATIONS
	AFSWC, Kirtland AFB, NM
1	(SWEH)
50	(SWOI)
5	(SWRS)
1	US Naval Weapons Evaluation Facility (NWEF) (Code 404), Kirtland AFB, NM

DISTRIBUTION (cont'd)

No. cys	
	OTHER AIR FORCE AGENCIES
1	Director, USAF Project RAND, via: Air Force Liaison Office, The RAND Corporation, ATTN: RAND Library, 1700 Main Street, Santa Monica, Calif
	ARMY ACTIVITIES
1	Director, Ballistic Research Laboratories (Library), Aberdeen Proving Ground, Md
1	Chief of Engineers, Department of the Army (ENGEB), Wash 25, DC
1	Office of the Chief, Corps of Engineers, US Army (Protective Construction Branch), Wash 25, DC
1	Director, Army Research Office, Arlington Hall Sta, Arlington, Va
	Director, US Army Waterways Experiment Sta, P.O. Box 60 Vicksburg, Miss
1	(WESTR)
1	(WESUC)
1	Commanding Officer, US Army Engineers, Research & Development Laboratories, Ft Belvoir, Va
	NAVY ACTIVITIES
1	Chief, Bureau of Yards and Docks, Department of the Navy, Wash 25, DC
1	Commanding Officer and Director, Naval Civil Engineering Laboratory, Port Hueneme, Calif
1	Commander, Naval Ordnance Laboratory, White Oak, Silver Spring, Md
	OTHER DOD ACTIVITIES
2	Chief, Defense Atomic Support Agency, ATTN: Mr. John Lewis, Blast and Shock Division, Wash 25, DC
1	Commander, Field Command, Defense Atomic Support Agency (FCAG3, Special Weapons Publication Distribution), Sandia Base, NM
20	ASTIA (TIPDR), Arlington Hall Sta, Arlington 12, Va
	AEC ACTIVITIES
1	Sandia Corporation (Technical Library), Sandia Base, NM

DISTRIBUTION (cont'd)

No. cys	
	OTHER
1	Florida State University, Director of Engineering Science, ATTN: Dr. Grover L. Rogers, Tallahassee, Fla
1	General American Transportation Corp., MRD Division, ATTN: Dr. Glen L. Neidhardt, 7501 N. Natchez, Niles, Ill
1	University of Missouri, School of Mines and Metallurgy, ATTN: Dr. Clark, Rolla, Mo
1	University of Illinois, ATTN: Dr. N. M. Newmark, 201 Civil Engineering Hall, Urbana, Ill
1	Paul Weidlinger, Consulting Engineer, 770 Lexington Ave., New York 21, NY
1	Armour Research Foundation, Illinois Institute of Technology, ATTN: Dr. E. Sevin, 10 West 35th Street, Chicago 15, Ill
1	Massachusetts Institute of Technology, Department of Civil and Sanitary Engineering, ATTN: Dr. Robert V. Whitman, Cambridge 29, Mass
1	University of New Mexico, Department of Civil Engineering, ATTN: Dr. E. Zwoyer, Albuquerque, NM
1	University of California, College of Engineering, ATTN: Prof. Martin Duke, Los Angeles, Calif
1	North Carolina State, Department of Civil Engineering, ATTN: Prof. Ralph Fadum, Raleigh, NC
1	St. Louis University, Institute of Technology, ATTN: Dr. Carl Kisslinger, 3621 Olive Street, St. Louis 8, Mo
1	University of Michigan, Department of Civil Engineering, ATTN: Prof. F. E. Richart, Jr., 313 West Engineering, Ann Arbor, Mich
1	University of Notre Dame, Department of Civil Engineering, ATTN: Prof. Harry E. Saxe, Box 598, Notre Dame, Ind
1	Purdue University, Department of Civil Engineering, ATTN: Prof. Gerald Leonards, West Lafayette, Ind
1	National Engineering Science Company, 711 South Fairoaks Avenue, Pasadena, Calif
1	Shannon and Wilson, ATTN: Mr. Stanley Wilson, 1105 North 38th Street, Seattle 3, Wash
1	E. H. Plesset Assoc., Inc. ATTN: Mr. Marc Peter, 6399 Wilshire Blvd., Los Angeles 48, Calif

DISTRIBUTION (cont'd)

No. cys	
1	University of Illinois, Theoretical and Applied Mechanics Dept., ATTN: Prof. A. P. Boresi, Urbana, Ill
1	The Mitre Corporation, ATTN: Warren McCabe, P. O. Box 208, Bedford, Mass
1	Official Record Copy (SWRS, Lt Hamada)

Air Force Special Weapons Center, Kirtland AF Base, New Mexico
Rpt No. AFSWC-TDR-63-26. THE DEVELOPMENT OF RECIPROCITY PROCEDURES FOR UTILIZING DATA FROM UNDERGROUND EXPLOSION TESTS. Final Report, May 1963. 90 p. incl illus, tables, 23 refs.

Unclassified Report

A procedure for predicting underground cavity motions resulting from surface air-blast loading is developed on the basis of a dynamic-reciprocity principle for a nonhomogeneous, anisotropic, linear, viscoelastic half space. A computer program for evaluating the integral equations for this medium is presented. Experimental measurements from the RAINIER Event of Operations PLUMBBOB are used to postulate cavity motions

1. Digital computers
2. Ground motion
3. Military facilities -- hardening
4. Rainier burst
5. Surface bursts
6. Underground structures
I. AFSC Project No. 1080, Task 108007
II. Contract AF 29(601)-5132
III. WEB No. 13.148
IV. Space Technology Labs., Inc., Redondo Beach, Calif
V. R.E. Hutton, S.Y. Yu, Y.C. Fung
VI. In ASTIA collection

Air Force Special Weapons Center, Kirtland AF Base, New Mexico
Rpt No. AFSWC-TDR-63-26. THE DEVELOPMENT OF RECIPROCITY PROCEDURES FOR UTILIZING DATA FROM UNDERGROUND EXPLOSION TESTS. Final Report, May 1963. 90 p. incl illus, tables, 23 refs.

Unclassified Report

A procedure for predicting underground cavity motions resulting from surface air-blast loading is developed on the basis of a dynamic-reciprocity principle for a nonhomogeneous, anisotropic, linear, viscoelastic half space. A computer program for evaluating the integral equations for this medium is presented. Experimental measurements from the RAINIER Event of Operations PLUMBBOB are used to postulate cavity motions

1. Digital computers
2. Ground motion
3. Military facilities -- hardening
4. Rainier burst
5. Surface bursts
6. Underground structures
I. AFSC Project No. 1080, Task 108007
II. Contract AF 29(601)-5132
III. WEB No. 13.148
IV. Space Technology Labs., Inc., Redondo Beach, Calif
V. R.E. Hutton, S.Y. Yu, Y.C. Fung
VI. In ASTIA collection

Air Force Special Weapons Center, Kirtland AF Base, New Mexico
Rpt No. AFSWC-TDR-63-26. THE DEVELOPMENT OF RECIPROCITY PROCEDURES FOR UTILIZING DATA FROM UNDERGROUND EXPLOSION TESTS. Final Report, May 1963. 90 p. incl illus, tables, 23 refs.

Unclassified Report

A procedure for predicting underground cavity motions resulting from surface air-blast loading is developed on the basis of a dynamic-reciprocity principle for a nonhomogeneous, anisotropic, linear, viscoelastic half space. A computer program for evaluating the integral equations for this medium is presented. Experimental measurements from the RAINIER Event of Operations PLUMBBOB are used to postulate cavity motions

1. Digital computers
2. Ground motion
3. Military facilities -- hardening
4. Rainier burst
5. Surface bursts
6. Underground structures
I. AFSC Project No. 1080, Task 108007
II. Contract AF 29(601)-5132
III. WEB No. 13.148
IV. Space Technology Labs., Inc., Redondo Beach, Calif
V. R.E. Hutton, S.Y. Yu, Y.C. Fung
VI. In ASTIA collection

Air Force Special Weapons Center, Kirtland AF Base, New Mexico
Rpt No. AFSWC-TDR-63-26. THE DEVELOPMENT OF RECIPROCITY PROCEDURES FOR UTILIZING DATA FROM UNDERGROUND EXPLOSION TESTS. Final Report, May 1963. 90 p. incl illus, tables, 23 refs.

Unclassified Report

A procedure for predicting underground cavity motions resulting from surface air-blast loading is developed on the basis of a dynamic-reciprocity principle for a nonhomogeneous, anisotropic, linear, viscoelastic half space. A computer program for evaluating the integral equations for this medium is presented. Experimental measurements from the RAINIER Event of Operations PLUMBBOB are used to postulate cavity motions

1. Digital computers
2. Ground motion
3. Military facilities -- hardening
4. Rainier burst
5. Surface bursts
6. Underground structures
I. AFSC Project No. 1080, Task 108007
II. Contract AF 29(601)-5132
III. WEB No. 13.148
IV. Space Technology Labs., Inc., Redondo Beach, Calif
V. R.E. Hutton, S.Y. Yu, Y.C. Fung
VI. In ASTIA collection

arising from a surface burst at the RAINIER site. The effects of variations in the cavity pressure signature, number of measured ground motions, and instrumentation errors are examined. Recommendations are made for experimental programs to obtain needed additional data, and, in general, to ascertain the applicability of the reciprocity to soils.		arising from a surface burst at the RAINIER site. The effects of variations in the cavity pressure signature, number of measured ground motions, and instrumentation errors are examined. Recommendations are made for experimental programs to obtain needed additional data, and, in general, to ascertain the applicability of the reciprocity to soils.	
arising from a surface burst at the RAINIER site. The effects of variations in the cavity pressure signature, number of measured ground motions, and instrumentation errors are examined. Recommendations are made for experimental programs to obtain needed additional data, and, in general, to ascertain the applicability of the reciprocity to soils.		arising from a surface burst at the RAINIER site. The effects of variations in the cavity pressure signature, number of measured ground motions, and instrumentation errors are examined. Recommendations are made for experimental programs to obtain needed additional data, and, in general, to ascertain the applicability of the reciprocity to soils.	